DEPARTMENT OF TRANSPORTATION

Cost-benefit analysis of fuel-efficient speed control using signal phasing and timing (SPaT) data: evaluation for future connected corridor deployment

Michael Levin, Principal Investigator
Civil, Environmental, and Geo- Engineering
University of Minnesota

MARCH 2023

Research Report
Final Report 2023-06

To request this document in an alternative format, such as braille or large print, call 651-366-4718 or 1-800-657-3774 (Greater Minnesota) or email your request to ADArequest.dot@state.mn.us. Please request at least one week in advance.

Technical Report Documentation Page

1. Report No.	2.	3. Recipients Accession No.
MN 2023-06		

4. Title and Subtitle	5. Report Date
Cost/benefit analysis of fuel-efficient speed control using signal phasing and timing (SPaT) data: evaluation for future connected corridor deployment	March 2023
	6.

7. Author(s)	8. Performing Organization Report No.
Michael W. Levin, Zongxuan Sun, Shi'an Wang, Wenbo Sun, Suiyi He, Bohoon Suh, Gaonan Zhao, Jacob Margolis, Maziar Zamanpour	

9. Performing Organization Name and Address	10. Project/Task/Work Unit No.
Department of Civil, Environmental, and Geo- Engineering University of Minnesota 500 Pillsbury Drive S.E. Minneapolis, MN 55455-0116	CTS #2021009
	11. Contract (C) or Grant (G) No. (c) 1036220

12. Sponsoring Organization Name and Address	13. Type of Report and Period Covered
Minnesota Department of Transportation Office of Research & Innovation 395 John Ireland Boulevard, MS 330 St. Paul, Minnesota 55155-1899	14. Sponsoring Agency Code

15. Supplementary Notes

http://mdl.mndot.gov/

16. Abstract (Limit: 250 words)

The objective of this methodology is to refine the preliminary results from previous work (11% fuel savings for one vehicle, one intersection) to an entire corridor of SPaT signals, with different CV market penetration, and with driver awareness of fuel savings benefits. The research will proceed in three parts. First, several vehicles will be instrumented with DSRC receivers and GPS tracking to record SPaT data and the vehicle trajectories together. Offline, the project team will optimize the speed and powertrain control based on recorded SPaT data, using the recorded vehicle trajectories to identify the constraints of traffic flow. A living lab consisting of a GM car engine loaded by a transient hydrostatic dynamometer will be used to measure the fuel consumption with and without speed control. Second, the project team will conduct traffic flow simulations to study the impacts of higher market penetration on the overall fuel benefits, including the benefits to legacy vehicles which unintentionally use SPaT based speed controls by following CVs. Third, network models will be used to predict changes in route choices as drivers recognize the benefits of fuel savings in the route utility. The numerical predictions of fuel savings will be combined into cost/benefit analyses to inform MnDOT on the future deployment of SPaT on other corridors.

17. Document Analysis/Descriptors	18. Availability Statement
Connected vehicles, Autonomous vehicles, Intelligent transportation systems, Traffic signal timing, Traffic signal phases, Traffic models, Power trains	No restrictions. Document available from: National Technical Information Services, Alexandria, Virginia 22312

19. Security Class (this report)	20. Security Class (this page)	21. No. of Pages	22. Price
Unclassified	Unclassified	129	

Cost/benefit analysis of fuel-efficient speed control using signal phasing and timing (SPaT) data: evaluation for future connected corridor deployment

FINAL REPORT

Prepared by:

Michael W. Levin[1]
Zongxuan Sun[2]
Shi'an Wang[1]
Wenbo Sun[2]
Suiyi He[2]
Bohoon Suh[2]
Gaonan Zhao[2]
Jacob Margolis[1]
Maziar Zamanpour[1]

[1]Civil, Environmental, and Geo- Engineering
[2]Mechanical Engineering
University of Minnesota

March 2023

Published by:

Minnesota Department of Transportation
Office of Research & Innovation
395 John Ireland Boulevard, MS 330
St. Paul, Minnesota 55155-1899

Acknowledgements

We gratefully acknowledge the assistance and support of the following Technical Advisory Panel members: Michael Levin, Marcus Bekele, Kevin Chan, Michael Fairbanks, Catherine Huebsch, Cory Johnson, Derek Lehrke, Micaela Resh, Daniel Rowe, Brent Rusco, and Ray Starr.

List of Abbreviations

CV - Connected Vehicle

CAV - Connected Autonomous Vehicle

SPaT - Signal Phasing and Timing

HIL - Hardware in the Loop

Contents

List of Figures

List of Tables

Executive Summary

Due to rising fuel costs and environmental impact, consumers are increasingly aware of fuel efficiency (MPG) in the vehicles they purchase. A major source of fuel consumption is acceleration/deceleration cycles caused by stopping at red lights. Anticipating future signal phases creates significant opportunities for individual vehicles to optimize their speed profiles on arterial corridors. By preemptively reducing speed before a red light, vehicles can avoid coming to a full stop, thereby reducing the fuel consumption needed to accelerate again. The objective of this methodology is to refine the preliminary results to gain a fuel optimal control method for connected vehicles. The analysis is applied to an entire corridor of SPaT signals, with different CV market penetration rates, and with driver awareness of fuel savings benefits. The research team mainly completes the following tasks:

Task 1: Initial Memorandum on Expected Research Benefits and Potential Implementation Steps. The research team selected key benefits to clearly define the benefits the state will receive from the results and conclusions of this research as an initial assessment.

Task 2: Data collection of SPaT messages. In this task, the research team obtained the real-world traffic information in various traffic conditions using OBUs. Then, the team conducted multiple test drives on the TH-55 corridor using the instrumented vehicles. The objective was to record vehicle trajectories and SPaT broadcasts together.

Task 3: Fuel-efficient speed control based on short-term traffic flow prediction. The speed control was adjusted to match the predicted time the vehicle could pass through the traffic signal given the estimated queue lengths. Flow and density estimations from traffic flow theory is used to predict the queue length. The real-time traffic estimation provides specific constraints to the target vehicle speed optimization algorithm.

Task 4: Living lab experiments and analysis of speed control benefits. All vehicle and powertrain models were calibrated using actual vehicle testing data. HIL experiments were conducted for validation work of the proposed co-optimization strategy of task 3. Research team also showed that a controlled vehicle can achieve a substantial fuel benefit compared with the base vehicle.

Task 5: Analysis on Various Market Penetrations of Connected Automated Vehicles. The research team developed a holistic simulation methodology to predict the benefits in fuel consumption for vehicle platoons at various market penetration rates of CAVs.

Task 6: Network model of SPaT corridors and route choice. The research team tried to model the magnitude of fuel savings at the network-level (for major corridors) by dynamic traffic assignment

Task 7: Cost-benefit analyses of connected corridor installation. The research team computed the long-term cost-benefit ratio of installing a SPaT corridor to find optimal timing for options.

Task 8: Final Memorandum on Research Benefits and Implementation Steps. The research team provided a qualitative and quantitative discussion of the estimated benefits.

Key Findings

SPaT can successfully provide concrete fuel savings.

In a long-term horizon such as 10 years, it is financially reasonable to install and run SPaT corridors.

Fuel Saving by SPaT is possible even in low market penetration rates.

Impacts of SPaT deploying varies according to the target corridor.

Chapter 1

Introduction

Vehicle fuel consumption is a major concern of our society for many reasons including fuel costs and environmental impacts. Studying traffic patterns can reveal some solutions for this problem. Vehicles deceleration and accelerations when approaching signalized intersections causes a huge amount of fuel consumption. For a traditional human-driven vehicle, it is common that the driver will try to accelerate when approaching an intersection to pass it with the current green light. However, the signal light may turn red before the vehicle reaches the intersection. In this case, the vehicle must decelerate to stop before the stop line and keep idling for the next green light. These sharp accelerations/decelerations and idling will lead to unnecessary fuel consumption at signalized intersections. Connected autonomous vehicles technology may create a novel response to this issue. By communicating with traffic signals, connected vehicles (CVs) have the potential to avoid this kind of energy waste.

A CV is equipped with sensors to collect real-time traffic data, including preceding vehicles' and other CVs' locations and speeds through vehicle to vehicle (V2V) communication, and the signal phase and timing (SPaT) information through vehicle to infrastructure (V2I) communication. The newly available information makes it possible for a CV to anticipate future traffic conditions. This process provides a control which is optimal for fuel consumption. Thus, if a corridor becomes equipped with this mechanism, connected vehicles can enjoy this efficiency. Generally, every signalized corridor can provide some certain amount of fuel saving based on traffic demand.

Deploying SPaT will require initial cost for installation and equipment while fuel saving benefits will appear gradually as more connected vehicles use that corridor. These benefits will help road users to save fuel costs in the long-term. Therefore, costs are invested immediately at the start point and benefits appears over time after deployment. The current study provides an optimal control on connected vehicles using SPaT on different

corridors to evaluate whether deploying SPaT infrastructure would be beneficial.

Chapter 2

Task 2: Data collection of SPaT messages

March 31 2021

2.1 Introduction

Connected vehicle (CV) applications present new solutions to many energy optimization problems. However, it is challenging to evaluate various optimizations and controls with real-world testing due to safety and technical concerns. Therefore, most previous research depends on traffic simulation software for evaluation and testing. Even though simulation software is a great tool for evaluating different traffic solutions, it might lack realism. The connected corridor on TH-55 enables us to overcome these shortcomings. It allows real vehicles to interact with real-world traffic signals via dedicated short range communications (DSRC). Our previous work also used wireless communications to obtain information from traffic signals and adjacent vehicles, and evaluate the optimal controls for CVs. However, both broadcasting device and receiving device were customized for the research. Also, the evaluation included only an intersection and simple traffic scenario (car-following). Therefore, it is not guaranteed that results of the optimal controls can be generalized and expanded to the real-world traffic including varying traffic conditions. The purpose of Task 2 is to record vehicle trajectories and signal phasing and timing (SPaT) and MAP data together in diverse traffic scenarios. We classified traffic scenarios in peak time versus off-peak time and four different patterns of real road driving. Those recorded data sets will be used to evaluate the speed and powertrain optimization of connected vehicles and to identify the constraints of the traffic flow. These provide a more realistic representation of traffic flow and the signal information, and therefore the research team can verify the performance of optimal control framework with the realistic data.

2.2 In-Vehicle Equipment

2.2.1 Purpose

In-Vehicle Equipment is an installed instrument on a vehicle to enable communication with other vehicles and infrastructures using DSRC . It includes on-board units (OBU).

Input:

- From roadside units (RSUs): Signal Phase and Timing (SPaT) and MAP data
- From surrounding vehicles: Basic Safety Message (BSM) of other vehicles

Output:

- To surrounding vehicles: BSM of the instrumented vehicle
- To RSUs: BSM of the instrumented vehicle

2.2.2 Vendors and Procurement

During task 2, the project team researched vendors of connected vehicle equipment, then discussed the requirements for software, hardware, and warranty support. More than 10 different vendors used to sell OBUs in the market. However, many vendors including LEAR discontinued producing OBUs or providing technical support for OBUs. Based on our research, OBUs from SAVARI and COHDA are only vendors still available for purchase.

In the meantime, the research team had an opportunity to rent SAVARI OBUs from the Connected and Automated Vehicle Support Services provided by the U.S. department of transportation (DOT). The compatibility with LEAR RSU used on the connected corridor was the most important factor to consider. Theoretically, any DSRC devices from different suppliers can communicate with each other if they meet SAE J2735 standard. However, there are possibilities that DSRC devices from different brands interpret the SAE J2735 standard differently and configure the DSRC message structure in a different manner. Therefore, the research team conducted confirmation tests with rented SAVARI OBUs and verified that they receive DSRC messages from the LEAR RSUs on TH-55.

Based on provided details and confirmation tests, SAVARI was chosen as the OBU supplier for this project. SAVARI has two different models of OBU: MOBIWAVE (MW) 1000 and 2000. The MW1000 is the DSRC version, and the MW2000 is the CV2X (Cellular) version. They do not have a dual mode version currently available. As a result, the MW1000 was selected as the in-vehicle equipment for this project.

Vendors	OBU models	Price
SAVARI	MOBIWAVE 1000	$1,219/EA
COHDA	MK5	$1,791/EA
LEAR	LOCOMATE ROADSTAR	Discontinued

Table 2.1: OBU models of each vendors

2.3 Testing vehicle instrumentation

2.3.1 Pre-Installation

Figure 2.1 shows parts lists of the equipment for the driving test. It consists of OBU, integrated GPS and DSRC antenna and 12V power cable. All OBUs are updated with the latest version of the firmware to guarantee the wireless communication via DSRC between RSUs and OBUs. Older versions of the firmware were developed based on the older versions of SAE standards. Therefore it is not possible to receive SPaT and MAP messages using OBUs with older firmware. Moreover, the OBUs need to be configured and tested before collecting data. It is necessary to confirm the configuration regarding channel numbers, PSID, security features, and data storage.

Figure 2.2 shows the instrumentation of a testing vehicle. The OBU (SAVARI MW1000) is installed to obtain vehicle speed and location based on GPS. The OBU also receives signal status from the RSU. As shown in Figure 2.2, the GPS and DSRC antenna of the OBU is located at the center of the dashboard of the vehicle to ensure a good signal reception and avoid any damages during the tests. Since the location of the antennas affects the range of communication between the RSU and OBU, the antenna is mounted at the same spot of the dashboard every time. The OBU will be installed on the test vehicles with HMI. In the test, the laptop is used as HMI. We can run the software for data collection, and check if OBUs are receiving SPaT and MAP adequately. Both OBU and HMI are powered through the cigarette plug.

Equipment parts lists		
No.	Item	Quantity
1	SAVARI Moviwave 1000	1
2	Integrated GPS/DSRC Antenna	1
3	12volt Adaptor plug	1

Figure 2.1: OBU parts list

Figure 2.2: OBU installation diagram

2.4 SPaT and MAP message

2.4.1 SPaT

The SPaT message is used to convey the current status of signalized intersections. The primary information used is the current state of the intersection, at what time the current state is most likely to have begun, and the range of times for which it could end. Along with the MAP message (which describes a full geometric layout of an intersection) the receiver of this message can determine the state of the signal phasing and when the next expected phase will occur [SAE]. The OBU receives the SPaT messages broadcast at the intersection via the RSU 10 times per second. Since DSRC messages are encoded in Unaligned Packed Encoding Rules (UPER) and shown as hexadecimals, decoding is required to use the messages for our research. To interpret messages fast and accurately, the open-source packet analyzer 'Wireshark' and a plugin tool [wir] that is a custom software based on SAE J2735 [SAE] are used. Using them, SPaT messages are interpreted automatically. The messages are then exported as a human-readable file (e.g. .txt) and the exported files are processed in MATLAB. This way, SPaT messages became legible without dealing with line by line interpretation. From the interpreted messages, we can figure out the location of intersections, signal phase, and timing for signal changes.

Figure 2.3 shows an example of a SPaT message interpreted from the open-source packet analyzer. In figure 2.3, the data element 'id: 5401' indicates that the message was broadcast at S Shore Dr. The intersection ID was assigned by the Minnesota DOT when the connected corridor was launched. Next, the data element 'moy: 365477' indicates 253 days 19 hours and 17 minutes (which is 7:17 PM on September 10th), and the data element

'timeStamp: 12296' indicates 12.296 seconds. Therefore, by combining the moy and the timeStamp, we can figure out that the message was created at 7:17:12 PM on September 10th, 2020.

The signal group ID is used to map the movements for which the signal phase and timing information applies. For instance, if a connected vehicle was driving in a straight lane from west to east at the S Shore Dr intersection, the data element 'signal group: 2' would need to be checked according to the MAP message. The data element 'eventState: protected-Movement-Allowed' describes that the signal is green. The data element 'minEndTime' and 'maxEndTime' indicate the possible time, in units of 1/10th of a second in the current or next hour, at which the phase could change. Therefore, 'minEndTime: 33817' indicates 3381.7 seconds (which is 56 minutes 21 seconds). Therefore, we can determine that the signal phase for signal group 2 will change at 7:56:21 PM.

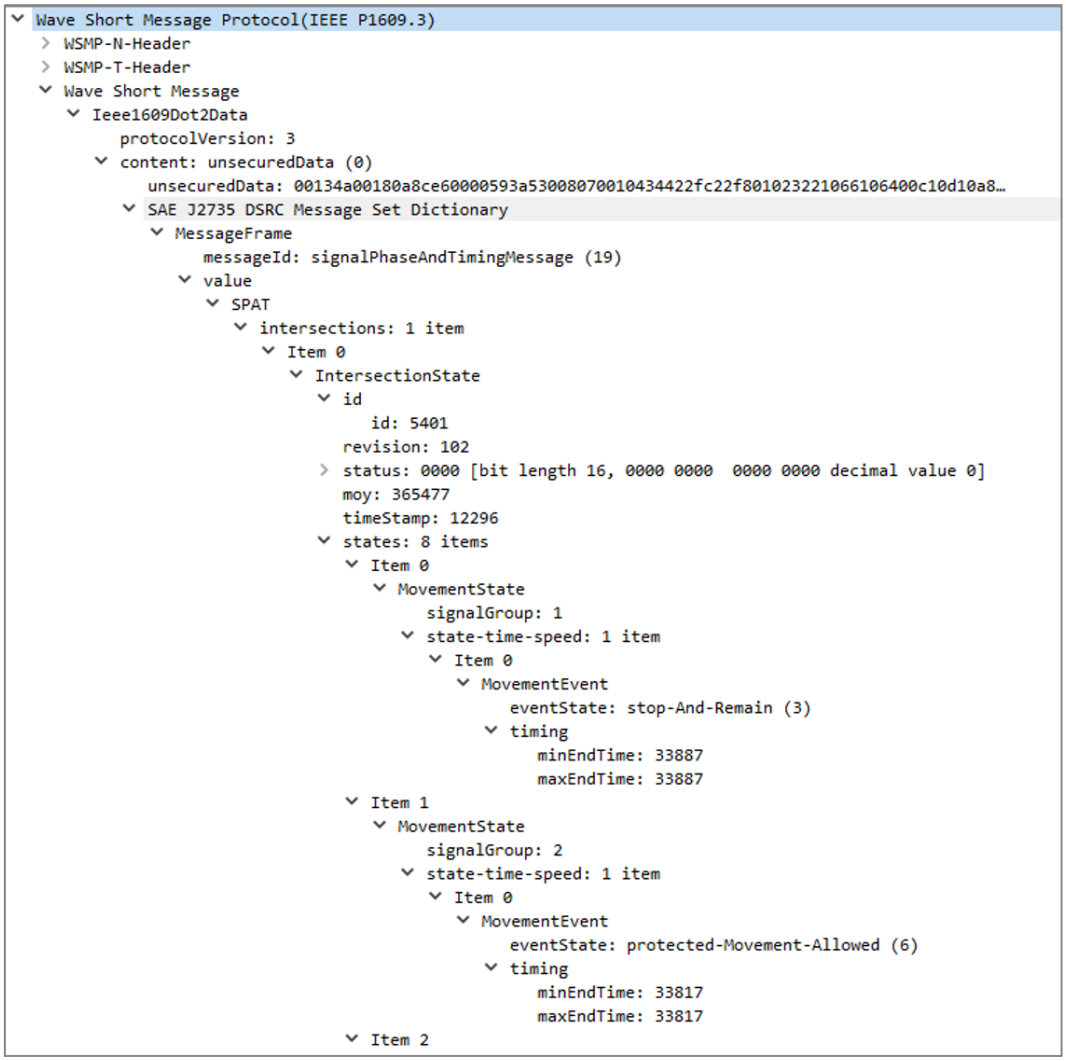

Figure 2.3: An example of a decoded SPaT message

2.4.2 MAP

The MAP message is used to convey many types of geometric information of the intersection. At the current time its primary use is to convey intersection lane geometry maps. The map message is used by other messages to relate additional information (for example, the signal phase and timing via the SPaT message) to events at specific geographic locations on the roadway [SAE]. The OBU receives the MAP messages broadcast to CVs at the intersection via the RSU once per second. In order to interpret the MAP messages, an online automotive ASN.1 message decoder [MAR] provided by Marben-Products is used. This online decoder allows decoding of encoded MAP messages into human-readable files. From the interpreted messages, we can figure out the location of intersections and signal groups.

Figure 2.4 shows an example of a MAP message interpreted from the online ASN.1 message decoder. In Figure 2.4, the data element 'id: 5401' indicates that the message was broadcast at S Shore Dr intersection. The data element 'refPoint' provides a precise location of the intersection in the GPS coordinates. Therefore, the GPS coordinates of the center of this intersection is latitude 44.9880245 and longitude -93.4197414. The data element 'laneID: 15' indicates that the assigned index for the lane is 15. Therefore, it is noticed that the following information is applied to lane 15. The data element 'directionalUse: 10' indicates that lane 15 is an ingress lane. If directionalUse is 01, then it means lane 15 is an egress lane. The data element 'maneuvers: 100000000000' represents that a straight movement is allowed from lane 15. The data element 'NodeXY' presents a single node point in a path. Each selected node has an X and Y offset from the prior node point. X-axis runs from west to east, and Y-axis runs from south to north. The node list for a lane is made up of a sequence of these points to describe the center line of the lane. For example, the first node is located -25.71m to the east which means 25.71m to the west, and -5.99m to the north which means 5.99m to the south from refPoint. The MAP message also contains connection information. For example, in the data element 'connectingLane', we can see that lane 15 is connected to lane 24 where the straight movement is allowed.

Figure 2.4: An example of decoded MAP messages

2.5 Data collection

From September 2020, the research team has been conducting driving tests along the connected corridor in varying traffic conditions aiming to collect data for evaluating traffic prediction and fuel-efficient control as well as providing thorough perspective and insight for potential of the connected corridor and CVs. As shown in Figure 2.5, three or four actual testing vehicles instrumented with OBUs were driven by human drivers to pass real-world intersections at TH-55. During the driving tests, OBUs installed in vehicles receive SPaT and MAP messages from RSUs on the traffic signal at intersections and store all received messages in the memory space of OBUs. Moreover, OBUs record the longitudinal and lateral location of vehicles received from the GPS in the memory space.

Figure 2.5: Test vehicles equipped with OBUs

As an initial step, the research team collected naturalistic driving data in varying demand periods. (e.g., peak and off-peak times). Figure 2.6 shows the traffic flow of each time window. The green traffic flow line describes normal traffic, the yellow line represents medium flow, and the red line indicates heavy traffic. As shown in Figure 2.6, TH-55 mostly has normal traffic flow, and it does not have heavy traffic even in rush hours such as 7-8 AM, and 5-6 PM. Therefore, the research team assigned a time window between 12 PM and 4 PM as peak traffic time and the others as off peak traffic time. Driving tests have been conducted with respect to the classification of peak and off peak time. And data was collected in diverse traffic conditions.

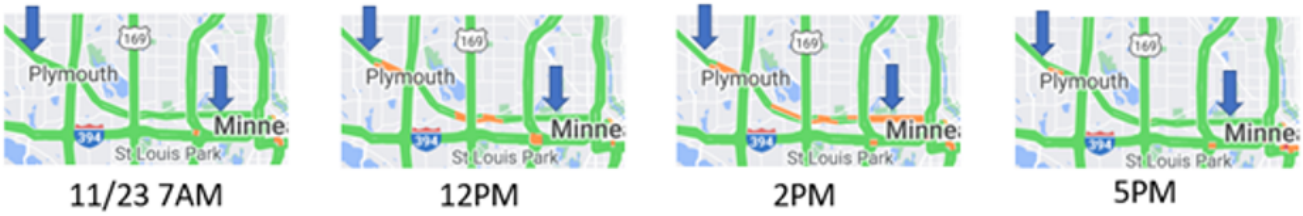

Figure 2.6: Traffic map on TH 55

In the second phase, the research team defines more detailed traffic scenarios which indicate typical driving patterns that can be observed in the real-world. Four driving patterns in Figure 2.7 are implemented in driving tests: (a) car-following, (b) cut-in, (c) cut-out: highway exits, (d) cut-out: lane change. Each test scenario was implemented recursively between Winnetka Ave to County Road 6. The whole list of collected datasets is shown in Table 2.2. The third column describes the number of testing vehicles equipped with the OBU. The fourth column displays the number of intersections with operational RSUs versus intersections that the testing vehicles passed. The fifth column shows the number of tests conducted.

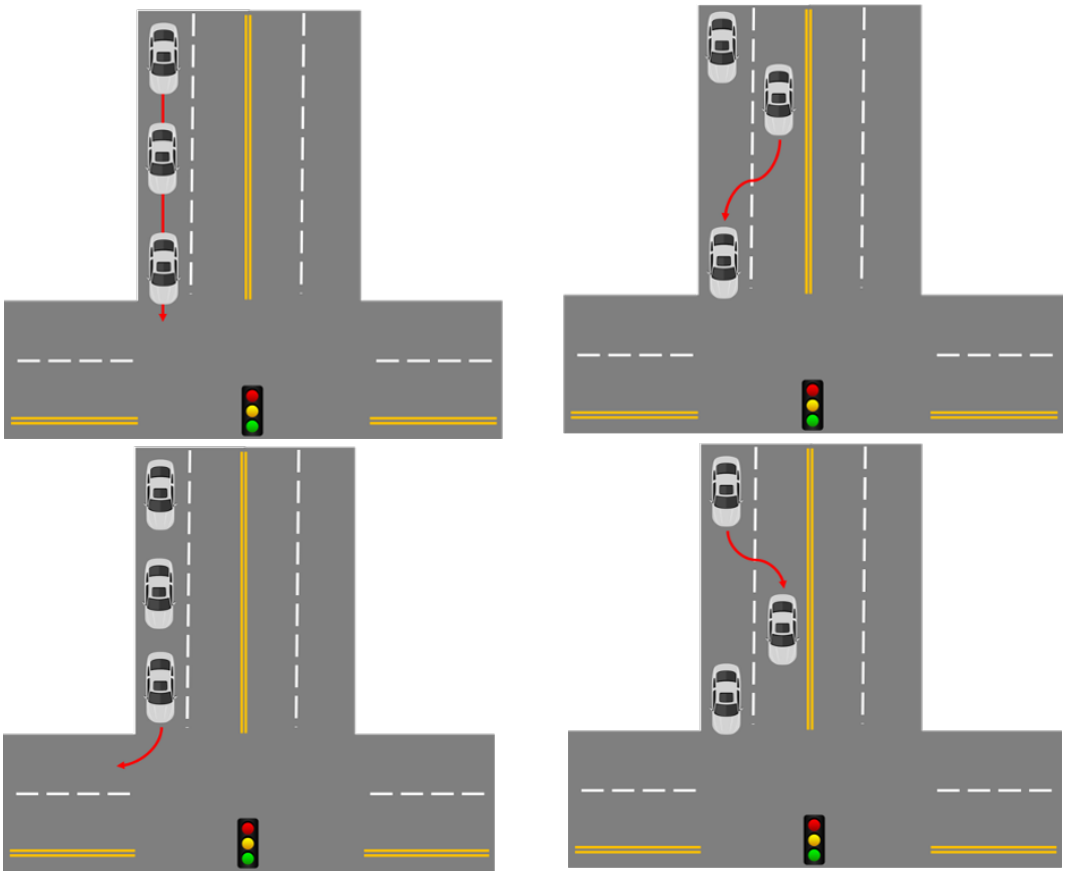

Figure 2.7: (a) car-following, (b) cut-in, (c) cut-out: highway exits, (d) cut-out: lane change

Scenario	Date	Time	Number of vehicles	Number of intersections (Operating/Passed)	Number of tests
Peak	9/10/20	4pm	1	20/22	4
	10/1/20	12pm	2	3/6	1
	10/21/20	3pm	1	7/22	2
	1/10/21	4pm	1	17/22	2
	2/3/21	12pm	2	17/22	1
Off peak	9/22/20	5pm	1	3/6	2
	10/9/20	5pm	1	7/22	2
	10/21/20	5pm	4	7/22	2
	1/13/21	8am	2	17/22	2
Cut-in	2/15/21	12pm	3	6/6	4
Cut-out: hwy exit	3/1/21	11am	3	6/6	6
Cut-out: Lane change	3/12/21	11am	3	6/6	4
Car-Following	3/12/21	12pm	3	6/6	4

Table 2.2: Data Collection History

2.6 Analysis of SPaT and MAP

2.6.1 Communication Reliability

The performance and reliability of DSRC were tested through driving tests. The research team first investigated the maximum and effective range of message reception. Theoretically, DSRC messages can be transferred up to 500m [Savari Inc.]. The range of communication depends on geographic location of traffic signals and roadways, obstruction from static (e.g., buildings) and moving objects (e.g., vehicles), the location of the antenna in the vehicle, and weather conditions [Xianan Huang, Ding Zhao, and Huei Peng]. Collected data shows that communication ranges vary for each intersection. Some intersections have relatively larger communication ranges, but others have smaller ones. Also, communication ranges are not consistent due to the effect of the surrounding environment at the time for data collection. The average communication ranges of each intersection are described in Figure 2.8. Generally, CVs start receiving SPaT messages 300m ahead of traffic signals and receive for 300m after passing the intersections. The maximum range of reception is 600m ahead of intersections.

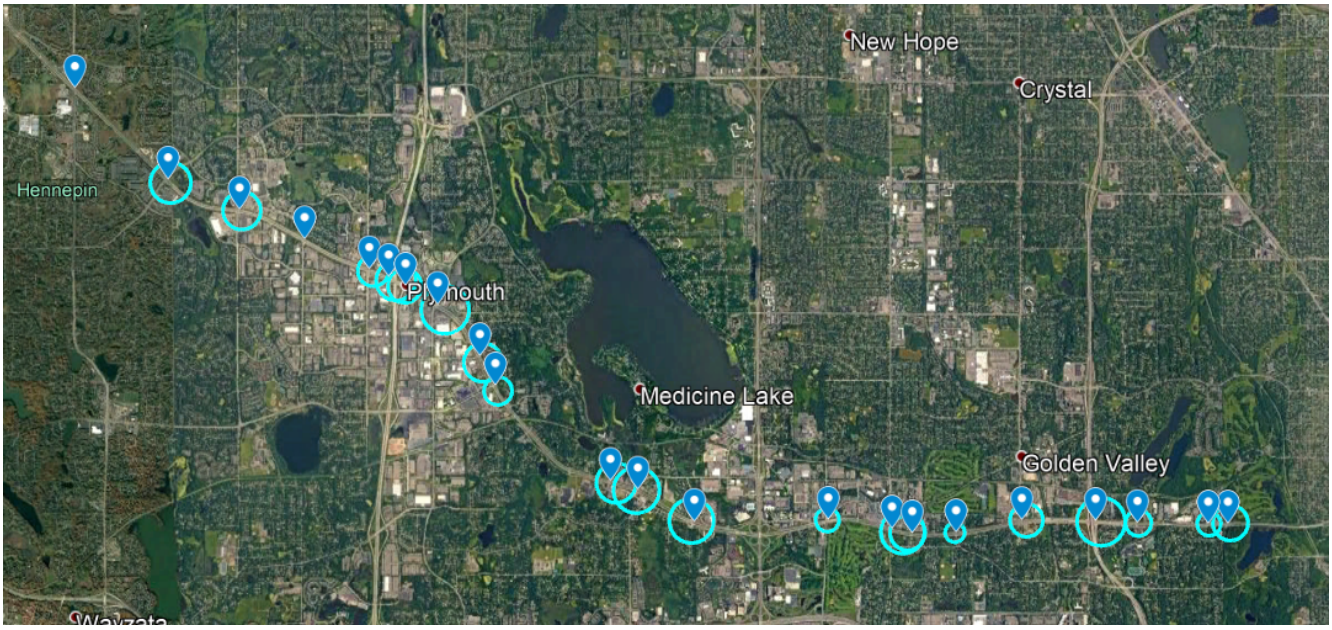

Figure 2.8: DSRC range at each intersections

2.6.2 Issues on SPaT

While reviewing collected data, the research team ran into a few issues on the SPaT messages. Especially, after updating traffic signal controllers and their software on the connected corridor as of December 2020, more issues are observed from the SPaT messages. Issues from new controllers will be discussed in the next section.

2.6.2.1 Time offsets

The current time information in the SPaT message was not accurate and was offset by 15 hours and 33 minutes. According to the SAE J2735, the data element minute of the year (moy) expresses the number of elapsed minutes of the current year. Taken together with timeStamp, it provides a range of one full year with a resolution of 1 millisecond. It is typically used to provide a time stamp indicating when a message was created. However, the indicated time on SPaT is 15 hours 33 minutes faster than real time. For example, the figure shown below is an excerpt of SPaT collected around 8:30 am on January 13, 2021.

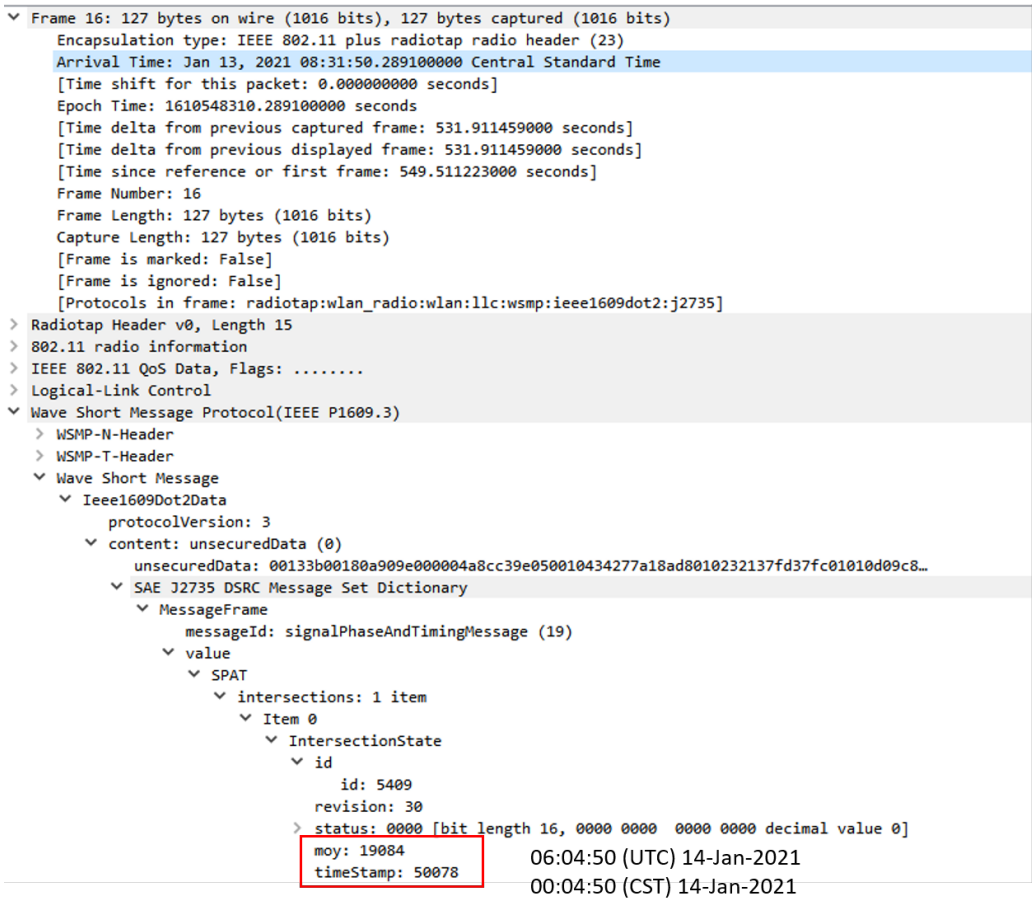

Figure 2.9: An excerpt of SPaT which has offset on 'moy'

Figure 2.9 was decoded in ASN.1 UPER. Therefore, the OBU time was not incorporated in the decoding process. The arrival time of the message indicates the exact time when the OBU received the message. In the blue highlight, it can be seen that the arrival time is 08:31:50am (CST), which is 02:31:50pm (UTC) on January 13, 2021. Central Standard Time (CST) is six hours behind Coordinated Universal Time (UTC).

In Figure 2.9, the time indicated with the red box represents 06:04:50 (UTC), which is 00:04:50 (CST) on January 14, 2021. From the difference between collected time and recorded time, we can see that the current time information in SPaT messages is 15 hours 33 minutes faster than real time. This issue is observed in 15 intersections among the 17 total functioning intersections. Among the 17 intersections, only Rockford and Vicksburg have accurate moy. As the offsets occur consistently, we compensate '-15 hours 33 minutes' to the SPaT time in the data processing process. It would be much more efficient if accurate moy is available from the SPaT data. We believe it is important to expand usability of the connected corridor.

2.6.2.2 Signal timing range

Signal timing information is not aligned with real-world traffic signal changes. The data element minEndTime is used to convey the earliest time possible at which the phase could change. The data element maxEndTime is used to convey the latest time possible which the phase could change. The data minEndTime and maxEndTime provide a possible time window for signal change. Therefore, the maxEndTime is greater or equal to minEndTime if both are in the current hour. When maxEndTime is in the next hour, the maxEndTime is smaller than minEndTime. For example, if the current time is 2:58:00 pm, and the signal phase change will happen between 2:59:00 pm to 3:01:00 pm. In this case, maxEndTime will be smaller than minEndTime where minEndTime and maxEndTime will be 35400 and 600 respectively. Generally, minEndTime and maxEndTime have less than a few minutes difference. However, it is noticed that both intersections at Theodore Wirth Pkwy and Meadow Ln have about 49 minutes difference between minEndTime and maxEndTime.

Figure 2.10 shows an excerpt of SPaT collected at 4pm (CST) on January 10th 2021 from the Meadow Ln intersection. In figure 2.10, minEndTime is 246 which represents 0.41 minutes and maxEndTime is 29669 which indicates 49.45 minutes. It is noted that maxEndTime is greater than minEndtime, which means both are in the current hour, and they are 49 minutes apart.

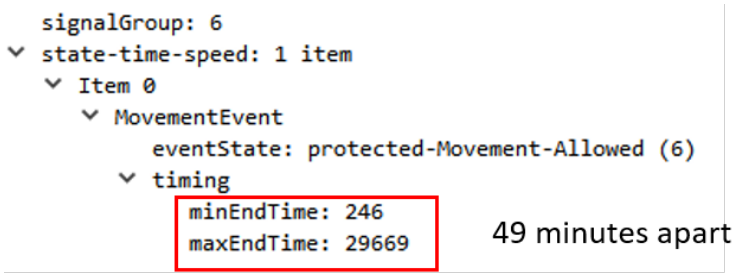

Figure 2.10: An excerpt of SPaT collected at Meadow

Figure 2.11 is an another excerpt of SPaT collected at 8am (CST) on January 13th 2021 from the Meadow Ln intersection. In Figure 2.11, minEndTime is 19805 which represents 33.01 minutes and maxEndTime is 13022 which indicates 21.7 minutes. In this case, it is noted that maxEndTime is less than minEndtime, which means maxEndTime is in the next hour, and they are 49 minutes apart.

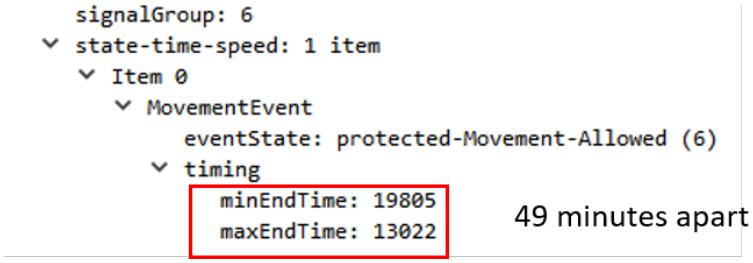

Figure 2.11: An excerpt of SPaT collected at Meadow

This issue was continuously observed from the recurring driving tests at Theodore Wirth Pkwy and Meadow Ln. The research team has been extracting signal timing information from the collected SPaT messages by averaging the minEndTime and maxEndTime. However, this strategy needs to be altered depending on the intersections because of the unrealistic difference between minEndTime and maxEndTime. Therefore, the research team uses minEndTime only to obtain signal timing for the SPaT messages from the two intersections during data processing.

2.6.2.3 Unstable signal timing

Signal timing is unstable at the intersection of Schaper Rd and Th 55. In order to use SPaT messages for CV applications, it is necessary to convey reliable information to CVs. Therefore, signal timing has to be consistent across a period of time during any given signal phase. However, in the SPaT message collected at Schaper Rd, it is noticed that the signal timing changed abruptly within a matter of milliseconds, so CVs cannot reliably expect when the signal will change to the next stage. For instance, Figure 2.12 shows two SPaT messages collected in consecutive sampling time (0.1 second). It can be seen that minEndTime changed from 693 to 715 and maxEndTime changed from 693 to 1594. This issue is observed only at Schaper Rd. Therefore, the research team uses the last SPaT messages only among the recorded messages at each intersection.

```
signalGroup: 6
state-time-speed: 1 item
    Item 0
        MovementEvent
            eventState: protected-Movement-Allowed (6)
            timing
                minEndTime: 693
                maxEndTime: 693
```

```
signalGroup: 6
state-time-speed: 1 item
    Item 0
        MovementEvent
            eventState: protected-Movement-Allowed (6)
            timing
                minEndTime: 715
                maxEndTime: 1594
```

Figure 2.12: An excerpt of SPaT collected at Schaper

2.6.3 Issues on MAP

Generally, Map messages have no issues. But, the messages broadcast at Douglass Dr intersection have the wrong signal group allocation. In the beginning stage, the research team created geometric maps of the locations of signal groups at each intersection. When the locations of the signal groups are consistent, it becomes more efficient to interpret SPaT and MAP messages with the premade geometric maps. While building the map, it was noticed that signal groups at Douglass Dr intersection are assigned to the wrong number, and it caused improper interpretation of SPaT and MAP messages. Figure 2.13 shows an example of geometric maps of locations of signal groups. As shown in Figure 2.13, Lane 3,4, and 5 are assigned with Signal group 1. However, the signal phase of signal group 1 is not matched with the real traffic signal. For example, a test vehicle was passing the intersection, but recorded SPaT messages that said it was a red signal at that intersection. The research team concluded that signal group 6 is more adequate based on the information of signal phase and timing. Furthermore, all the other intersections

have signal group 6 at the same lanes. Therefore, lanes 3, 4, and 5 are assumed to be in signal group 6, rather than group 1.

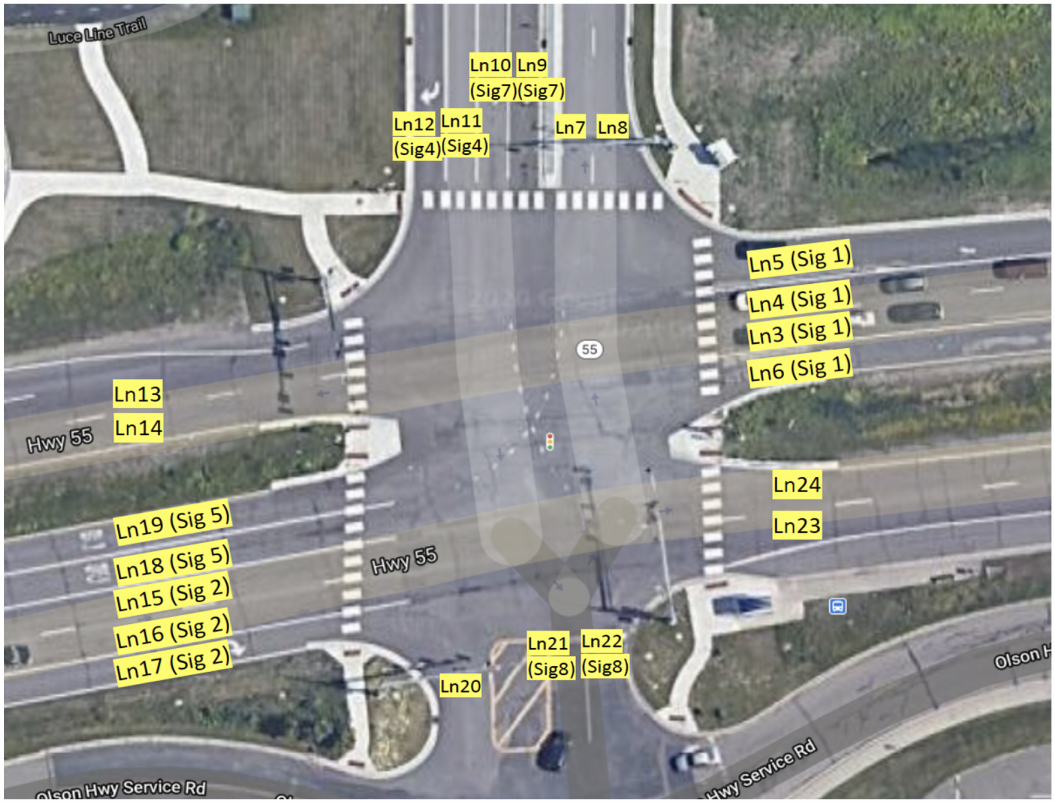

Figure 2.13: An example of geometric maps of locations of signal groups

2.6.4 Experiment results

Figure 2.14 shows the vehicle trajectories of CVs and signal phase and timing at each intersection. A green line describes that the traffic light is green and it's length indicates the time duration of green light. Likewise, a yellow and a red line represents a yellow light and a red light accordingly. The blue and pink line indicate the vehicle trajectory of each CV. For instance, a dataset for car following scenario is plotted in Figure 2.14. It can be seen that all the CVs pass intersections when the light is green. CVs stop at intersections when the light is red.

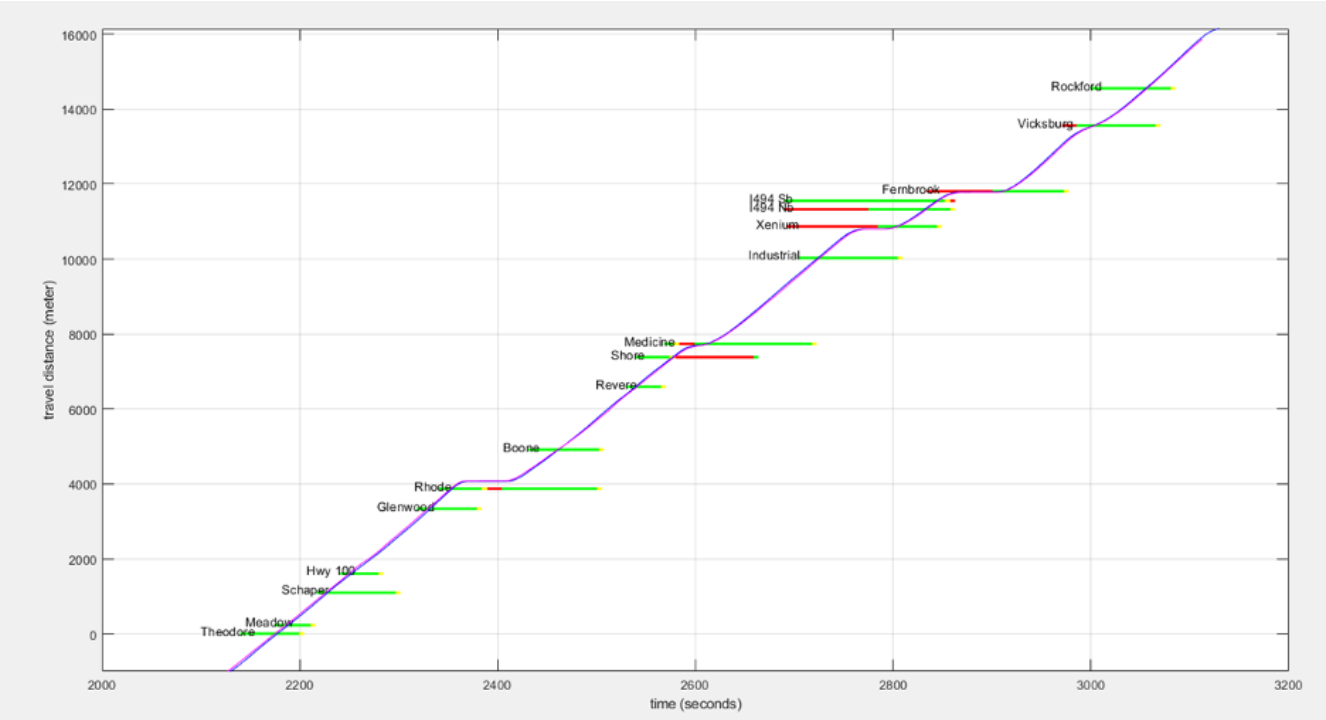

Figure 2.14: Vehicle trajectories and SpaT for a car following scenario

2.7 Summary

In this work, the real-world traffic information is obtained in various traffic conditions using OBUs. OBUs on the testing vehicles record the vehicle trajectories and traffic signal information broadcast from the RSUs. This information will enable various CV applications to be evaluated in realistic roadway conditions.

Our analysis results show that the SPaT messages broadcast at Theodore Wirth Pkwy, Meadow Ln and Schaper Rd include a few issues: 1) time offsets, 2) inaccurate signal timing, and 3) unsteady signal timing. It is also noticed that the MAP messages broadcast at Douglass Dr have the wrong signal group allocation. Therefore, the research team corrects the issues in the data processing process.

Through this project, the performance of traffic prediction and optimal control for energy saving will be demonstrated with the collected and preprocessed data.

Chapter 3

Task 3: Fuel-efficient speed control based on short-term traffic flow prediction

March 31 2021

Description: Using published literature on traffic state estimation and vehicle speed control using SPaT, the project team developed the traffic flow prediction model and speed control method with preliminary numerical results.

3.1 Introduction

Vehicle fuel consumption has been a major concern of our society. For a traditional human-driven vehicle, it is common that the driver will try to accelerate when approaching an intersection to pass it with the current green light. However, the signal light may turn red before the vehicle reaches the intersection. In this case, the vehicle must decelerate to stop before the stop line and keep idling for the next green light. These sharp accelerations/decelerations and idling will lead to unnecessary fuel consumption at signalized intersections. By communicating with traffic signals, connected vehicles (CVs) are a potential road to avoid this kind of energy waste.

A CV is equipped with sensors to collect real-time traffic data, including preceding vehicles' and other CVs' location and speed through vehicle to vehicle (V2V) communication, and the signal phase and timing (SPaT) information through vehicle to infrastructure (V2I) communication. The newly available information makes it possible for a CV to anticipate future traffic conditions (next 10-15s) using the traffic flow model, as the other vehicles' speed and location can be used to estimate the speed and the density of the traffic flow and the SPaT information provides the current and future signal states at the intersection. One advantage of this approach is that it works with different CV market penetrations, from 0% to 100% (when there is no other CV on the road, the target CV can use the speed and location of the preceding vehicle to estimate the traffic state). The prediction of future traffic conditions determines the car following constraints for the target CV. Under all constraints, the speed control of the target CV can be obtained by solving an optimal control problem, which aims for minimum fuel consumption. The target CV with speed control method can accelerate and decelerate smoothly, avoid unnecessary braking and idling, and operate the powertrain system more efficiently. Published papers have shown that for a single CV approaching an isolated intersection, fuel benefits increase from 5.3% to 9.4% as the penetration rate of connectivity increases [26]. However, the previous work only considers one intersection, and the traffic data is generated by a microscopic traffic simulator VISSIM. In this report, the proposed approach can be applied on a corridor with multiple intersections and is verified by real traffic data.

The optimal control will be solved and implemented in a model predictive control (MPC) framework. The control will be updated every N_{UD} time steps (selected as 1 second in this report) as new traffic information becomes available. The optimal control strategy will be solved for the next N_{PH} time steps (prediction horizon, selected as 15 seconds in this report). Figure 3.1 shows the flowchart of the project framework. (a) At the beginning of each update instance k, new information is obtained through connectivity, including preceding connected vehicles' location and speed, and SPaT. (b) Real-time information from connected vehicles and signal lights provides 'partial' measurement of the traffic states. a state observer (Unscented Kalman Filter) is used to estimate the current traffic states of the entire roadway. (c) Once the traffic states of the entire roadway are known, future traffic states

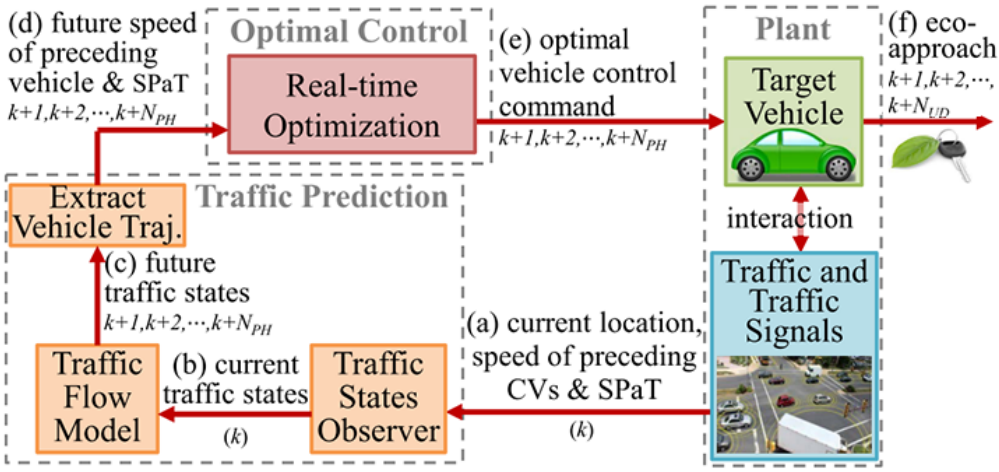

Figure 3.1: Flowchart of the project framework.

are predicted by propagating a traffic flow model forward in time for the prediction horizon (next N_{PH} time steps). (d) Using these future traffic states, future trajectory of the preceding vehicle is obtained. (e) The vehicle speed optimization is developed for the target connected autonomous vehicle (CAV). The future trajectory of the preceding vehicle is used to define the car-following distance constraint. The future SPaT is used to define the signal constraint. Then the optimization problem is solved to obtain the optimal control (vehicle speed control command) of the target CAV for the prediction horizon (next N_{PH} time steps). (f) The first N_{UD} steps of the optimal control are implemented on the target vehicle to achieve eco-approach then the entire process will be repeated. The traffic prediction and speed control are described in detail below.

3.2 Traffic Flow Model

Various continuous-time traffic flow models have been developed and widely adopted over the past several decades, with the notable ones proposed by Lighthill and Whitham [14] and Richards [21] (known as the LWR model). In the LWR model traffic is restricted to equilibrium states. In other words, the flow q follows the equilibrium relationship $q = f_*(\rho)$, where ρ is traffic density and $f(\cdot)$ is a nonlinear function. The notation $*$ is used to indicate the traffic state at equilibrium. This is also known as the fundamental diagram in transportation engineering. In reality, traffic is however generally observed in non-equilibrium states. One of the most well-known non-equilibrium traffic flow models is the Payne-Whitham (PW) model [20, 34]. The PW model is given by the following set of

partial differential equations:

$$\frac{\partial \rho}{\partial t} + \frac{\partial q}{\partial x} = 0 \tag{3.1}$$

$$\frac{\partial v}{\partial t} + v\frac{\partial v}{\partial x} + \frac{c_0^2}{\rho}\frac{\partial \rho}{\partial x} = \frac{v_*(\rho) - v}{\tau} \tag{3.2}$$

where

$\rho(x,t)$ = traffic density at location x at time t,

$v(x,t)$ = traffic speed at location x at time t,

$v_*(\cdot)$ = equilibrium speed as a function of density ρ,

$c_0 > 0$ = traffic sound speed,

τ = relaxation time for vehicles to reach the equilibrium speed.

Clearly, the PW model is able to mathematically describe the evolution of traffic density and speed on the road. However, we are devoted to predicting traffic in front of but not including the controlled target vehicle as shown in Figure 3.1. In addition, the function $v_*(\cdot)$ may take various forms, depending on the fundamental diagram used. For example, a triangular fundamental diagram is employed in the sequel to characterize the equilibrium traffic speed $v_*(\rho)$.

Despite the fact that the second-order traffic flow model (3.1)–(3.2) is capable of capturing the evolution of traffic density and speed, it unfortunately does not explicitly account for lane-changing behavior in a heterogeneous traffic flow. In what follows, we are devoted to extending the existing traffic flow model (3.1)–(3.2) to incorporate traffic behavior due to lane-changing.

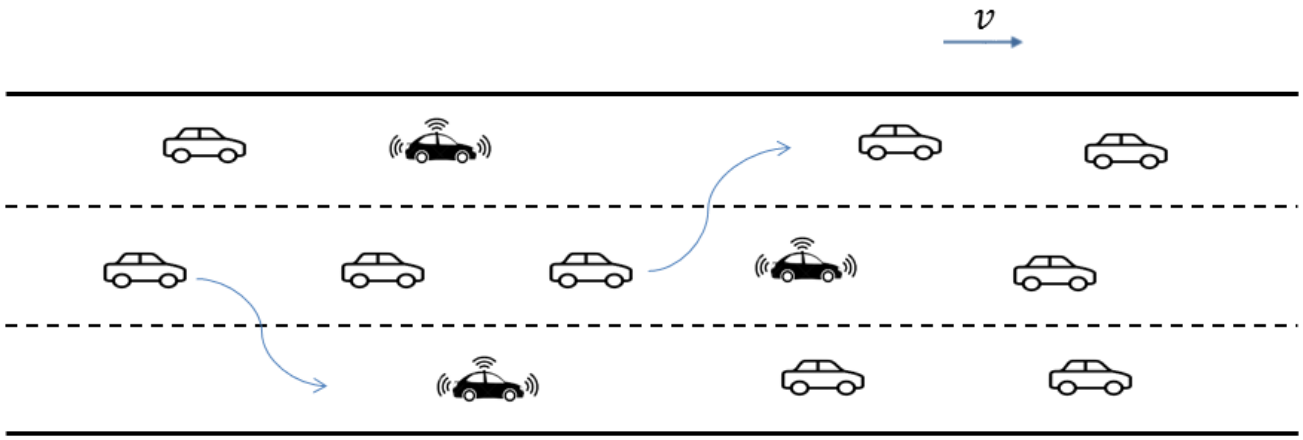

Figure 3.2: A typical illustration of lane changing.

A typical illustration of lane-changing in a heterogeneous traffic flow is presented in Figure 3.2. When there are fewer vehicles in the surrounding traffic, one is more likely to cut into a neighboring lane when it is safe

to do so. For a road with multiple lanes, the conservation equation for a single lane is given by [12]:

$$\frac{\partial \rho}{\partial t} + \frac{\partial q}{\partial x} = \Phi \tag{3.3}$$

where Φ is an inhomogeneous term representing the net lane-changing rate onto the target lane, with unit vehicle/time-distance.

Lane-changing is a microscopic driving behavior, which one may wish to fully capture with as much detailed information as possible. That is, it might be easier to describe lane-changing behavior accounting for complete traffic information, particularly density, available for all lanes. Since the PW model is employed, together with the data provided by connected vehicles, to propagate traffic states of the lane where the target vehicle is located, the explicit traffic information of other lanes is hardly available for the modeling of lane-changing. In the following, we present an alternative to modeling lane-changing behavior with limited traffic information available.

It is assumed that vehicles are more likely to change lanes to the neighboring lanes when the current location has a traffic density greater than the critical density ρ_c, whilst vehicles are more likely to join the current location from neighboring lanes when the current traffic density is smaller than ρ_c. It is possible that lane changing could occur when two neighboring lanes have densities greater (or less) than ρ_c. This is captured by the lane-changing adaptation rate introduced in the sequel. For example, when two neighboring lanes have densities larger than ρ_c, lane changing is less likely but still possible to occur due to already congested traffic. Hence, the parameter for lane-changing adaptation to be estimated will take smaller values. In other words, it is always possible for vehicles to come to and leave from a location x due to lane-changing when safe to do so. The net lane-changing rate Φ is negative at the current location when $\rho > \rho_c$, whilst it is positive when $\rho \leq \rho_c$. That is, due to lane-changing there are more vehicles likely to come to the current location than those leaving from the same site if the traffic density is relatively low, i.e., $\rho \leq \rho_c$. Hence, a unified expression of the net lane-changing rate Φ is given by:

$$\Phi = \alpha(\rho_c - \rho)v/dx \tag{3.4}$$

where dx is a sufficiently small time period for discretization in the sequel; $\alpha \geq 0$ is the lane-changing adaptation rate to be estimated.

Discretizing (3.3) in space and time with Φ given by (3.4), it follows that:

$$\frac{\rho_i(k+1) - \rho_i(k)}{dt} + \frac{\rho_i(k)v_i(k) - \rho_{i-1}(k)v_{i-1}(k)}{dx} = \frac{\alpha_i(k)}{dx}\big(\rho_c - \rho_i(k)\big)v_i(k) \tag{3.5}$$

where dx is the length of each cell after discretization; $\rho_i(k)$ and $v_i(k)$ are the density and average traffic speed of

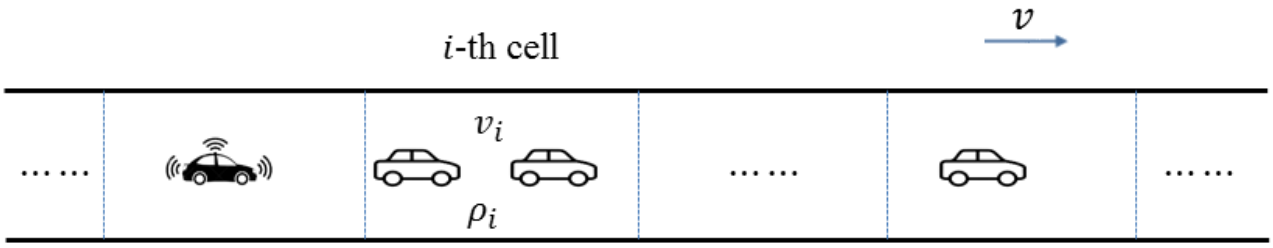

Figure 3.3: An illustration of lane discretization.

cell i at time k as illustrated in Figure 3.3; $\alpha_i(k)$ is the lane-changing adaptation rate corresponding to cell i at time k, as introduced in (3.4).

Rearranging (**??**) one can easily obtain the following difference equation describing the evolution of cell density.

$$\rho_i(k+1) = \rho_i(k) - \frac{dt}{dx}\big[\rho_i(k)v_i(k) - \rho_{i-1}(k)v_{i-1}(k)\big] + \frac{dt}{dx}\alpha_i(k)\big[\rho_c - \rho_i(k)\big]v_i(k) \tag{3.6}$$

It is assumed that vehicles leaving the current cell by lane-changing have a positive impact on the traffic speed of the cell since more space is created, while those joining the cell from other lanes have a negative impact on the traffic speed of the cell [32]. In other words, the collective impact of lane-changing on the traffic speed of a cell could be positive or negative, depending on the net lane-changing rate, i.e., inflow to or outflow from the cell. To this end, incorporating lane-changing behavior (3.2) can be rewritten as:

$$\frac{\partial v}{\partial t} + v\frac{\partial v}{\partial x} + \frac{c_0^2}{\rho}\frac{\partial \rho}{\partial x} = \frac{v_*(\rho) - v}{\tau} - \Lambda \tag{3.7}$$

where Λ denotes the impact of lane-changing on traffic acceleration and is given by:

$$\Lambda = \frac{\beta}{dx}\frac{(\rho_c - \rho)v}{\rho}v \tag{3.8}$$

where $\beta \geq 0$ is the speed adaptation parameter to be estimated. Equation (3.8) basically indicates that there will be a collectively negative impact on traffic speed due to lane-changing when traffic density is small, specifically less than the critical density ρ_c. That is, more vehicles are likely to join a cell compared to the number of vehicles leaving due to lane-changing. Discretizing (3.7) with Λ given by (3.8) one can obtain:

$$\begin{aligned}\frac{v_i(k+1) - v_i(k)}{dt} + \frac{v_i(k)[v_i(k) - v_{i-1}(k)]}{dx} + \frac{c_0^2}{dx}\frac{[\rho_i(k) - \rho_{i-1}(k)]}{\rho_i(k) + \epsilon} \\ = \frac{v_*(\rho_i(k)) - v_i(k)}{\tau} - \frac{\beta_i(k)}{dx}\frac{[\rho_c - \rho_i(k)]v_i(k)}{\rho_i(k) + \epsilon}v_i(k)\end{aligned} \tag{3.9}$$

where ϵ is a small positive number to avoid zero denominator. Rearranging (3.9) one obtains the following expression describing traffic speed evolution:

$$v_i(k+1) = v_i(k) - \frac{dt}{dx} v_i(k)[v_i(k) - v_{i-1}(k)] - \frac{dt}{dx} \frac{c_0^2[\rho_i(k) - \rho_{i-1}(k)]}{\rho_i(k) + \epsilon} + \frac{dt[v_*(\rho_i(k)) - v_i(k)]}{\tau} - \frac{dt}{dx} \frac{\beta_i(k)[\rho_c - \rho_i(k)]v_i(k)}{\rho_i(k) + \epsilon} v_i(k) \tag{3.10}$$

In case a triangular fundamental diagram is used, the equilibrium speed-density function $v_*(\cdot)$ is given by:

$$v_*(\rho_i(k)) = \begin{cases} v_0, & \rho_i(k) \leq \rho_c \\ c\big(\rho_{\text{jam}}/\rho_i(k) - 1\big), & \rho_i(k) > \rho_c \end{cases} \tag{3.11}$$

where the critical density ρ_c is given by:

$$\rho_c = \rho_{\text{jam}}/(v_0/c + 1) \tag{3.12}$$

where ρ_{jam} is jam density, and c is the slop of density drop when traffic is beyond road capacity. Based on the discretization shown above, one can readily propagate traffic flow using (3.6) and (3.10).

3.3 Traffic Prediction

The goal of traffic prediction is to predict the trajectory of the immediate preceding vehicle. In this report, the prediction horizon is defined as a distance used for traffic prediction. In general, a vehicle can only travel 300–500 meters at most in 10–15 seconds, so the prediction horizon should be longer than 500 meters but it should not be too long. If we divide the prediction horizon into M cells and propagate the aforementioned traffic flow model, then the trajectory of the preceding vehicle can be extracted from the predicted traffic states. To deal with a corridor with multiple intersections, currently, the project team has two methods. One is the fixed prediction horizon, the other is the moving prediction horizon.

Fixed prediction horizon takes inspiration from previous work [26] in which the prediction horizon remains unchanged when the target vehicle does not pass the intersection and is shown in Figure 3.4a. For a corridor with N intersections, it can be divided into $N + 1$ links by intersections. As long as the target vehicle does not pass an intersection (does not change a link), the prediction horizon remains the same. The first cell is the beginning of the current prediction horizon. Each cell has a length of dx (set as 25 m in this report) and is described by two state variables, traffic speed v_i and traffic density ρ_i. Supposing the preceding traffic signal is in Cell j, then M should be larger than j to make sure the target vehicle is able to predict the trajectory and speed of the preceding vehicle when it is approaching the intersection. As long as the target vehicle passes the intersection and enters into a new

link, the prediction horizon changes and the new prediction horizon should be divided into M' cells by a length of dx, where the first cell of the new prediction horizon is Cell $j+1$ in the old prediction horizon. Supposing the next intersection located in Cell j', then M' should be larger than j' for the same reason mentioned before. It is clear that there are some overlaps between the new prediction horizon and the old prediction horizon. To initialize the states of each cell in the new prediction horizon, the overlapped cells inherit from the old prediction horizon, while the other new cells are initialized with the same states as the last cell of the previous prediction horizon. By changing the prediction horizon when the target vehicle passes the intersection, the fixed prediction horizon method can be used to make traffic predictions in a scenario with multiple intersections.

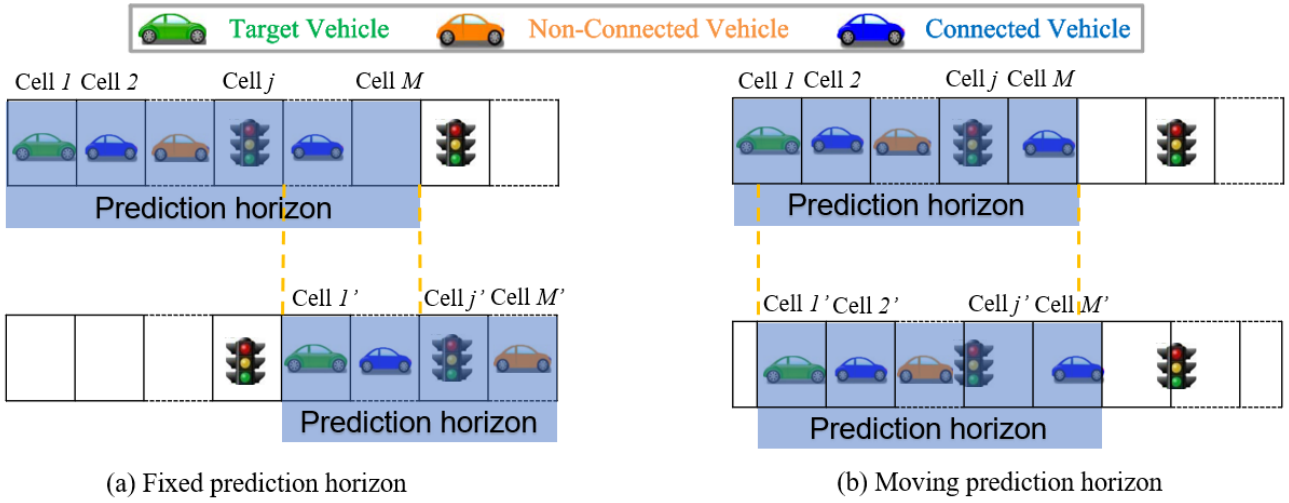

Figure 3.4: Traffic prediction horizon.

Moving prediction horizon is another method to deal with a corridor with multiple intersections, as shown in Figure 3.4b. In moving prediction horizon, the prediction horizon updates every second. For each update, the first cell is defined at the location where the target vehicle at. The length of the moving prediction horizon is a constant value. Thus, the number of the cells, M, is equal to the length of the prediction horizon divided by the length of one cell dx. As the prediction horizon updates every second and the target vehicle will not move a long distance in one second, there is a large overlap between the new and old prediction horizon. For the new cells in the overlapped segment, the states can be obtained by interpolating from the old prediction horizon. The states of other new cells, if any, can be initialized as the states of the cell M in the previous prediction horizon. Since the moving prediction horizon is defined based on the location of the target vehicle, it can be easily applied in a scenario with multiple intersections.

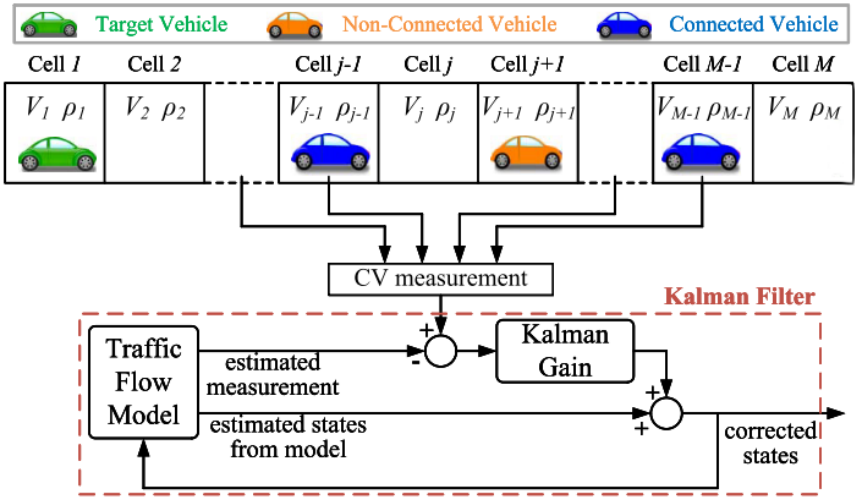

Figure 3.5: Diagram of the traffic states prediction.

For both fixed prediction horizon and moving prediction horizon, we can propagate the traffic flow model to predict the states of each cell at future time steps, as shown in Figure 3.5. It is assumed that v_j is the traffic speed at the center of the jth cell, ρ_j (veh/meter) is the density of the jth cell. The location of the CVs will not always coincide with the center of a cell. The following approximation is used to describe each preceding CV's speed as the linear interpolated speed of two cells that are adjacent to the preceding vehicle's location.

$$y_i(k) = \alpha_i(k) v_{j_{\text{adj}}+1}(k) + (1 - \alpha_i(k)) v_{j_{\text{adj}}}(k) + w_{v_i} \tag{3.13}$$

where $y_i(k)$ is the speed of the ith preceding CV; j_{adj} is the index of the last cell the preceding vehicle passed; $\alpha_i(k) = d_i/dx - j_{\text{adj}}$ is the interpolation coefficients; d_i is the location of the ith preceding CV; w_{v_i} is the Gaussian random variable to model measurement uncertainties.

As there may be non-connected vehicles on the road, only partial traffic states are 'measured' by preceding CVs. The rest unknown traffic states can be estimated by an observer. The unscented Kalman filter (UKF) [27] is used in this project since it can handle the non-smooth nonlinearities and consider modeling and measurement uncertainties. Essentially, UKF provides a systematic approach to use the partial traffic states obtained from CVs (measurement) to correct the state estimation from the traffic flow model. Detailed information can be found in [28].

3.4 Speed Control Method

The speed control method aims at minimizing the target vehicle's energy consumption, so it can be formulated as an optimization problem. Fuel efficiency can be improved at two levels [Shao and Sun]: vehicle level and powertrain level. Co-optimization of both levels offers the maximum energy saving. At the vehicle level, based on the anticipated future driving conditions mentioned above, the target vehicle can adjust its speed and following distance to operate with the most fuel efficient vehicle power demand. At the powertrain level, for the same vehicle speed and power demand, the powertrain system can be further optimized to operate in the most efficient regions. This leads to a hybrid optimal control problem as the vehicle speed is continuous and the gear position is discrete.

The following proposes a framework that can be used to formulate such problems for different CAV applications. Traffic information is the input (enabled by connectivity), and the objective is to minimize fuel consumption. The state equations depend on the vehicle and powertrain models. The constraints include physical limitations (e.g., maximum engine torque constraint), traffic constraints (e.g., a safe car-following distance), and drivability constraints (e.g., avoid engine lugging and shift busyness). Different CAV applications pose different traffic constraints. Usually, the fuel consumption model of a vehicle is nonlinear and depends on the powertrain states (engine speed and engine torque). Vehicle and powertrain models are nonlinear as well and depend on the roadway slope profile, which may be complex and have no analytical form. All these nonlinearities and the nature of the hybrid control problem bring challenges to develop a real-time implementable control.

To reduce the computational burden, optimization variables are carefully selected so that simplification techniques can be applied to formulate the original nonlinear hybrid optimal control problem as a mixed integer problem with a convex quadratic objective function and linear constraints. Simplification techniques are carefully selected to avoid sacrificing the accuracy of the vehicle and powertrain models. Then the optimization problem is solved by an efficient numerical state-of-the-art mixed-integer solver (Gurobi).

3.5 Problem Formulation

In this section, the fuel efficient vehicle speed and transmission gear position optimal control problem is formulated. The objective is to minimize fuel consumption while maintaining satisfactory drivability, mobility and driving comfort. The control inputs are vehicle acceleration (engine torque), vehicle braking force, and gear position (discrete). The state equations depend on the vehicle and powertrain models. The constraints include physical limitations (e.g., maximum engine torque constraint), traffic constraints (maintain a safe car-following distance and pass the intersection only when the signal is green), and drivability constraints (avoid engine lugging and shift busyness).

3.5.1 State equation

A point mass vehicle model is used. Denote state vector as $\boldsymbol{x}$, target vehicle's location, speed, and acceleration as d, v, a, then:

$$\dot{\boldsymbol{x}}(t) = \begin{bmatrix} \dot{d}(t) \\ \\ \dot{v}(t) \end{bmatrix} = \begin{bmatrix} v(t) \\ \\ a(t) \end{bmatrix} \tag{3.14}$$

3.5.2 Vehicle and powertrain models

The vehicle and powertrain models are:

$$\omega_e(t) = n(t) \cdot v(t), \quad n(t) = r_t(t) r_f(t) / r_r \tag{3.15}$$

$$T_e(t) \cdot n(t) = \underbrace{f_\varphi(t) + C_{\text{wind}} \cdot v^2(t) + m \cdot a(t)}_{F_r} + F_b(t) \tag{3.16a}$$

$$\text{and} \qquad f_\varphi(t) = \mu m g \cdot cos[\varphi(d(t))] + mg \cdot sin[\varphi(d(t))] \tag{3.16b}$$

where n is the lumped gear ratio (discrete); ω_e is the engine speed; r_t is the transmission gear ratio (discrete); r_f is the final drive ratio; r_r is the wheel radius; f_φ is the sum of rolling and grade resistance; φ is the roadway slope angle, which is a function of the target vehicle's location d; μ is the rolling friction constant; m is the vehicle mass; g is the gravitational constant; $C_{\text{wind}} = 0.5 C_d \rho_a A$ is the wind resistance constant; C_d is the drag coefficient; ρ_a is the density of air; A is the vehicle frontal area; F_b is the vehicle braking force.

3.5.3 Objective function

The objective function is defined as:

$$J = \underbrace{\phi(\boldsymbol{x}(t_f))}_{J_{\text{final}}} + \int_{t_0}^{t_f} [\underbrace{\dot{m}_f(t)}_{J_{\text{fuel}}} + \underbrace{w_1 \cdot a^2(t)}_{J_{\text{comfort}}}] \, dt \tag{3.17a}$$

$$\phi(\boldsymbol{x}(t_f)) = \psi_1 \cdot (d(t_f) - d_f)^2 + \psi_2 \cdot (v(t_f) - v_f)^2 \tag{3.17b}$$

where, $\dot{m}_f(t)$ is the fuel consumption rate model; J_{fuel} penalizes the fuel consumption; J_{comfort} ensures ride comfort with positive weight factor w_1; ψ_1,ψ_2 are large positive numbers to penalize the vehicle's final states; d_f, v_f are desired final location and speed of the target vehicle. Final states are penalized to ensure the target vehicle and the preceding vehicle (baseline vehicle) will travel the same distance in same time and reach the same final speed

for a fair comparison.

$$\dot{m}_f(t) = p_{00} + p_{01} \cdot \omega_e(t) + p_{11} \cdot P_e(t) \tag{3.18a}$$

$$P_e(t) = \omega_e(t) \cdot T_e(t) \tag{3.18b}$$

where p_{00}, p_{01}, and p_{11} are coefficients of the fitted polynomial. The order of the polynomial is selected to ensure both low computational burden and high accuracy. P_e is the power of the engine.

3.5.4 Constraints

Some constraints should be satisfied when solving the optimization problem.

3.5.4.1 Physical constraints

3.5.4.1.1 Engine torque dynamics constraint

To account for the engine torque dynamics, the torque change rate is constrained:

$$-\Delta T_{e_{\max}} \leq \dot{T}_e(k) \leq \Delta T_{e_{\max}} \tag{3.19}$$

3.5.4.1.2 Physical bounds

The vehicle speed and engine torque cannot be less than the idling speed $\omega_{e_{\text{idle}}}$ and idling torque $T_{e_{\text{idle}}}$, and the engine speed cannot be higher than the maximum engine speed $\omega_{e_{\text{ub}}}$. The vehicle speed is positive and the acceleration is bounded:

$$\omega_{e_{\text{idle}}} \leq \omega_e(t) \leq \omega_{e_{\text{ub}}}, T_{e_{\text{idle}}} \leq T_e(t) \tag{3.20a}$$

$$0 \leq v(t), \quad a_{\min} \leq a(t) \leq a_{\max} \tag{3.20b}$$

3.5.4.2 Traffic constraints

The traffic constraints depend on the specific CAV application such as whether there is a nearby preceding vehicle or a signalized intersection.

3.5.4.2.1 Car-following distance constraint

Because the target vehicle is following a preceding vehicle, the car-following distance constraint should be satisfied:

$$d_{\min} + h_{\min} \cdot v(t) + \beta \cdot \sigma[d_p(t)] \leq d_p(t) - d(t) \leq d_{\max} - \beta \cdot \sigma[d_p(t)] \tag{3.21}$$

where d_p is the estimated location of the immediate preceding vehicle; $d_p - d$ is the following distance; $d_{\max}$ is the upper bound to ensure a satisfactory and realistic traffic throughput; $h_{\min}$ is the time headway in seconds; $d_{\min}$ is the minimum following distance when the target vehicle has 0 speed; To improve the robustness of the control, the uncertainties coming from the prediction of preceding vehicle's location d_p are considered. $\sigma[d_p(t)]$ is the standard deviation of the estimated immediate preceding vehicle's location, and β determines the confidence level and is selected to be 1 in this report.

Moreover, uncertainties in the prediction can result in an actual car-following distance that is near the constraints or even violates the constraints. This brings in challenges to exactly satisfy the constraints at all time. In this case, 'soft constraints' are adopted in the car following constraints, which allow violation of the constraints with additional slack variables s_1, s_2:

$$d(t) \geq d_p(t) + \beta \cdot \sigma[d_p(t)] - d_{\max} - s_1(t) \tag{3.22}$$

$$d(t) \leq d_p(t) - \beta \cdot \sigma[d_p(t)] - (d_{\min} + h_{\min} \cdot v(t)) + s_2(t) \tag{3.23}$$

$$s_1(t) \leq 0, \quad s_2(t) \leq 0 \tag{3.24}$$

In the objective function, additional terms are added to penalize the sum of violations at each time step:

$$J = \phi(\boldsymbol{x}(t_f)) + \int_{t_0}^{t_f} [\dot{m}_f(t) + w_1 \cdot a^2(t) + w_2 \cdot s_1^2(t) + w_3 \cdot s_2^2(t)]\, dt \tag{3.25}$$

where w_2, w_3 are two positive weighing factors.

3.5.4.2.2 Signal constraint

The target vehicle can pass the intersection only when the signal is green:

$$d(t_r) \leq d_{\text{sig}}, \quad d(t_g) \geq d_{\text{sig}} \tag{3.26}$$

where t_r and t_g are the time instances of the beginning of 'next' red light and green light; d_{sig} is the location of the intersection.

3.5.4.3 Drivability constraints

The following constraints are enforced to ensure a satisfactory drivability performance:

$$T_e(t) + T_{\text{rsrv}}(t) \leq T_{e_{\max}}(\omega_e(t)) \tag{3.27}$$

where $T_{e_{\max}}$ describes the maximum torque line and is a nonlinear function of engine speed, which can be approximated using piecewise linear functions; T_{rsrv} is the torque reserved.

$$T_e(t) + T_{\text{rsrv}}(t) \leq \max_{i=1,2,3} \{k_{Te}^i \cdot \omega_e(t) + b_{Te}^i\}, \tag{3.28}$$

Moreover, the minimum time duration between two gear shifts should be constrained:

$$n(t + t_i) = n(t), \quad \forall t_i \in [0, t_g), \quad \forall t \in \{t_0, t_0 + t_g, t_0 + 2t_g, ...\} \tag{3.29}$$

where, t_0 is the first time when the gear shift can happen, and t_g forces that the gear shift can only occur every t_g seconds.

3.5.4.4 Initial and final conditions

At each update instance, the initial vehicle location, speed, and gear position are known:

$$d(t_0) = d_0, \quad v(t_0) = v_0, \quad g(t_0) = g_0 \tag{3.30}$$

The final location and speed of the target vehicle are bounded to the neighborhood of the predicted final location and speed of the preceding vehicle for a fair comparison:

$$d_p(t_f) - \delta_d \leq d(t_f) \leq d_p(t_f) + \delta_d \tag{3.31}$$

$$v_p(t_f) - \delta_v \leq v(t_f) \leq v_p(t_f) + \delta_v \tag{3.32}$$

To reduce the computational burden and not to sacrifice the accuracy of the control, simplifications are made with carefully selected optimization variables using the Big-M technique [Bemporad and Morari] and McCormick relaxation method [13]. Moreover, the problem is discretized using the pseudo-spectral method [22] which can generally give better accuracy with low computational burden compared with Euler or Runge-Kutta methods. The optimization problem can be summarized as:

$$\min_{v,a,n} J = \phi(\boldsymbol{x}(N_{\text{PH}})) + \sum_{k=1}^{N_{\text{PH}}} [\dot{m}_f(k) + w_1 \cdot a^2(k) + w_2 \cdot s_1^2(k) + w_3 \cdot s_2^2(k)] \tag{3.33}$$

$$
\begin{aligned}
\text{s.t.} \quad & d(k+1) = d(k) + v(k) \cdot dt && \text{(3.34a)}\\
& v(k+1) = v(k) + a(k) \cdot dt && \text{(3.34b)}\\
& \omega_e(k) + (1 - g_i(k)) \cdot (n_i \cdot v_{\max}) \geq n_i v(k) && \text{(3.34c)}\\
& \omega_e(k) + (1 - g_i(k)) \cdot (-\omega_{e_{\text{ub}}}) \leq n_i v(k) && \text{(3.34d)}\\
& T_e(k) \cdot n_i + (1 - g_i(k)) \cdot (F_{r_{\max}} + F_{b_{\max}}) \geq F_r(k) + F_b(k) && \text{(3.34e)}\\
& T_e(k) \cdot n_i + (1 - g_i(k)) \cdot (F_{r_{\min}} + F_{b_{\min}} - T_{e_{\max}} n_i) \leq F_r(k) + F_b(k) && \text{(3.34f)}\\
& T_{e_{\text{idle}}} \omega_e(k) + \omega_{e_{\text{idle}}} T_e(k) - \omega_{e_{\text{idle}}} \cdot T_{e_{\text{idle}}} \leq P_e(k) && \text{(3.34g)}\\
& T_{e_{\text{ub}}} \omega_e(k) + \omega_{e_{\text{ub}}} T_e(k) - \omega_{e_{\text{ub}}} \cdot T_{e_{\text{ub}}} \leq P_e(k) && \text{(3.34h)}\\
& (3.19)\text{–}(3.24), \text{and} (3.26)\text{–}(3.32)
\end{aligned}
$$

where (3.34a)–(3.34b) are the discrete form of the state equation (3.14). The powertrain model (3.15) is converted to (3.34c)–(3.34d) by the Big-M technique. Similarly, the vehicle model (3.16a) is converted to (3.34e)–(3.34f). d_g is the number of gear ratios of the vehicle transmission. When the gear i is engaged, $g_i(k) = 1$, otherwise, $g_i(k) = 0$. n_i is the gear ratio of the ith gear. The non-convex equation (3.18b) is transformed to (3.34g)–(3.34h) by the McCormick relaxation.

Then the optimization problem is solved under all constraints using an efficient nonlinear programming solver (Gurobi) [25].

3.6 Simulation Results

A preliminary result is shown in this section using the proposed traffic prediction method and speed control method, but all simulation results do not consider lane changing behaviors. In other words, the $\alpha_i(k)$ in (3.6) and $\beta_i(k)$ in (3.10) are set as 0 when propagating the traffic flow model. Currently, the project team has four DSRC receivers, so a maximum of four vehicles' trajectories and SPaT data can be recorded at the same time when driving on the TH-55.

3.6.1 Traffic scenarios

The preliminary result focuses on a segment of TH-55 consisting of four intersections, as shown in Figure 3.6. The four 'CAVs' are driven from the West to the East (left to right in the figure).

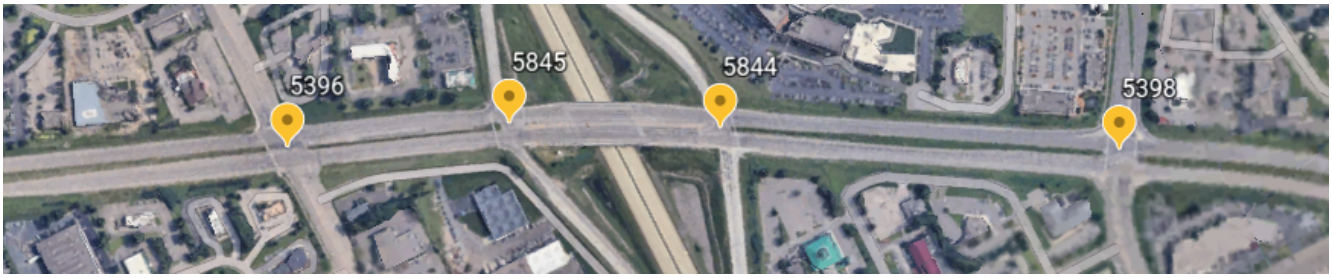

Figure 3.6: A segment of TH-55 consisting 4 intersections.

Figure 3.7 shows the location and speed of the four vehicles. The four vehicles passed intersection 5396 and intersection 5398 with a green signal but stopped at intersection 5845 and intersection 5844 because of the red light. It is assumed that the target vehicle follows the last vehicle in the platoon and all of the four vehicles are considered as CVs that can broadcast their location and speed information to the target vehicle.

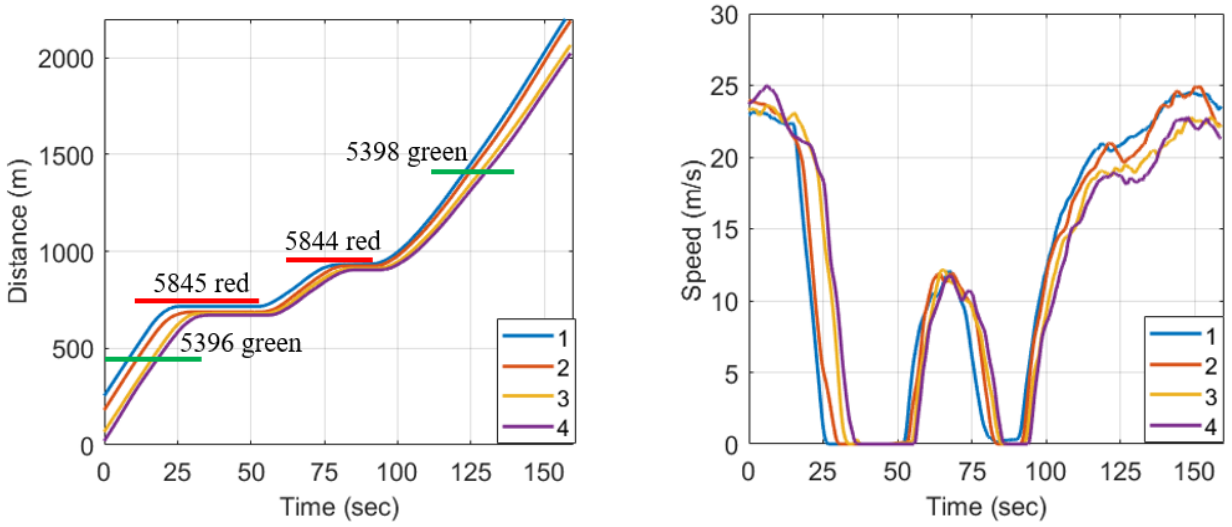

(a) Location of four vehicles

(b) Speed of four vehicles

Figure 3.7: Traffic scenario

3.6.2 Results of traffic prediction

In the prior framework, the traffic prediction horizon is invariant with only one intersection taken into account [26]. In practice, the target vehicle is likely to pass multiple intersections before reaching its final destination. Hence, it is necessary to generalize the existing framework to incorporate a number of intersections. As mentioned before, there are two approaches possible for traffic prediction in the presence of multiple intersections. The first approach uses a fixed prediction horizon for each link (i.e., a road segment), whereas the other one employs a moving prediction horizon. In what follows, a detailed comparison of these two approaches for traffic prediction is presented.

The simulation results of traffic prediction are shown in Figure 3.8, where the traffic prediction is updated every 1 second. The blue curve represents speed of the preceding vehicle, whilst the red curves denote the speed prediction of the first 5 seconds at each updating instance.

The root-mean-square error (RMSE) of the speed prediction is used to represent its accuracy. The RMSE is defined as:

$$RMSE = \sqrt{\frac{1}{m}\sum_{k=1}^{m}(v_p(k) - \hat{v}_p(k))^2} \tag{3.35}$$

where m is the number of time steps; $v_p(k)$ and $\hat{v}_p(k)$ are the actual speed and its prediction of the preceding vehicle at time step k, respectively.

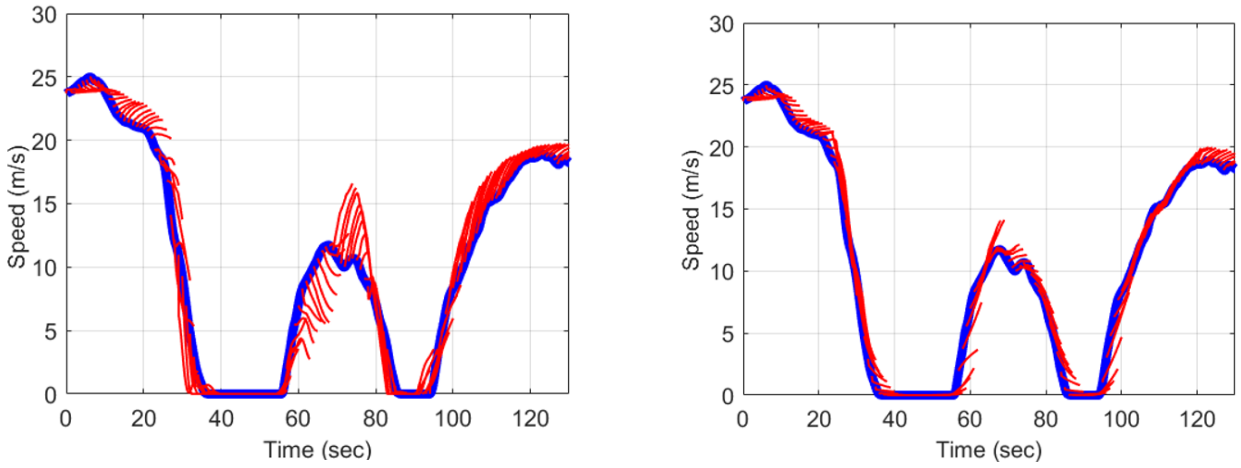

(a) Fixed prediction horizon

(b) Moving prediction horizon

Figure 3.8: Traffic prediction

For the first 5 seconds, the RMSE using the fixed prediction horizon is 1.7472 m/s, while it is 1.0483 m/s using the moving prediction horizon. Figure 3.9 shows the five-second RMSE at each prediction update. The moving prediction horizon performs better for a short-time prediction since it is challenging for the fixed prediction horizon to achieve an accurate prediction when changing links (e.g., passing an intersection), especially when two intersections are closely located. For example,comparing to the moving prediction horizon, the fixed prediction horizon performs worse during 60–80 s. It is observed from Figure 3.8a that the predicted speed of the preceding vehicle decreases while its actual speed increases during 60–70 s, whereas the predicted speed increases while the actual speed decreases during 70–80 s. In practice, the vehicle passes the intersection 5845 until after 70 s. The next intersection (i.e., intersection 5844) is located only 240 m away from the intersection 5845. Due to close proximity of these two intersections, when traffic signal is green at the intersection 5845 while the vehicle has not passed

it, it is predicted that the vehicle will approach the intersection with a low speed. The vehicle will accelerate as soon as passing the intersection. Once the vehicle passes the intersection, the prediction horizon changes in the way as mentioned before. The states of the first few cells in the new prediction horizon are inherited from the previous prediction horizon. Thus, the predicted speed increases after 70 s, but the actual speed decreases due to red traffic signal at the intersection 5844. As time goes by, the UKF estimates more accurate states of each cell. As a result, the prediction results appear to be more reasonable. For the moving prediction horizon, as shown in Figure 3.9b, the RMSE is higher when the vehicle is going to pass an intersection (i.e., 50–60 s and 90–100 s) after a red signal. More studies can be done in the future to model the start-stop traffic wave and improve the prediction accuracy. Overall, the moving prediction horizon has a better prediction accuracy for the five-second prediction as the prediction horizon will not change dramatically when changing links.

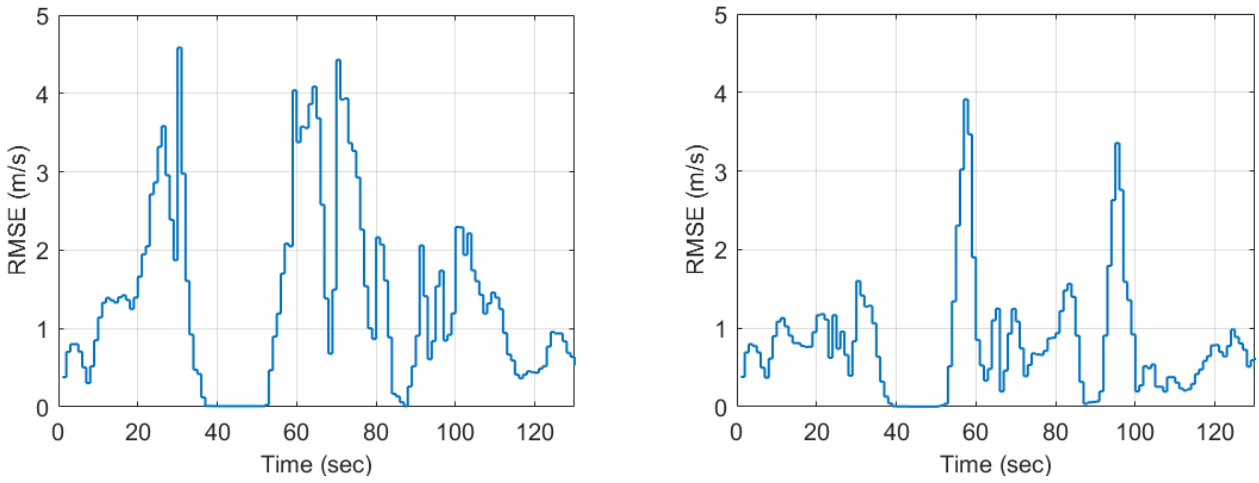

(a) Fixed prediction horizon

(b) Moving prediction horizon

Figure 3.9: Five-second RMSE at each prediction update

For the 15 seconds, the RMSE using fixed prediction horizon is 3.0068 m/s, whereas it is 3.1292 m/s using moving prediction horizon. The RSMEs for these two approaches appear to be close, which might be due to the challenge of predicting the speed of the preceding vehicle for the next 15 seconds.

Since the dynamics of real-world traffic are highly non-linear, more detailed studies will be conducted in the future to investigate the nonlinear nature of the traffic and to improve the prediction accuracy. Moreover, it is worth mentioning that, although these two approaches reach a similar result for the next fifteen-second prediction, the moving prediction horizon has less computational burden because the length of the fixed prediction depends on the distance between two intersections which is always longer than the length of the moving prediction horizon.

3.6.3 Optimization results

Figure 3.10 shows the simulated results of car-following distance, vehicle speed, gear position, and energy consumption. The moving prediction horizon is used for traffic prediction in this part. The initial following distance is set as 20 m. The maximum following distance is set as 40 m, and the minimum following distance changes with the preceding vehicle speed according to (3.22). With collision avoidance control, the target vehicle will decelerate when the following distance becomes critically small.

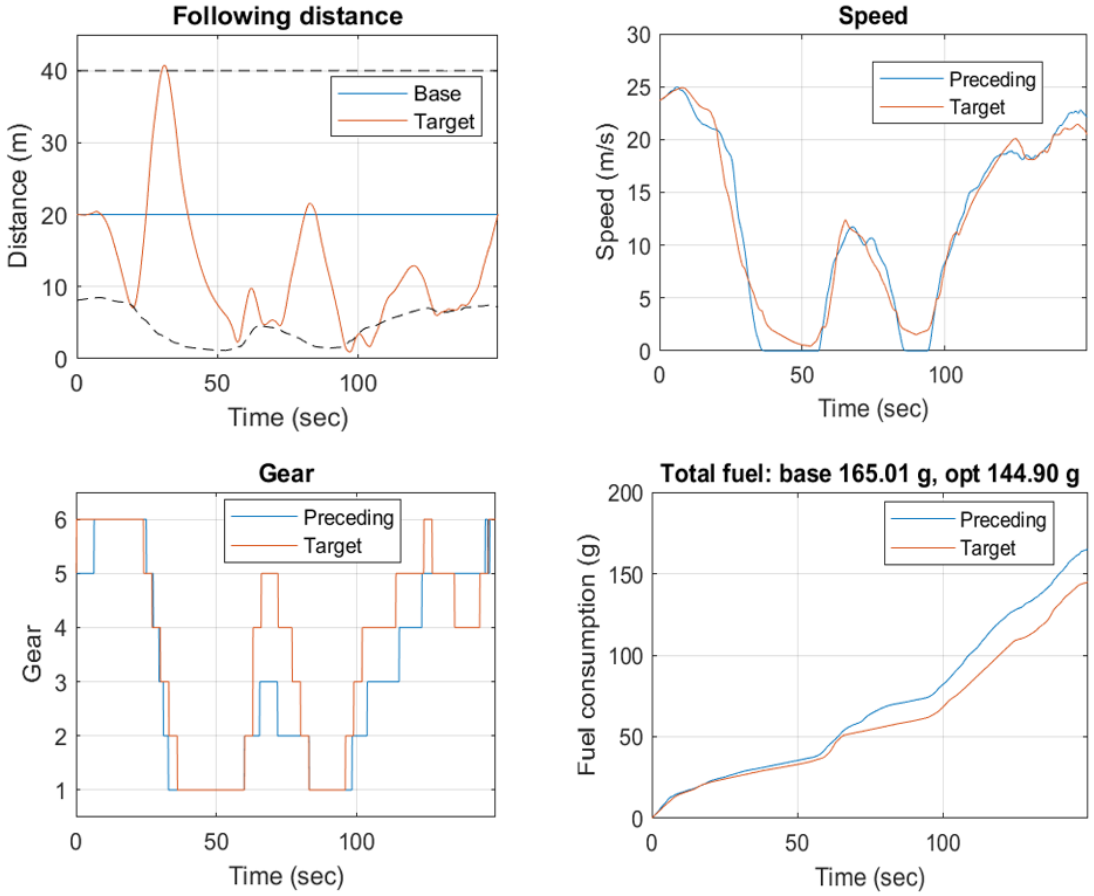

Figure 3.10: Optimization result.

With co-optimization of vehicle speed and gear position, the target vehicle achieves 12.19% benefits on fuel consumption. On the one hand, the energy benefits come from less deceleration when approaching the intersections when the signal is red, and smoother acceleration when leaving intersections. Taking actions of the target vehicle during 35 s to 55 s for example, it knows the signal is red when it is approaching the intersection and knows when the signal will change to green. Thus, the following distance reaches the maximum as the target vehicle avoids stops by decelerating earlier, and reaches the minimum when the signal light changes to green and the preceding vehicle starts to accelerate. In the process of passing the intersection, the target does not stop, which reduces the

amount of braking and avoids idling waste. On the other hand, some energy benefits come from the optimization of gear position. With the optimal gear position, the internal combustion engine can work in more efficient regions with the same vehicle speed.

3.7 Summary

This report shows the technical details of the traffic prediction and speed control method. The traffic prediction is based on the second order traffic flow model and can be applied to mixed-traffic scenarios where both connected and non-connected vehicles are on the road. The moving prediction horizon makes it easy and reasonable to deal with the road with multiple intersections and leads to less computational burden compared with the fixed prediction horizon. Real-time information from connected vehicles and signal lights provides a 'partial' measurement of the traffic states. The unknown traffic states are estimated using an observer (Unscented Kalman Filter). The traffic prediction works as an input into the speed control problem, and the optimal speed control can be obtained by solving a formulated optimization problem. The optimization variables are carefully selected and appropriate simplification is applied to formulate the problem to reduce its computational burden so that the proposed method has the potential to be applied in real-time. The preliminary results show that, for a segment of road with 4 intersections, the fuel benefits can be 12.19%. In the future, the proposed speed control method will be implemented on the corridor with 22 intersections, and the project team will work on further improving the accuracy of traffic prediction and reducing the computational burden.

Chapter 4

Task 4: Living lab experiments and analysis of speed control benefits

August 31 2021

Description: Using the data collected on TH-55 and a hardware-in-the-loop testbed, we evaluate the fuel consumption benefits of the vehicle speed control with SPaT signal.

4.1 Introduction

Transportation energy consumption is a significant part of the national energy usage. Recently with the emerging V2V and V2I technologies, it becomes clear that connected and autonomous vehicles can help to reduce energy consumption for transportation.

To achieve this objective, a co-optimization strategy of vehicle speed and gear position was proposed by our research team to realize the fuel consumption saving [26]. The key idea of this method is that the target connected vehicle (CV) can collect the real-time location speed information of other CVs and the signal phase and timing (SPaT) information by communication, which makes it possible for the target CV to predict the future traffic condition for the next 10-15 seconds by implementing the traffic flow model. By acquiring that critical information and exploiting optimization technique, the target CV can plan its speed when approaching the intersections to avoid sharp acceleration/deceleration, to reduce the amount of braking, and to prevent unnecessary idling, leading to the significant energy saving. Meanwhile, the optimization of the gear position will force the internal combustion engine to operate in a more efficient region with the same vehicle speed and less fuel.

In the report of Task 3, the detailed co-optimization strategy was presented, including the traffic flow model, the traffic prediction, speed control method, and optimal control problem formulation. In section 6, one can find that the co-optimization method was validated by a numerical simulation. The four 'CVs' formed a platoon, which was driven from the West to the East on a segment of TH-55 including four intersections. From the simulation results, one can find that the target vehicle can achieve 12.19% benefits on fuel consumption by exploiting the co-optimization technique, which can verify that the proposed technique was effective and efficient.

In this task, a hardware-in-the-loop (HIL) testbed is used to experimentally evaluate the performance of the target vehicle. HIL testbed allows a virtual target vehicle to interact with traffic while maintaining the fidelity of the fuel measurement with laboratory instruments. A laboratory powertrain research platform is employed to represent the virtual target vehicle, including an actual engine, an engine loading device (hydrostatic dynamometer), and vehicle dynamic models. The main advantage, with the actual engine, the target vehicle simulated by the powertrain research platform can accurately represent the dynamics of the target vehicle without safety concerns.

In this report, the profiles of three different target vehicles will be implemented in the HIL testbed, named 'base one', 'opt one', and 'opt two'. The base one is the traditional vehicle with fixed distance (20m) to the preceding vehicle. The opt one is the connected and autonomous vehicle driven by the proposed co-optimization technique. The opt two is a traditional vehicle controlled by an intelligent driver model (IDM) following the opt one. The objective of the testbed experiment would like to evaluate: 1). Fuel consumption benefit of opt one vs base one. 2). Fuel consumption benefit of opt two vs base one.

4.2 HIL testbed configuration

4.2.1 Overview

Figure 4.1 shows the overall architecture of the HIL testbed. The blocks in blue indicate actual hardware, such as the actual engine, hydrostatic dyno, and all components of the living lab (i.e., actual testing vehicles, signal cabinet, RSU); the blocks in orange color indicate software including all controllers, and vehicle models. The engine is controlled using a three-level control architecture similar to [Wang and Sun]. With

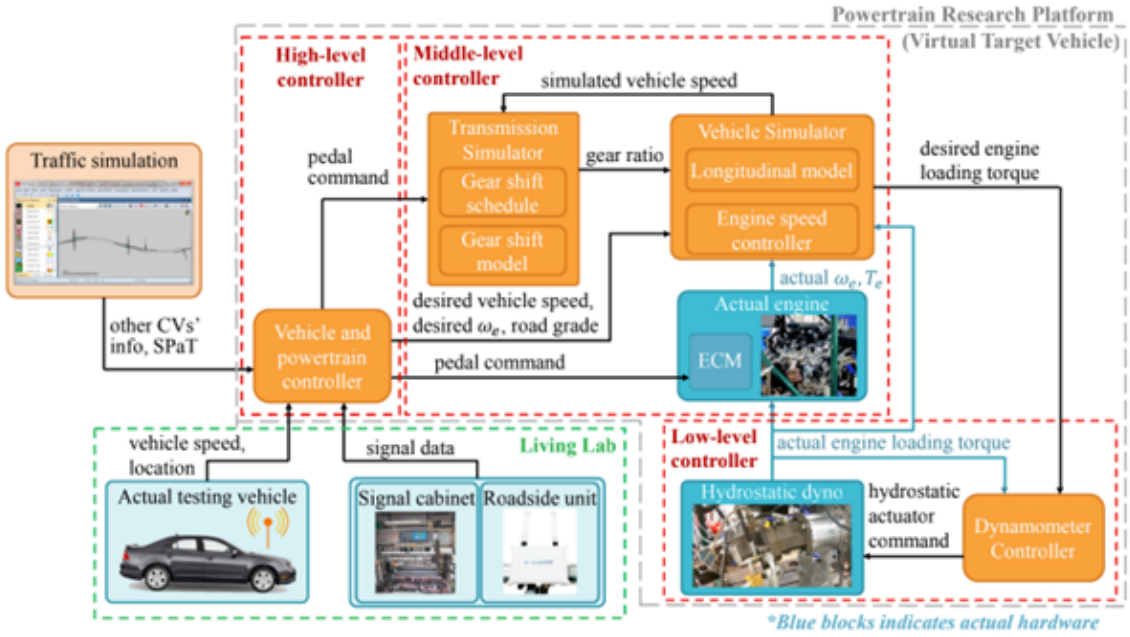

Figure 4.1: Overall Architecture of the HIL Testbed

4.2.1.1 High-Level Controller

The high-level controller receives the same traffic conditions as the target vehicle (speed limit, preceding vehicle's speed and location, etc.), and commands the same vehicle trajectories (vehicle's location, speed, acceleration, etc.), and powertrain states (engine speed, engine torque, etc.) as the target vehicle. To match the performance of an actual vehicle the same roadway conditions are input to this controller, and the controller commands the same vehicle trajectories and powertrain states as the actual vehicle. For an energy focused CAV application, this controller is essentially an optimization algorithm for fuel improvement.

4.2.1.2 Middle-Level Controller

The middle-level controller includes the transmission model (powertrain model) and the vehicle model. To match the performance of an actual testing vehicle, these models were carefully calibrated using actual vehicle data generated

from a FHWA research project [J.Ma and J.Hu] [16] The transmission model contains a shift schedule and a gear shift model. The shift schedule determines the current gear ratio between the engine speed and the vehicle wheel speed and was obtained using actual vehicle testing data. The gear shift model describes the dynamics of the gear shifting process. The vehicle model has a vehicle longitudinal model and an engine controller. The longitudinal model simulates the vehicle dynamics and outputs the simulated vehicle longitudinal speed. The engine controller determines the desired engine loading torque based on the longitudinal dynamics, desired and actual engine speed.

4.2.1.3 Low-Level Controller

The low-level controller receives the desired engine loading torque command from the middle-level controller, and it controls the hydrostatic dynamometer to provide that loading torque to the actual engine. A feedback linearization controller [Y. Wang, Z. Sun and K.A. Stelson] is used to achieve precise loading torque tracking.

In the following sections, each element of the HIL testbed will be described in detail.

4.2.2 Engine

The engine for a 2013 Cadillac SRX was installed, which is a General Motors (GM) LFX 3.6L V6 engine. A transient hydrostatic dynamometer was used to motor or load the engine [Y. Wang, Z. Sun and K.A. Stelson]. Figure 4.2 shows the overview of the powertrain research platform after all configurations. All necessary mechanical and electronic components of the engine were installed, including the engine control module (ECM), harness cables and relay fuse box. The stock ECM software is used to operate the engine. Therefore, the engine control strategies (e.g., spark timing, fuel injection timing) remain the same as in an actual vehicle. The desired engine operating points (engine speed and engine torque) are determined by the high-level controller (as in Figure 4.1) and commanded using two control signals sent from the real-time controller. These two control signals mimic the output signals from an actual accelerator pedal (driver's command). The ECM receives these signals and then commands the engine throttle opening to change the engine output power.

The real-time engine speed and torque are measured by a high precision Hottinger Baldwin Messtechnik GmbH (HBM) T12 torque/speed transducer. It was installed between the engine crankshaft and the engine loading pump/motor shaft. Both the engine and the loading pump/motor were mounted through customized engine mount, casing and adapters. The same air intake manifold as an actual vehicle is used, while the engine cooling system was redesigned with customized coolant tank and radiator. The outlets of the catalytic converters were connected to the building exhaust through customized pipes as well. Necessary connecting hoses were installed to connect the precise fuel consumption and emission measurement systems to the engine. The fuel measurement system is a P402 from AVL with measurement uncertainty of 0.1% and output frequency of up to 80 kHz.

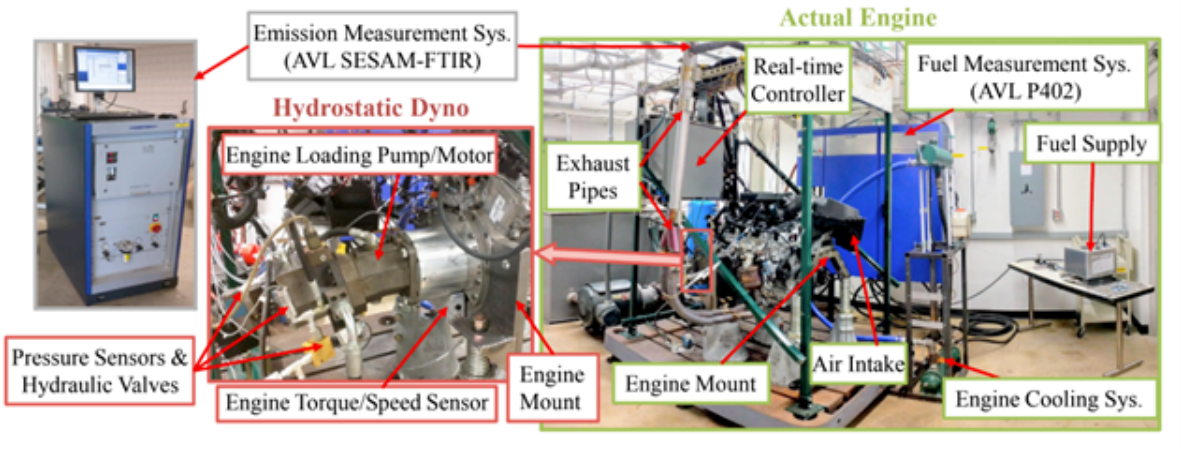

Figure 4.2: Overview of the powertrain research platform

4.2.3 Engine Maps Developement

Engine maps are necessary for developing the three-level controller of the HIL testbed and for calibrating vehicle and powertrain models. In total, three steady-state engine maps were obtained in the lab:

4.2.3.1 Engine Speed, Throttle, and Engine Torque Map

Both the engine speed and throttle trajectories were recorded from actual vehicle, but the engine torque was not measured due to the lack of a torque sensor on the actual vehicle. With this engine map, the corresponding engine torque can be obtained which is important for both the transmission model calibration and the vehicle model calibration.

4.2.3.2 Engine Speed, Throttle, and Accelerator Pedal Map

The throttle is commanded indirectly by sending the accelerator pedal signals to the ECM. With this engine map, the correct pedal command can be determined given recorded engine speed and throttle commands from the actual vehicle.

4.2.3.3 Engine Speed, Throttle and Fuel Consumption Map

This engine map is crucial for developing the fuel consumption model of the target vehicle. This model is necessary for designing optimization algorithms in a CAV application. In addition, it could be used as a benchmark to validate the engine maps obtained on the HIL testbed by comparing the calculated fuel consumption from the engine map against the measured fuel consumption from the actual vehicle.

To develop these engine maps, the engine was controlled to run through different steady state operating points and the corresponding data was measured and recorded. The following procedures were adopted: First, the

testing points were determined for both the engine speed and throttle based on their operating ranges from actual vehicle tests. The engine speed was gridded every 100 revolutions per minute (RPM) step and the throttle was gridded every 1%. In certain regions where the engine torque is sensitive to the throttle changes, additional throttle grids were tested for every 0.5%. Second, the HIL testbed was controlled to hold both the engine speed and torque at steady state for each testing point. The corresponding data (engine speed, engine torque, pedal and throttle position, and fuel consumption) were measured and recorded. Each set point was held for at least 30 s to ensure the engine has reached steady state. Finally, all recorded data were processed to develop the engine maps. The outliers were excluded, and the measurements were averaged. Figure. 4.3 shows the three engine maps obtained through the above HIL experiments.

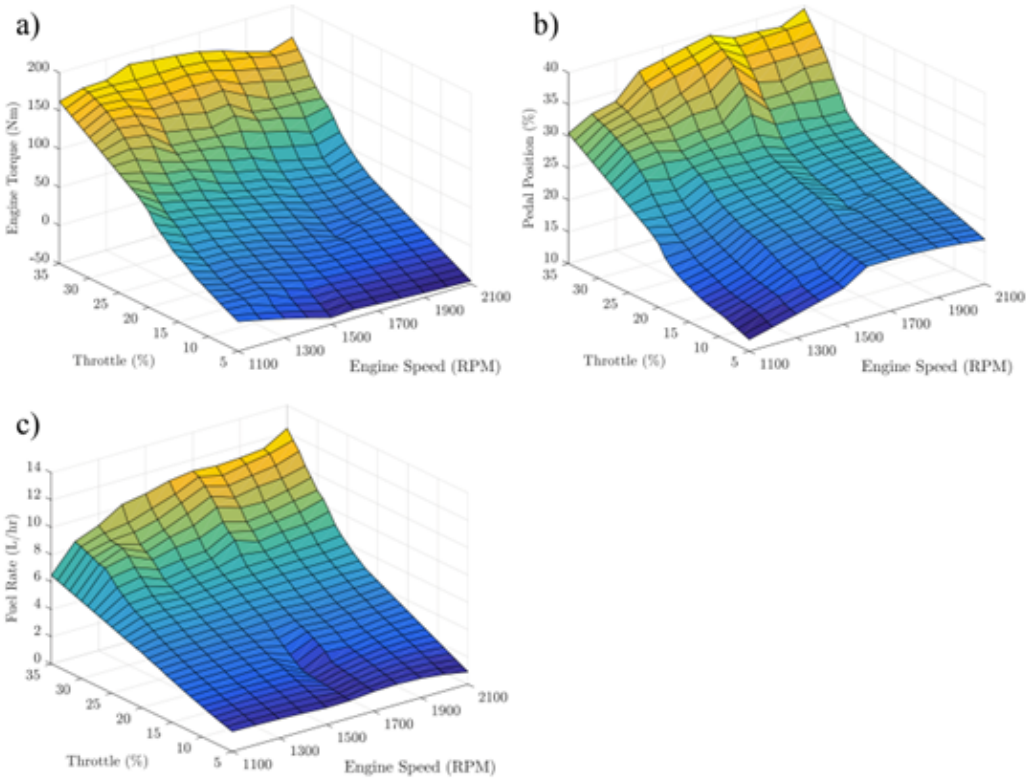

Figure 4.3: Engine Map: a) Engine Speed, Throttle, and Engine Torque Map; b) Engine Speed, Throttle, and Accelerator Pedal Map; c) Engine Speed, Throttle and Fuel Consumption Map

4.2.4 Transmission Model Development

An automatic transmission utilizes a shift schedule to determine the desired gear position and electronically control the gear ratio between the engine output shaft and the vehicle wheels. The shift schedule usually depends on the current vehicle speed and engine throttle position and it is determined by the car manufacturer through extensive calibrations to achieve objectives such as ride comfort, drivability and fuel economy. To match the performance of an actual vehicle, it is ideal to use the same shift schedule in the transmission model. However, this shift schedule

is not readily available. Therefore, the shift schedule is determined empirically using actual vehicle's data from a FHWA project [J.Ma and J.Hu] [16]. The result is shown in Figure 4.4. During the actual vehicle tests, all the vehicle speed, throttle position and gear position data were recorded. These data were used to determine a shift schedule. Essentially, it is to determine multiple curves of vehicle speed and throttle position relationships. The gear position changes when the operating points of vehicle speed and throttle position cross one of these curves. The first step was to extract actual vehicle data points whenever a gear-shift event occurs (i.e., the gear position changes). Next, curves of the shift schedule were obtained as piecewise linear curves that fit the extracted gear-shift event data points with the minimum error. Figure 4.5 a-1 and 4.5 b-1 shows the calibration results for two actual vehicle test scenarios. The blue lines indicate gear positions obtained from the shift schedule. The recorded vehicle speed and throttle position data were sent to the shift schedule to find the gear positions. The red dashed lines indicate gear positions recorded from the actual vehicle. It can be seen that the two gear positions match well which verified the shift schedule.

In addition, parameters of the following powertrain model were determined:

$$\omega_e(t) = \frac{R_{fd} GearRatio(t)}{R_{tire}} \cdot v(t) \tag{4.1}$$

where ω_e is the engine speed (rad/s); GearRatio is the transmission gear ratio; R_{fd} is the final drive ratio; R_{tire} is the wheel tire radius (m); v is the vehicle speed (m/s). The values of all transmission gear ratios (six for the six-speed transmission) and final drive ratio were obtained from the brochure. The tire radius was calibrated since the actual tire radius can be slightly different from the brochure due to the deformation of the tire. The same actual vehicle data from FHWA were used. The inputs are vehicle speed and actual gear ratio, the output is the calculated engine speed from the powertrain model Equation (4.1). The tire radius was determined to be the one that gives the minimum error between the calculated engine speed and the engine speed recorded from the actual vehicle. Calibration results from two actual vehicle testing scenarios are shown in Figure 4.5 a-2 and b-2. The blue lines indicate engine speeds calculated from the powertrain model and the red lines indicate engine speeds recorded from the actual vehicle. It can be seen that the two engine speeds match well which verifies the powertrain model.

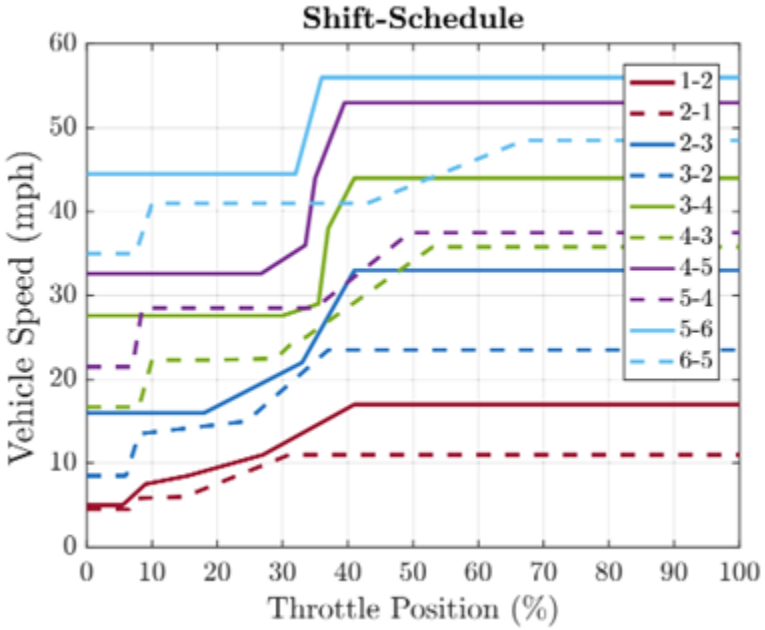

Figure 4.4: Empirical Transmission Shift Schedule

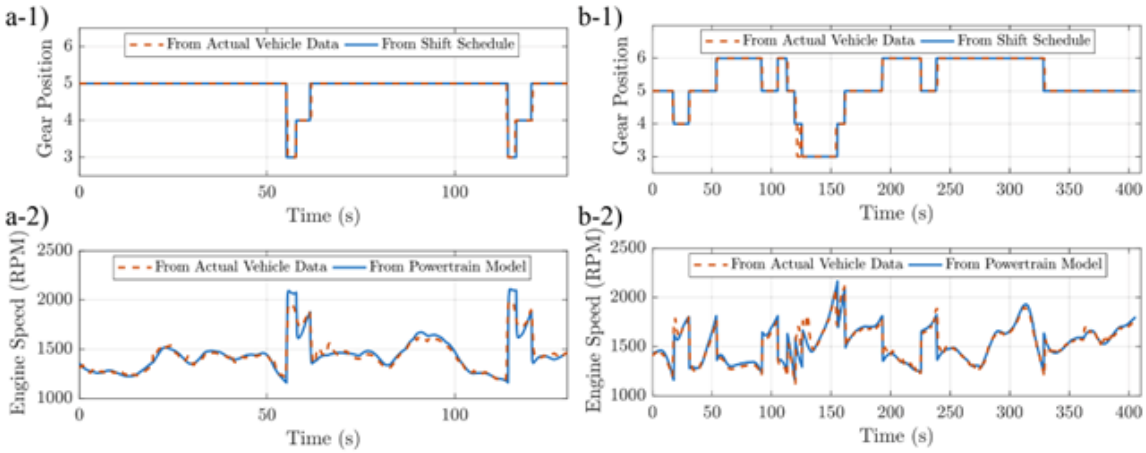

Figure 4.5: Transmission Model Calibration Results: (a) actual vehicle test one; (b) actual vehicle test two

4.2.5 Vehicle Model Development

The vehicle and powertrain dynamics are governed by the following equations:

$$J_e \omega \omega_e = T_e(t) - T_f(t) - T_d(t) \tag{4.2}$$

$$\frac{T_d(t) \cdot R_{fd} \cdot GearRatio(t)}{R_{tire}} - \{f_{tire} M_v g cos\phi(t) + \frac{1}{2} C_d \rho A v^2(t)\} = M_v a(t) \tag{4.3}$$

where T_e is the engine torque (Nm); T_f is the engine friction torque (Nm); T_d is the engine loading torque (Nm); a is the vehicle acceleration (m/s^2); f_{tire} is the rolling resistance friction constant; M_v is the vehicle mass (kg); g is the gravity constant; ϕ is the road slope angle (rad); C_d is the drag coefficient; ρ is the air density (kg/m^3); A is the vehicle frontal area (m^2).

From Equation (4.2), to ensure the performance of the virtual target vehicle matches the performance of an actual testing vehicle, both the engine output torque and the engine loading torque need to be the same as the actual vehicle. The engine torque can be controlled by sending the same accelerator pedal command as the actual vehicle. However, the desired loading torque has to be estimated using Equation (4.3) which includes several unknown parameters. As discussed in the previous section, the gear ratios and final drive values were already obtained from the brochure, and the tire radius was calibrated. The gravity constant is also a known constant. The remaining parameters that need to be calibrated are f_{tire}, M_v, and the lumped wind resistance constant $C_{wind} = \frac{1}{2} C_d \rho$.

These parameters were calibrated using the actual vehicle data from a FHWA project. For a well calibrated vehicle model, the calculated engine loading torque from Equation (4.3) should match the engine loading torque of an actual vehicle, given the same vehicle trajectory and roadway condition. During the actual vehicle tests, all the vehicle speed, acceleration, roadway slop, and gear positions were recorded. These data were sent to Equation (4.3) to obtain the calculated engine loading torque. Due to the difficulties in installing a torque sensor on an actual vehicle, the actual engine loading torque was not directly measured. It was estimated by an engine map using recorded engine speed and throttle of the actual vehicle. The model parameters of Equation (4.3) were selected as those giving the minimum error between the calculated engine loading torque and the estimated actual engine loading torque. The initial guess was based on the brochure and the ranges of these parameters were referred to [Z.Sun and G.G.Zhu].

In total, two FHWA data sets were used to calibrate the model: Aberdeen Track scenarios (data set 1) and rolling terrain scenarios (data set 2). The data set 1 was conducted on a relatively flat roadway and the effects of road grade angles are limited. A flat roadway is ideal for the longitudinal model calibration since the model is sensitive to the grade resistance term. Even for a roadway with small grade angle, the grade resistance term can become dominant compared to other resistances. Therefore, the data set 1 was used at beginning to obtain a preliminary calibration of the parameters though the nonlinear least square method. Once this was done, the model was further calibrated using the data set 2.

Figure 4.6a shows one calibration result from data set 1 and Figure 4.6b shows one calibration result from data set 2. The blue lines are estimated actual engine loading torque and the red lines are calculated engine loading torque using Equation (4.3). It can be seen that in both scenarios, the calculated engine loading torque match well with the estimated engine loading torque from actual vehicle data. This validates the vehicle model calibration. The root-mean-square-errors (RMSEs) are 3.08 and 18.30 respectively. The result from data set 2 has greater RMSEs due to more transient engine dynamins and more aggressive roadway slopes.

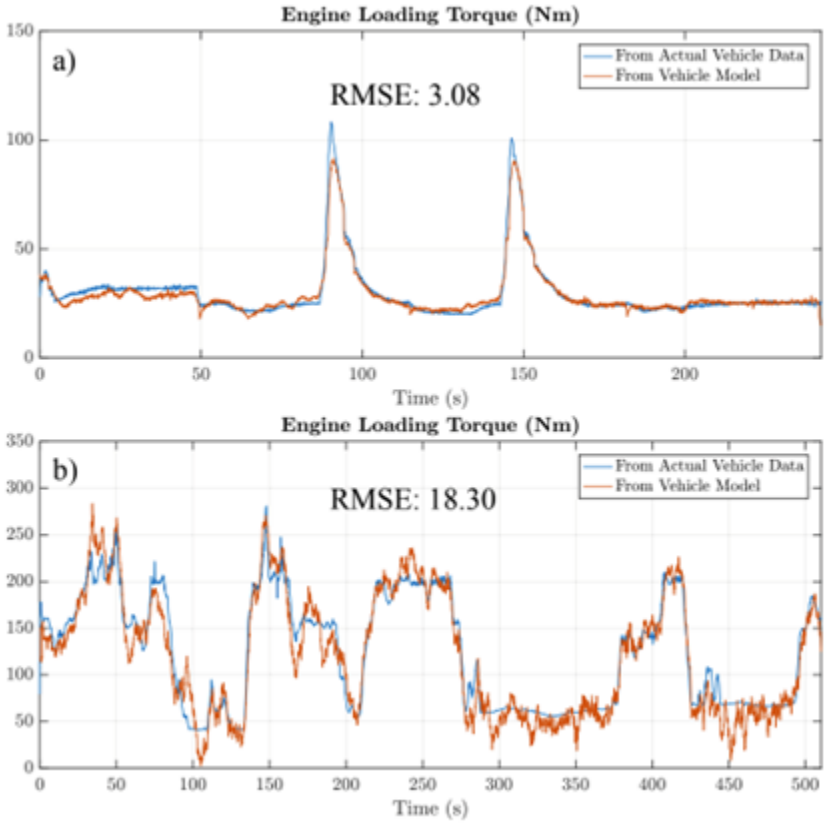

Figure 4.6: Vehicle Model Calibration Results

4.2.6 Implementation

Once all models and controllers were calibrated and verified, the performance of the virtual target vehicle represented by the powertrain research platform was compared against the performance of an actual vehicle. Given a testing scenario, first the high-level controller calculates the desired accelerator pedal command and engine torque using the engine maps and the calibrated longitudinal model. Next, these commands plus vehicle performance data (vehicle's speed, acceleration, etc.) and the testing scenario's roadway conditions (speed limit, the degree of road slope, etc.) are sent to the middle-level controller to determine the desired loading torque using both powertrain and vehicle models. This loading torque plus a compensation term from an engine controller (as shown in Figure 4.1) determines the final desired loading torque. This engine controller is a proportional-integral (PI) controller

based on engine speed feedback and compensates for uncertainties of the powertrain and vehicle models. Finally, the engine loading pump is controlled to provide the loading torque. The actual engine speed and torque are measured and sent to the vehicle model to simulate the performance of the virtual vehicle. The fuel consumption and emissions of the virtual target vehicle are measured using precise instruments and recorded as well.

Remark: In this report study, all inputs to the middle-level controller have been combined as a testing profile.

4.3 Experimental Validation Results and Analysis

4.3.1 Vehicle Base One

First, the base one was emulated by HIL testbed and experimental results of it were obtained. Figure 4.7 shows the results of reference profile and HIL testbed of base one, including engine speed, engine torque, throttle, vehicle speed, instant fuel consumption and cumulative fuel consumption. One can see that HIL testbed can track the reference profile well. The root-mean-square-error (RMSE) of the reference profile vehicle speed and the HIL testbed speed is 0.7903 m/s.

For the base one, the total fuel consumption of HIL testbed is 153.1372g, close to the result 158.3791g calculated by engine map.

4.3.2 Vehicle opt one

For vehicle opt one, all the results are shown in Figure 4.8 below, also including engine speed, engine torque, throttle, vehicle speed, instant fuel consumption and cumulative fuel consumption. The HIL testbed can track the reference profile very well. Besides, the RMSE of the reference profile vehicle speed and the HIL testbed vehicle speed is 0.4601 m/s.

The total fuel consumption of HIL test is 135.7545 g, almost the same as the result 136.1858 g calculated by engine map.

4.3.3 Vehicle opt two

For vehicle opt two, all the results are shown in Figure 4.9 below, including engine speed, engine torque, throttle, vehicle speed, instant fuel consumption and cumulative fuel consumption. The HIL testbed can track the reference profile well with the vehicle speed RMSE index of 0.7187 m/s.

The total fuel consumption of HIL test is 139.3844 g, close to the result 147.2292 g calculated by engine map.

4.3.4 Comparison

First, comparing the performances of the base one with opt one, the opt one can achieve 11.35% energy benefits, which can be found in the following Figure 4.10. The energy benefits come from less deceleration when approaching the intersections when the signal is red, and smoother acceleration when leaving intersections. Taking actions of both vehicles during 80 s to 100 s for example, the deceleration and acceleration of opt one (Figure 4.8.d) becomes smoother than the base one (Figure 4.7-d). The opt one does not stop, which reduces the amount of braking and avoids idling waste. Thus, the opt one can achieve great benefits on fuel consumption.

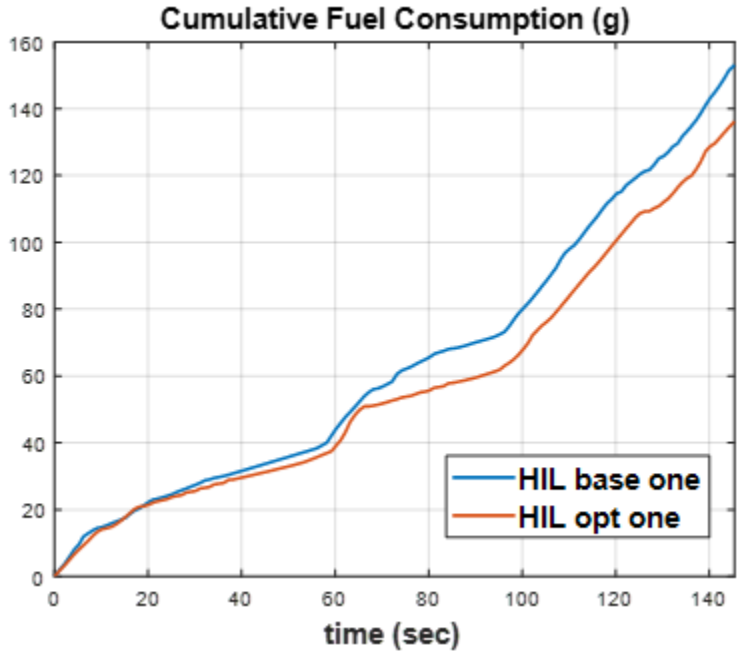

Figure 4.10: Comparison Between Base One and Opt One

Second, when comparing vehicle base one and opt two, one can see that even the traditional vehicle opt two following the opt one also can achieve good energy benefits. The cumulative fuel consumptions of these two vehicles are shown below. Quantitatively, it can save 8.98% fuel.

The reason can be smoother deceleration and acceleration process of the opt two when it followes the connected and autonomous vehicle opt one. Also taking the vehicle opt two (Figure 4.9.d) during 80 s to 100 s for example, it does not stop when approaching the intersections with red signal and it accelerates smoothly when leaving intersections because it follows the opt one. Thus, the traditional vehicle following the opt one can achieve some benefit on fuel consumption, too.

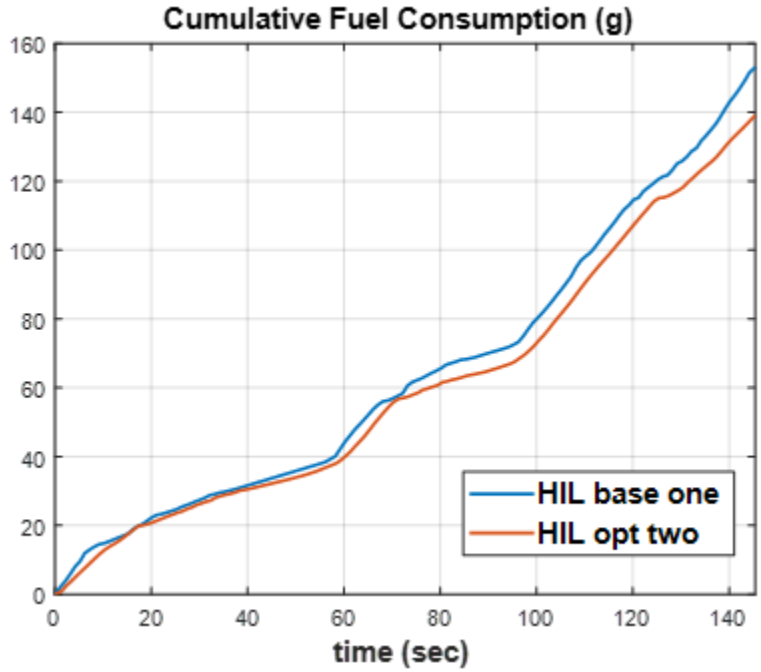

Figure 4.11: Comparison Between Base One and Opt Two

4.4 Summary

This report presented a brief introduction of the HIL testbed configuration. All vehicle and powertrain models were calibrated using actual vehicle testing data. HIL experiments were conducted for validation work of the proposed co-optimization strategy of task 3. Specifically, the HIL testbed results showed that the fuel benefits can be 11.35% for the target connected and autonomous vehicle vs a traditional vehicle. It also showed that a vehicle controlled by the intelligent driver model (IDM) following the connected and autonomous vehicle can achieve 8.98% fuel benefit compared with the base vehicle.

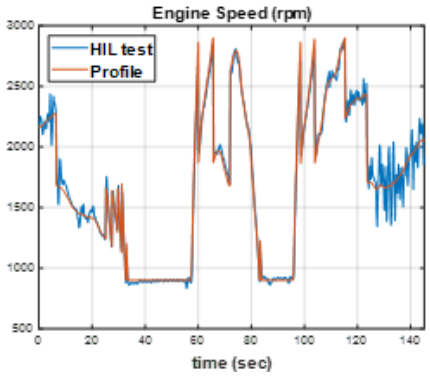

(a) Engine Speed (rpm)

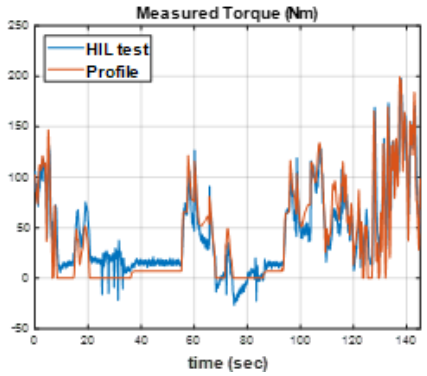

(b) Engine Torque (Nm)

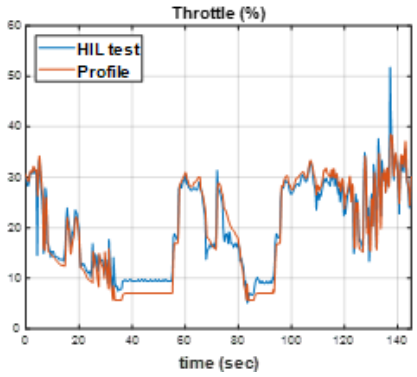

(c) Throttle (%)

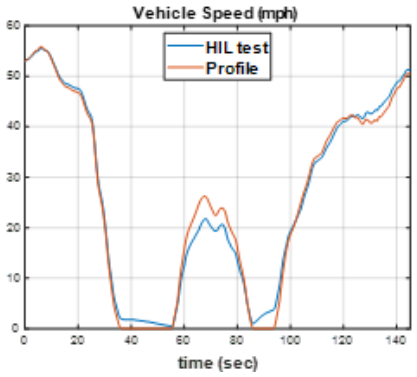

(d) Vehicle Speed (mph)

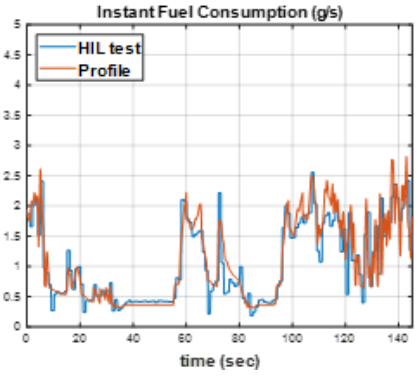

(e) Instant Fuel Consumption (g/s)

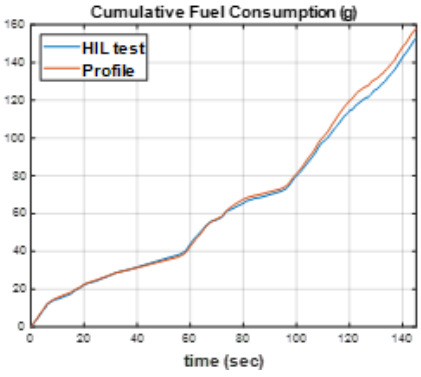

(f) Cumulative Fuel Consumption (g)

Figure 4.7: Illustration of various images

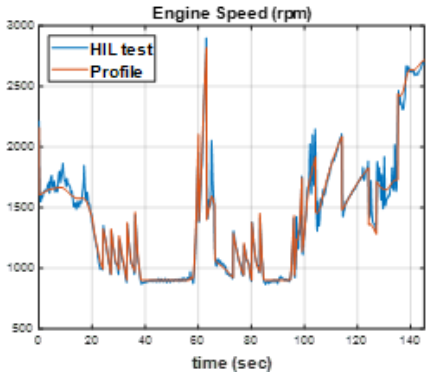

(a) Engine Speed (rpm)

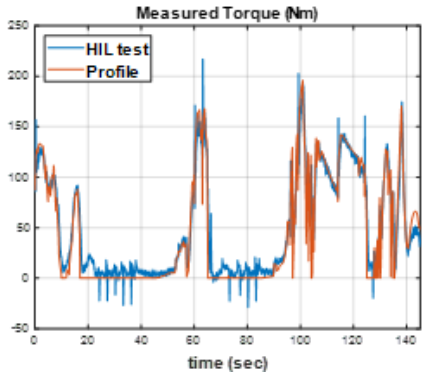

(b) Engine Torque (Nm)

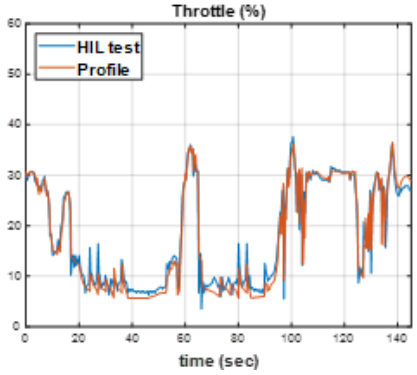

(c) Throttle (%)

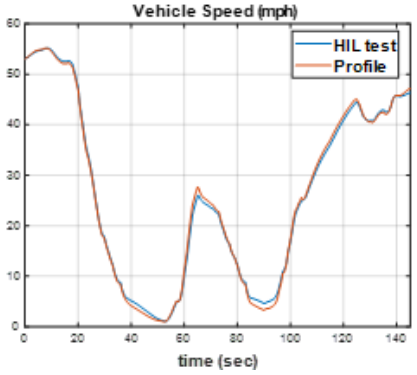

(d) Vehicle Speed (mph)

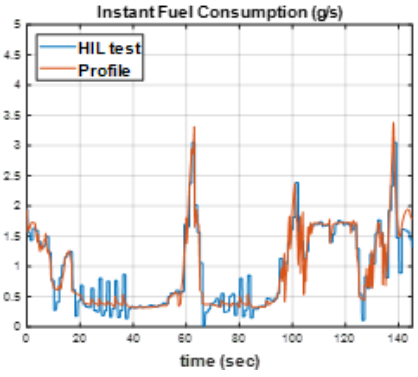

(e) Instant Fuel Consumption (g/s)

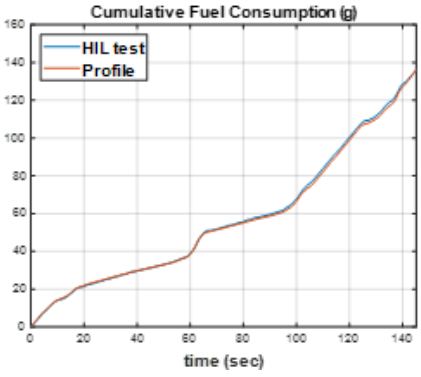

(f) Cumulative Fuel Consumption (g)

Figure 4.8: Experimental Results of Opt One

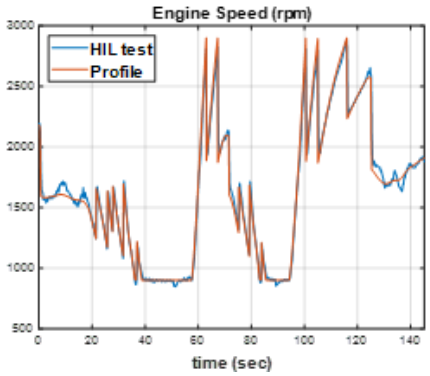

(a) Engine Speed (rpm)

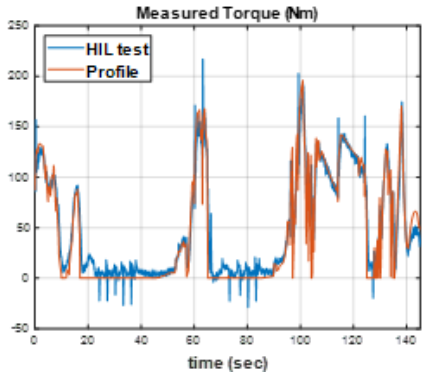

(b) Engine Torque (Nm)

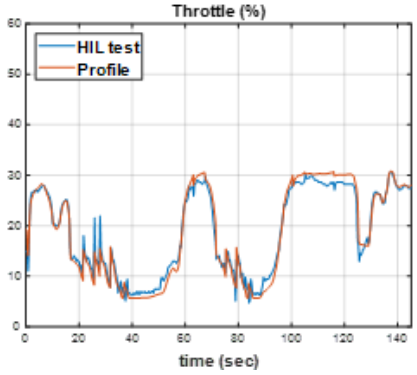

(c) Throttle (%)

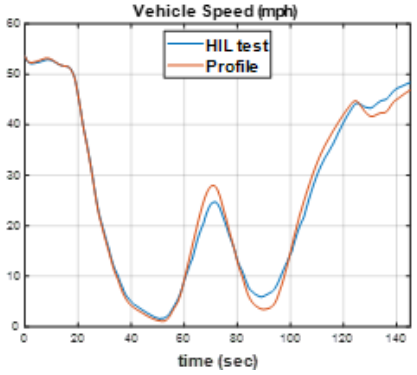

(d) Vehicle Speed (mph)

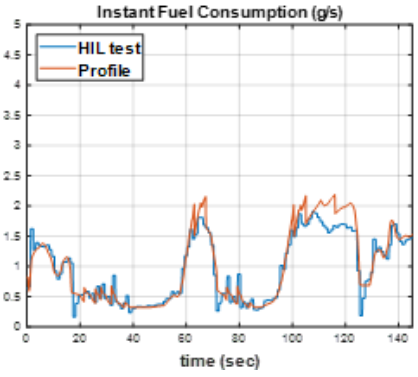

(e) Instant Fuel Consumption (g/s)

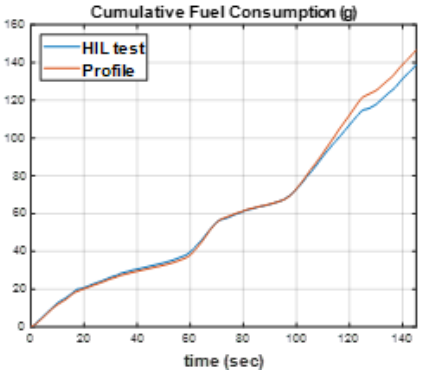

(f) Cumulative Fuel Consumption (g)

Figure 4.9: Experimental Results of Opt Two

Chapter 5

Task 5: Analysis on Various Market Penetrations of Connected Automated Vehicles

May 31, 2021

Description: Using the traffic prediction and vehicle speed optimization framework proposed in Task 3, the project team developed a holistic simulation methodology to predict the benefits in fuel consumption for vehicle platoons at various market penetrations of connected automated vehicles.

5.1 Introduction

In Task 3, preliminary results were presented on traffic prediction and vehicle speed optimization. The results showed that a fuel benefit of 12.19% could be achieved for the target connected automated vehicle (CAV) traveling through four consecutive intersections on Hwy 55 in Minnesota. When vehicles reduced speed preemptively corresponding to the predicted traffic conditions and the signal phase and timing (SPaT) information, they formed a moving bottleneck for surrounding vehicles. At low CAV market penetrations, these moving bottlenecks have only small effects on legacy vehicles (LVs). However, at larger (e.g., 30–40%) market penetrations, these moving bottlenecks will start to cause LVs to slow down as well. As a result, LVs following CAVs will likely experience benefits in fuel consumption as well.

In this report, we employ an improved traffic prediction method, which appears to be able to reduce prediction errors considerably, especially when vehicles approach signalized intersections. Further, the modified prediction method along with the vehicle speed control technique presented in Task 3 are applied to study the impact of CAV market penetrations on the fuel consumption of vehicle platoons. Each CAV makes prediction of future traffic based on the information collected from preceding CAVs, as well as the information obtained from the immediate preceding vehicle and SPaT at intersections. Once future traffic conditions are predicted for each CAV, they will be able to optimize their speed accordingly with the objective of minimizing fuel consumption. Unlike what was done in Task 3 where a single CAV was considered, in the present work we consider a vehicle platoon with a varying number of CAVs depending on the market penetration rate. For simulation studies, we use the vehicle speed data collected on Hwy 55 for the lead vehicle on the road. Each CAV in the platoon is intelligently controlled using the proposed speed control method, while all the LVs are represented using an intelligent driver model (IDM) [30].

5.2 Traffic Prediction and Vehicle Speed Control

As seen in Task 3, the well-known second-order Payne-Whitham (PW) model was used to propagate traffic states. This traffic flow model is developed in the context of highway traffic, with the underlying assumption that vehicles always tend to adjust their speed to reach the equilibrium value. While this is true for highway traffic, it does not always hold for a signalized arterial due to the presence of traffic lights. In this work, an appropriate modified equilibrium speed term is incorporated to overcome this challenge for improving accuracy of traffic prediction [29]. Once future traffic conditions are predicted for each CAV, their speed will be optimized using the technique proposed in Task 3 with the objective of minimizing fuel consumption. Unlike what was done in Task 3 where a single CAV was considered, in the present work we consider a vehicle platoon with a varying number of CAVs depending on the market penetration rate.

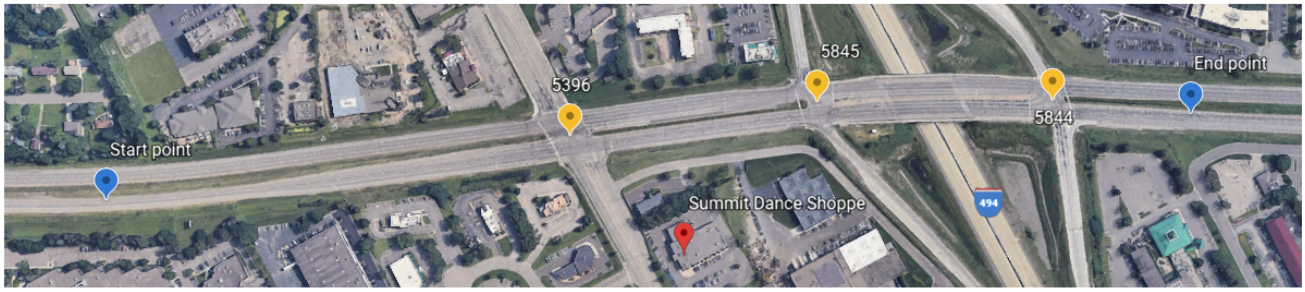

Figure 5.1: A segment of Hwy 55 where field experiments were conducted.

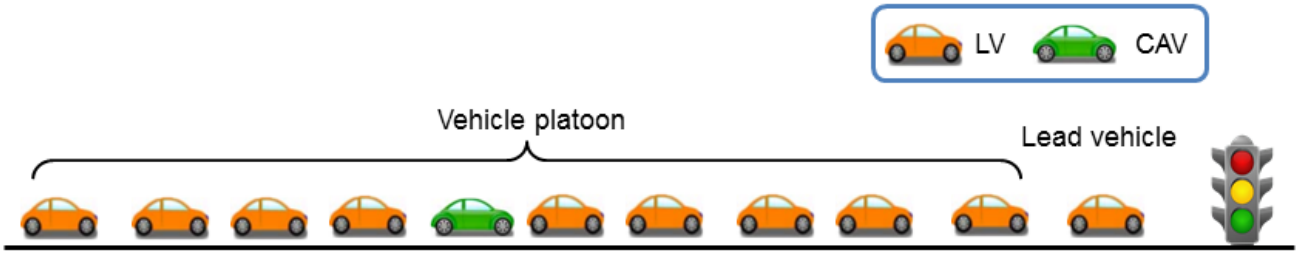

Figure 5.2: Illustration of the simulation setting.

5.3 Numerical Results

In this section, we present a series of numerical results for vehicle speed optimization with various market penetration rates of CAVs, where fuel benefits for the vehicle platoon are observed. The case study is conducted using real-world traffic data collected on Hwy 55 in Minnesota, as shown in Figure 5.1. Although the simulation study is carried out for a segment of Hwy 55, the solution method developed is readily applicable for other parts of the road given that SPaT information is available. In our field experiments, four testing vehicles equipped with on-board units (OBUs) were driven by human drivers to collect traffic data. OBUs can collect real-time vehicle data, such as GPS location, speed, and acceleration. The intersections are mounted with roadside units (RSUs) connected to the signal controller. Vehicles equipped with OBUs can receive SPaT information broadcast by RSUs within a certain range, e.g., 500 m. Therefore, vehicle trajectories and the SPaT information received at each intersection can be extracted from the data collected.

In the simulation studies, the speed profile of the lead vehicle leading the platoon follows the real-world data collected on Hwy 55 as used in Task 3. Specifically, the lead vehicle passed the intersection #5396 on a green light, whereas it had to stop at intersections #5845 and #5844 on red lights before the signal turned green. This is based upon the traffic data collected on Hwy 55. Clearly, there are a large number of traffic scenarios possible due to the presence of traffic lights. We conducted numerical experiments with vehicles entering the simulated space at various spacings and observed similar patterns in fuel benefits for the vehicle platoon. For brevity, we present here only a set of results with detailed interpretations. A platoon consisting of 10 vehicles is assumed to follow a lead

LV (11 vehicles in total), as shown in Figure 5.2. Any vehicle in the platoon can be either a LV or a CAV, which allows for the exhibition of various market penetration rates of CAVs. As commonly seen in the literature, all LVs are simulated using the intelligent driver model (IDM) [30]. CAVs are controlled using the speed control method presented in Task 3. They are assumed to be equipped with sensors such as RADAR and/or LIDAR, allowing for measuring speed and distance. Clearly, CAVs are able to obtain the information, e.g., speed and distance, of their immediate preceding vehicle, and traffic information from all preceding CAVs within the vehicle-to-vehicle communication range.

In this setting, 10 different penetration rates of CAVs are simulated, ranging from 10% to 100%. The baseline scenario is considered with a 0% penetration rate of CAVs, i.e., all the vehicles are LVs. (Note that LV refers to a legacy vehicle, not the lead vehicle.) The fuel consumption of each vehicle is calculated from the starting point d = 0 m to d = 1100 m covering all the intersections shown in Figure 5.1 (the third intersection #5844 is located at 960 m with respect to the starting point). Following its immediate preceding vehicle, each vehicle passes the starting point with the same speed at a desired spacing s^* determined by the IDM [30], which is given by

$$s^*(v, \Delta v) = s_0 + \max\left\{0, vT + \frac{v\Delta v}{2\sqrt{ab}}\right\}, \tag{5.1}$$

where v is the speed of the vehicle; Δv is the speed difference between the vehicle and its preceding one; s_0 is the minimum spacing; T is the desired time headway; and a and b are the maximum vehicle acceleration and comfortable braking deceleration, respectively. The set of parameters can be found in [31].

As shown in Task 3, CAVs could obtain fuel benefits using the optimal speed control method due to traffic prediction and the availability of SPaT information. Apart from that, in this task, we are also interested in studying the impact of CAVs driving behaviors on fuel consumption of the following LVs. To this end, four types of fuel benefit are defined in this section. The first type of fuel benefit is the overall fuel benefit of the platoon involving all the vehicles under consideration. The second type represents the average fuel benefit of all CAVs in the platoon, whereas the third type denotes the average fuel benefit of all LVs. The fourth one indicates the fuel benefit of all LVs behind CAVs. Specifically, the first one is calculated by comparing the total fuel consumption of all vehicles in the platoon with that of the baseline scenario. For the fourth one, it is computed taking into account all LVs appearing after the first CAV in the platoon. For example, in case the 4th and 7th vehicles are two CAVs in the platoon, the fuel benefit for LVs behind CAVs is calculated by comparing the total fuel consumption of the 5th, 6th, and 8th to 11th vehicles with that of the baseline scenario.

The set of simulation results on fuel benefits for the 10-vehicle platoon is shown in Figure 5.3 at various market penetration rates of CAVs. For a given penetration rate of CAVs, there are a number of possible permutations of vehicle location since each vehicle in the platoon can be either a CAV or a LV. For example, in a 10-vehicle

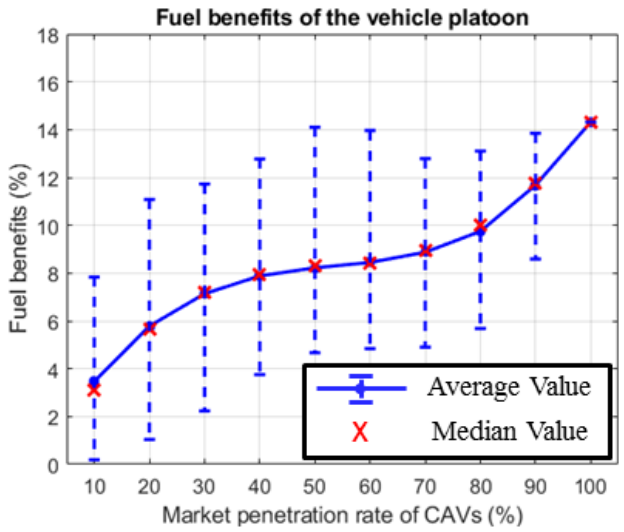

(a) Fuel benefits of the 10-vehicle platoon.

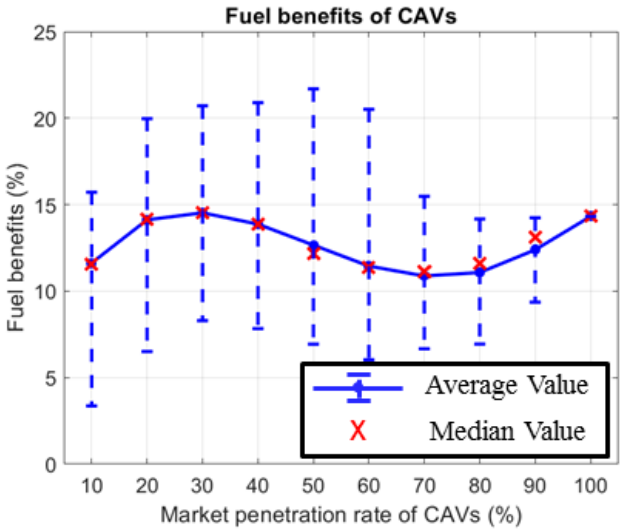

(b) Fuel benefits of CAVs.

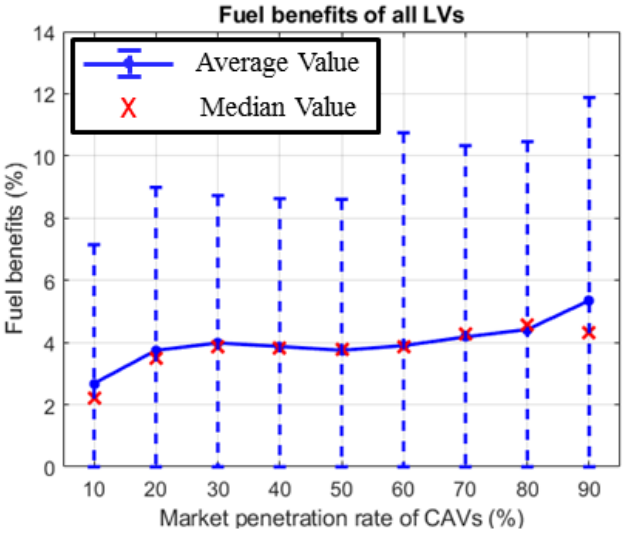

(c) Fuel benefits of all LVs.

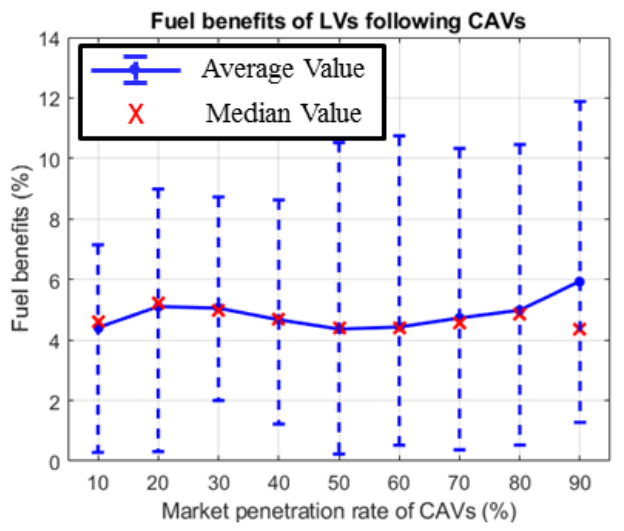

(d) Fuel benefits of LVs behind CAVs.

Figure 5.3: Vehicle fuel benefits at various market penetration rates of CAVs.

platoon with 10% penetration rate of CAVs, the only CAV can be any one in the platoon. In the simulation studies, more than 80% of all possible permutations are simulated for each market penetration rate. In Figure 5.3, the solid line shows the average fuel benefit of all simulated permutations with a varying range represented by the dotted line.

It is observed from Figure 5.3a that the fuel benefit of the vehicle platoon increases with the increase of the CAV market penetration rate, ranging from around 3% to 13%. Due to optimized CAV trajectories, LVs following CAVs also experience fuel benefits as observed in Figure 5.3d, ranging between 4% and 6% at various market penetration rates of CAVs. It is interesting to note that the fuel benefit of LVs behind CAVs does not

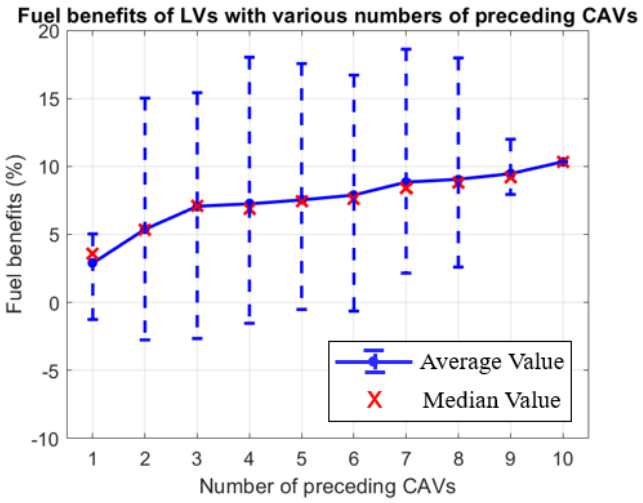

Figure 5.4: Fuel benefits of LVs with various numbers of preceding CAVs.

necessarily increase with the increase of the penetration rate. This is due to the fact that a higher penetration rate does not necessarily result in a larger number of CAVs driving ahead of a LV in the presence of permutations. A similar pattern in fuel benefits of all LVs is observed in Figure 5.3c. Comparing Figure 5.3c to Figure 5.3d, it is observed that the average fuel benefit of all LVs is smaller than that of LVs behind CAVs due to the fact that LVs ahead of the first CAV do not experience any fuel benefit.

For comparison, we present the fuel benefits of LVs with various numbers of CAVs ahead in Figure 5.4. It is clear that better traffic prediction can be achieved with a larger number of CAVs present, due to more available traffic information provided by CAVs. Figure 5.4 shows the fuel benefit of a LV increases with the increase of the number of its preceding CAVs. This is because the immediate preceding CAV of the LV drives in a smoother manner given a better traffic prediction. As a result, the LV following the optimized trajectory of CAVs will experience more fuel benefits.

It is also observed in Figure 5.3a that the increasing rate of fuel benefits for the vehicle platoon appears to be smaller when the penetration rate increases from around 40% to 70%, compared to other penetration rates. This is mainly due to the permutations of vehicle location in the platoon. Specifically, the fuel benefit of a single CAV is shown in Figure 5.5 corresponding to various locations in the vehicle platoon. It is observed that the CAV appears to be able to achieve more fuel benefits when located after the 7th position in the platoon. This is mainly due to two reasons. On the one hand, the optimal speed control of CAVs is obtained and implemented within a model predictive control (MPC) framework, as shown in Task 3. As a result, the fuel benefit obtained by a specific CAV may vary depending on different traffic states. That is, the number of preceding CAVs and their trajectories affect the results of traffic prediction. On the other hand, in the baseline scenario vehicles following the 7th vehicle experience a gear position shift in the first 23 secs (approximately), resulting in more fuel consumption,

as shown in (d) of Figure 5.6. A closer scrutiny on vehicle fuel benefits in the baseline scenario along with that of the optimized scenario is presented in Table 5.1. It is clearly observed that there is a significant increase in fuel consumption from vehicle 7 to the following ones due to gear shift. As a result, CAVs present at the back of the platoon with speed optimization appear to achieve a relatively higher percentage of fuel benefits, as observed in Figure 5.5.

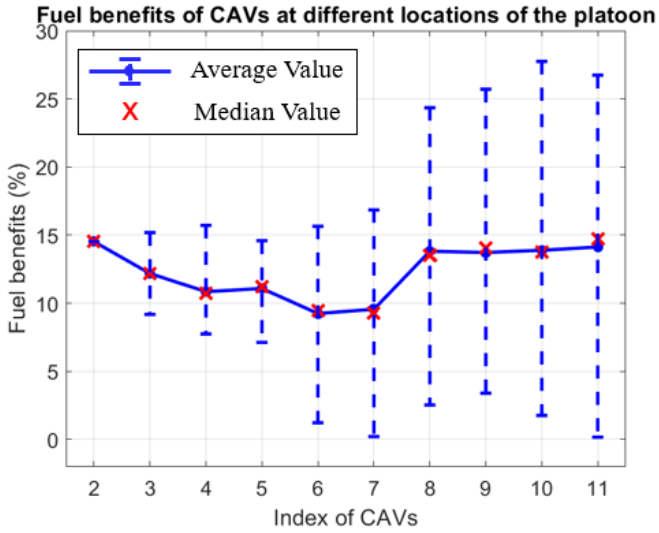

Figure 5.5: Fuel benefits of CAVs at different locations in the vehicle platoon.

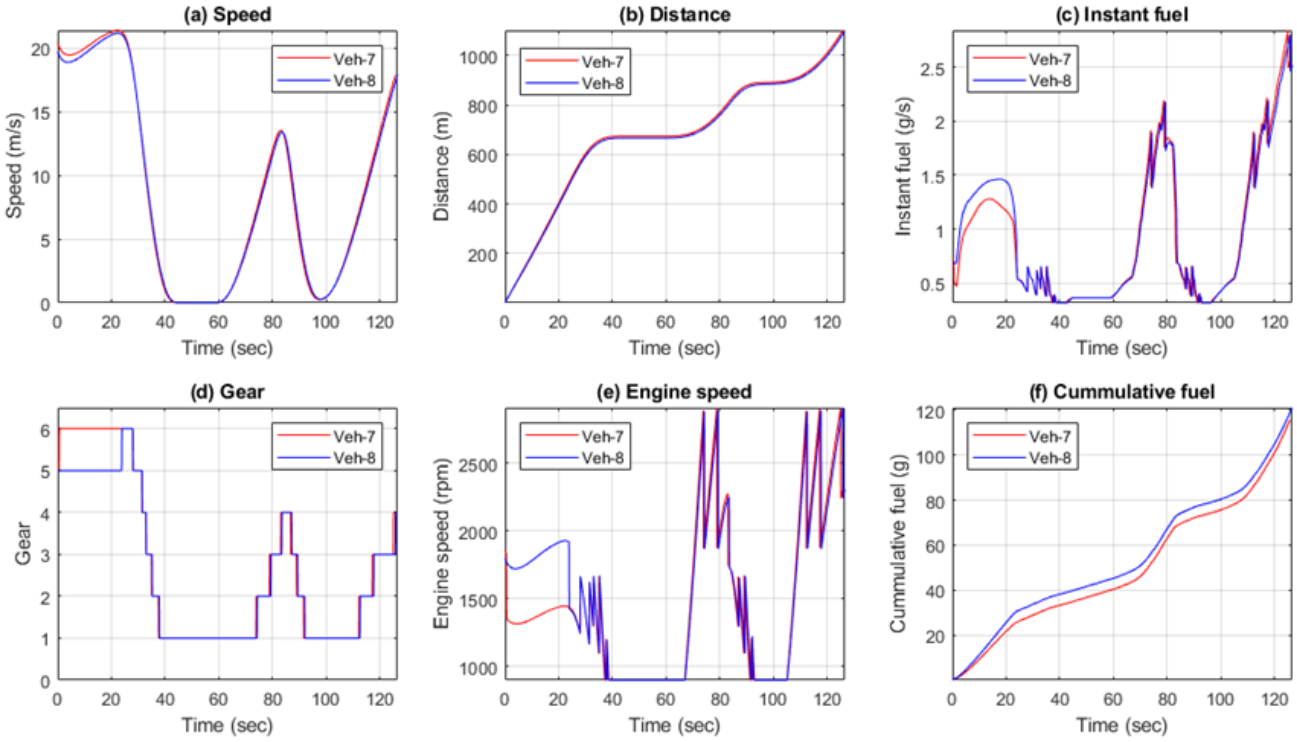

Figure 5.6: Simulation results of vehicles 7 and 8 in the baseline scenario.

As noted before, at a given penetration rate of CAVs there could be various possible permutations of

Table 5.1: Fuel consumption of each vehicle: baseline scenario vs. optimized scenario.

Vehicle index	2	3	4	5	6
Baseline (g/km)	99.03	100.72	102.24	103.38	104.23
Opt. average (g/km)	84.65	88.45	91.14	91.92	94.59
Vehicle index	7	8	9	10	11
Baseline (g/km)	105.01	110.03	110.70	111.05	111.67
Opt. average (g/km)	94.97	94.83	95.51	95.62	95.89

vehicle location in the platoon. It turns out that, at around 40%–70% penetration rates there is a larger percentage of cases involving vehicles 4 to 7 being CAVs. This percentage increases with the increase of penetration rate from 40% to 70%. As a result, fuel benefits of CAVs decrease over this range of penetration rates as observed in Figure 5.3b. As a *weighted sum* of the fuel benefits of CAVs and LVs, fuel benefits of the vehicle platoon experience a slight increase over the penetrations 40%–70%, as seen in Figure 5.3a. With continued increase of the penetration, any vehicle when being a CAV is likely to obtain more fuel benefits with more CAVs ahead due to better traffic prediction. Consequently, the increasing rate of fuel benefits for the platoon appears to be higher over the penetrations 70%–100%, as shown in Figure 5.3a.

To further study the impact of CAVs driving at optimized speeds, a platoon with more vehicles is also considered. That is, there are 20 vehicles in the platoon following a lead LV (21 vehicles in total). The simulation results on fuel benefits of the vehicle platoon are shown in Figure 5.7, with CAV market penetration rates ranging from 5% to 40%. It is observed that the fuel benefit of the vehicle platoon increases with the increase of CAV market penetration rate, which is consistent with the observation in Figure 5.3a. Vehicle fuel benefits are achieved as a result of smoother traffic due to optimized trajectories of CAVs. In other words, the optimally controlled CAVs are able to drive in a proactive manner to reduce shockwave when approaching red signals. For illustration, the trajectories of all vehicles in a 20-vehicle platoon following a LV are shown in Figure 5.8a when each vehicle is a LV. The formation of shockwave is clearly observed at intersections #5845 and #5844 due to red signals. As a comparison, a simple case is simulated where the 7th vehicle is the only CAV in the platoon. The corresponding vehicle trajectories are presented in Figure 5.8b. Clearly, starting from the CAV the shockwave is very much reduced compared to that in Figure 5.8a.

Comparing Figure 5.7 to Figure 5.3, a similar pattern is observed for each type of fuel benefit. However, there appears to be a higher fuel benefit obtained by LVs for the 20-vehicle platoon compared to that of a 10-vehicle platoon. This is due to a larger presence of LVs in a longer platoon at the same penetration rate of CAVs. As a result, for the given range of penetration rates the average fuel benefit of the platoon shown in Figure 5.7a is

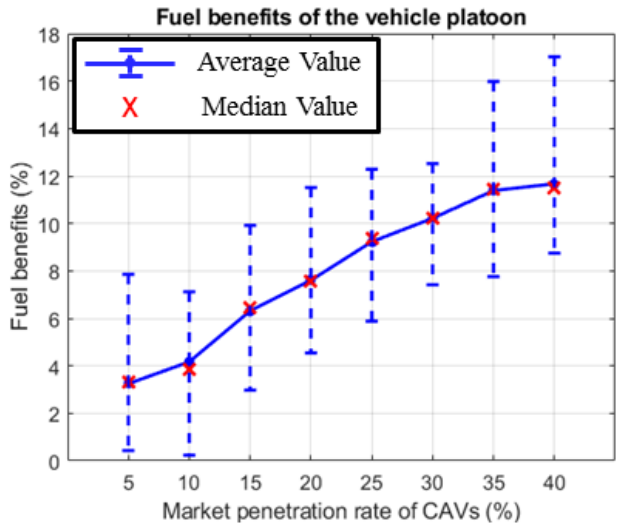

(a) Fuel benefits of the 20-vehicle platoon.

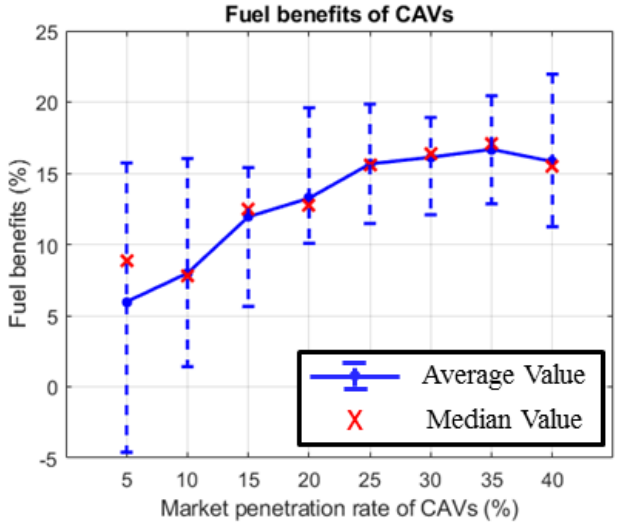

(b) Fuel benefits of CAVs.

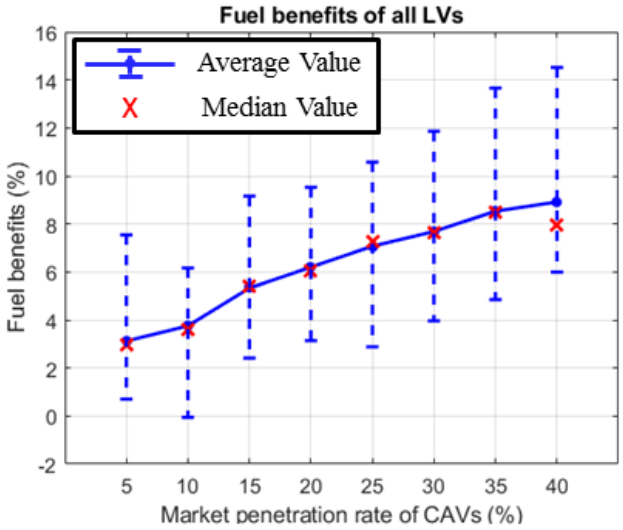

(c) Fuel benefits of all LVs.

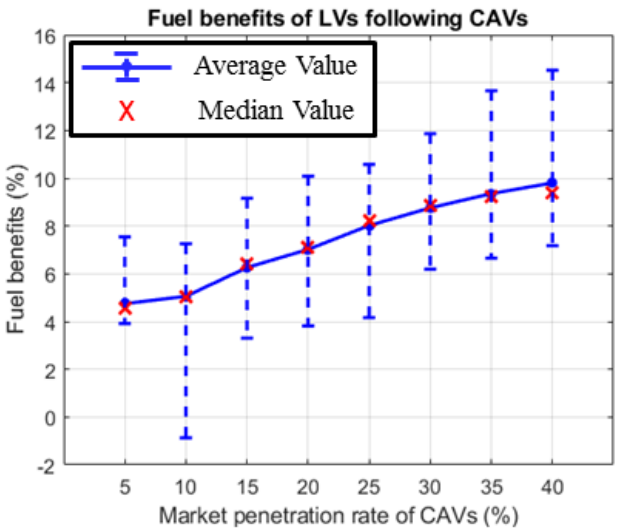

(d) Fuel benefits of LVs behind CAVs.

Figure 5.7: Vehicle fuel benefits at various market penetration rates of CAVs.

higher than that of Figure 5.3a. In the baseline scenario without CAVs, vehicles in the further back of the platoon are likely to experience larger speed disturbances due to amplification of deceleration of the preceding vehicles [35], resulting in more fuel consumption. Therefore, in the presence of CAVs the fuel benefit of all LVs and that of LVs behind CAVs continue to increase with the increase of the penetration rate from 5% to 40%, as shown in Figure 5.7c and Figure 5.7d, respectively.

In addition to fuel benefits, we are also interested in studying the impact of CAVs on travel time of the following LVs. A set of comparative results is shown in Figure 5.9 for the 10-vehicle platoon. It is observed from Figure 5.9 that the average travel time of LVs behind CAVs decreases with the increase of CAV penetration rate.

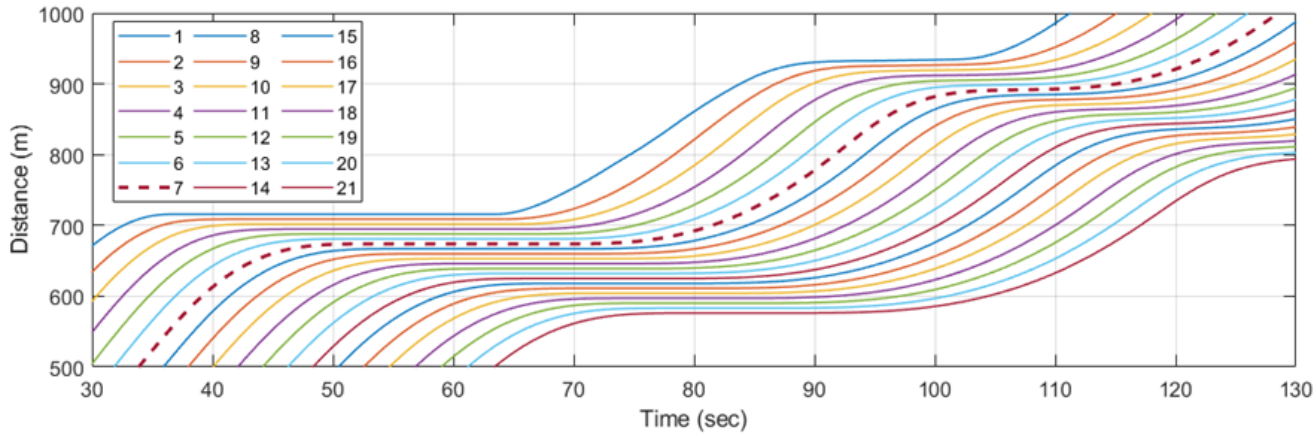

(a) Trajectory of all vehicles that are LVs.

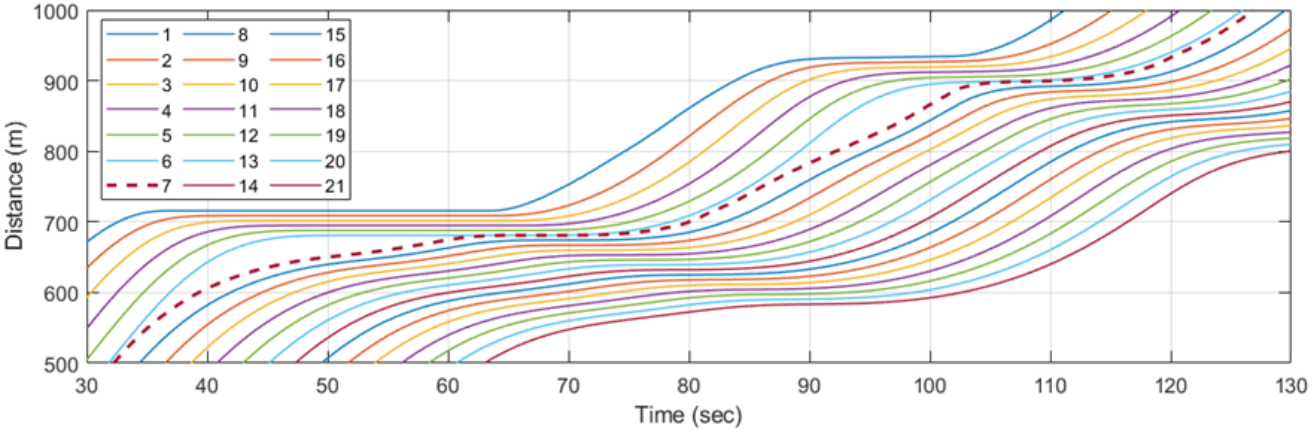

(b) Trajectory of all vehicles with 7 being a CAV.

Figure 5.8: Trajectory of all vehicles in a 20-vehicle platoon following a lead LV.

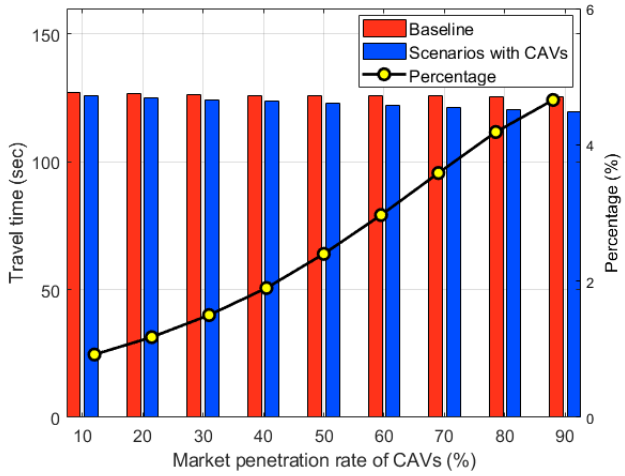

Figure 5.9: Comparison of travel time for LVs with and without CAVs.

With a penetration rate varying from 10% to 90%, the corresponding reduction in average travel time for LVs ranges from around 1% to nearly 5%. As observed before, this is possibly due to smoother traffic with a higher

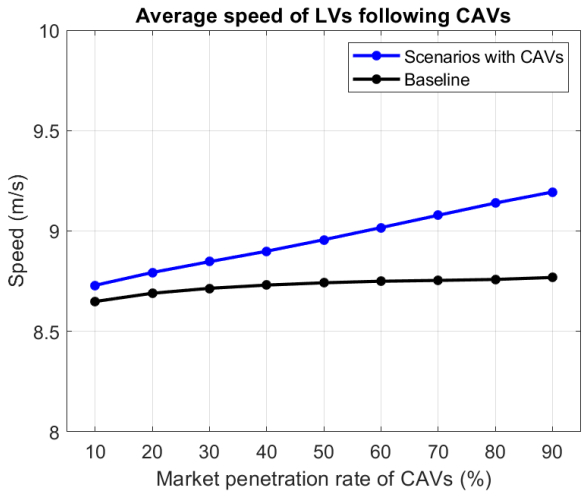

Figure 5.10: Average speed of LVs behind CAVs at various penetration rates.

penetration rate of CAVs. As a result, LVs experience a larger average speed at a higher penetration rate of CAVs, as opposed to the case with a lower penetration rate. It is observed in Figure 5.10 that the average speed of LVs behind CAVs increases with the increase of the penetration rate, resulting in a decreasing average travel time for LVs as observed in Figure 5.9.

5.4 Summary

Using the traffic prediction and vehicle speed optimization framework proposed in Task 3, we developed a holistic simulation methodology to predict the benefits in fuel consumption for vehicle platoons at various market penetration rates of CAVs. Specifically, we proposed an improved traffic prediction method which appears to be able to reduce prediction errors considerably, especially when vehicles approach an intersection [29]. Further, the modified prediction method along with the vehicle speed control technique presented in Task 3 are applied to study the impact of CAV market penetrations on the fuel consumption of vehicle platoons. For simulation studies, the vehicle speed data collected on Hwy 55 in Minnesota is used for the lead vehicle on the road. CAVs are intelligently controlled using the proposed speed control method, while all the LVs are simulated using an IDM.

A series of simulation experiments is conducted. It is observed from the results that fuel benefits of the vehicle platoon appear to increase with the increase of CAV penetrations due to smoother traffic. In addition to fuel benefits obtained by LVs behind CAVs, LVs also experience a smaller travel time compared to the case without CAVs. A positive correlation is observed between travel time reduction for LVs and the penetration rate of CAVs. The results are very encouraging in the sense that more vehicles driving on Minnesota roads will benefit from the deployment of future connected corridors with an increasing number of CAVs present.

Chapter 6

Task 6: Network model of SPaT corridors and Route Choice

October 31, 2021

Dynamic Traffic Assignment Model to Show Impact of Signal Phasing and Timing (SPaT) on Route Choice

Description: Limited deployment of SPaT corridors will change the utility of different routes for CV drivers. Due to significant fuel savings on SPaT corridors, CV drivers may prefer to use SPaT corridors even if it increases the travel time of their trip. The project team will construct a traffic assignment model of major corridors, using data from the 7-county DynusT model of the Twin Cities created by MnDOT. The traffic assignment will be solved using classic algorithms such as the method of successive averages. This network model will be used to evaluate various SPaT deployments at different CV market penetrations to predict how route choice changes will affect network-wide fuel savings.

6.1 Introduction

In the previous tasks, it was shown that the use of signal phase and timing (SPaT) can increase fuel efficiency when deployed with connected autonomous vehicles (CAVs). In Task 5, the traffic prediction and vehicle speed optimization data from Task 3 were used to develop a holistic simulation methodology to predict the benefits in fuel consumption for vehicle platoons at various market penetration rates of CAVs. This method was applied to study the impact of CAV market penetrations on fuel consumption of vehicle platoons using vehicle speed data collected along Trunk Highway 55. After a series of simulations were conducted, fuel benefits were observed with platoons of vehicles. It was found that the benefits increase with the market penetration rate of CAVs as the legacy human-driven vehicles (HVs) behind CAVs also benefited from the fuel efficiency.

In this report, we apply the fuel benefits data from Task 5 to demonstrate how vehicles will change their routes to use the connected corridor. Specifically, we model the fuel benefits that CAVs enjoy on a dynamic traffic assignment model. We define a generalized travel time cost function that models the trade-off that drivers make between potentially increased travel time but decreased fuel usage when routing to use a SPaT-enabled signal. Using a network model for the Twin Cities area, we track the market penetration rate, travel times, and fuel benefits of vehicles along the TH-55 connected corridor to see how many vehicles re-route to take TH-55 and enjoy the increased fuel benefits. We track the increase in CAVs using TH-55 at increasing levels of market penetration and determine how much fuel is saved by using the connected route to determine network-level savings.

6.2 Modified Dynamic Traffic Assignment Methodology

Traffic assignment modeling is the process of using networks to model real-life roadway conditions and congestion. The roadway system is modeled with links and nodes, where links represent roads and nodes represent intersections. A traffic assignment model is used to predict the flow of drivers on each roadway segment, called a link flow. There are two main types of traffic assignment models, static and dynamic.

Static models were the first to be developed, and do not consider the element of time. They assign trips from the demand data and predict travel times using a link performance function, typically dependent on the free flow time and capacity of each link. Dynamic traffic assignment models track changes to congestion over time, which requires storing the location of vehicles on the network at the same level of detail as the link flows to be tracked. As congestion changes over time, the model is solved when *dynamic user equilibrium* is reached. This is achieved when all the paths used by drivers departing the same origin, for the same destination, at the same time, have equal and minimal travel times. Due to the dynamic nature of dynamic traffic assignment, it is possible for there to be multiple equilibrium states or no equilibrium. In dynamic user equilibrium, drivers choose routes based off of their experienced travel times, with the underlying assumption being that drivers are familiar enough with

the network to anticipate likely changes in congestion (and thus travel time) in order to make an informed decision on their route choice. As we model the morning commute in this study, this is a reasonable assumption. This means that it is only possible to solve the problem through an iterative process, such as the method of successive averages used in this study. [7].

As this task uses dynamic traffic assignment, we will focus solely on it. There is a three step process for dynamic traffic assignment.

1. Network Loading: The traffic flow model is used to predict the time dependent travel times on each link, with the routes and departure times of drivers as input.

2. Path Finding: With the travel time of each link obtained from network loading, all the drivers at a certain time find the shortest route to their destination

3. Route Updating: Vehicles are shifted from their current paths onto the new, shorter paths. The traffic flow model is updated with the new vehicle paths.

To perform the network loading step, it is necessary to model the state of each link and node. As the model is time dynamic, time is discretized into time steps Δt. Each link outputs a sending and receiving flow $S(t), R(t)$ for a particular timestep, which denotes the number of vehicles leaving and entering the link respectively. Nodes, which are between links, take the sending flow of all the links going to the node and the receiving flow of the links going from the node and calculate the turning movement flow for each possible movement (ie, which link a vehicle turns onto when as it crosses an intersection). The Newell-Daganzo method is used to calculate the sending and receiving flow for links ([18], [8]).

In order to have a realistic model of vehicle flows, it is necessary to use traffic flow theory. The most basic assumption in traffic flow theory is from the Lighthill-Whitham-Richards model relating flow q (rate at which vehicles pass a certain point), density k (spatial concentration of vehicles), and speed u (the average rate of travel) [14].

$$q = uk \tag{6.1}$$

To use traffic flow theory to find the counts of vehicles at certain points on the network, we introduce another variable $N(t, x)$ which is defined as the cumulative count of vehicles that have passed point x at time t. This allows

us to create the relationship between q, u, and k:

$$\frac{\partial N}{\partial t} = q \tag{6.2}$$

$$\frac{\partial N}{\partial x} = -k \tag{6.3}$$

$$\frac{\partial q}{\partial x} + \frac{\partial k}{\partial t} = 0 \tag{6.4}$$

This allows us to find the flow $q(t,x)$, density $k(t,x)$, and speed $u(t,x)$ if we are given $N(t,x)$ [18].

With this traffic theory in mind, we now seek to find the cumulative counts at both ends of each link. Let L be the length of a given link, u_{f} the free flow speed of the link, w the congested wave speed, k_{j} the jam density, and $q_{\max}$ the link capacity. We use the Newell-Daganzo [18] method to find the fundamental diagram (in this case, trapezoidal):

$$Q(k) = \min\{u_{\mathrm{f}}k, q_{\max}, w(k_{\mathrm{j}} - k)\} \tag{6.5}$$

In this study, we use the link transmission model to calculate the sending and receiving flows for links [38]. It only involves calculations at each end of the link, but requires storing the previous values of information about the link. We use the Newell-Daganzo method to calculate the upstream and downstream cumulative vehicle counts for a given node at a point Δt in the future:

$$N^{\downarrow}(t+\Delta t) = \min\{N^{\uparrow}((t+\Delta t) - \tfrac{L}{u_{\mathrm{f}}}), q_{max}\Delta t\} \tag{6.6}$$

We can then get the sending flow as the difference between $N^{\downarrow}(t+1)$ and $N^{\downarrow}(t)$.

$$S(t) = \min\{N^{\uparrow}((t+\Delta t) - \frac{L}{u_{\mathrm{f}}}) - N^{\downarrow}(t), q_{max}\Delta t\} \tag{6.7}$$

In order to get the receiving flow, we have to consider the congested wave speed $-w$ to include the case where the upstream end of the link is congested. We consider the difference between a stationary point at the start of the link $N(0,t)$ and the point at the end of the link $N(L, t - \frac{L}{w})$ along with the possible flows from (6.5) to get:

$$N^{\uparrow}(t+\Delta t) = \min\{N^{\uparrow}(t) + q_{max}\Delta t, N^{\downarrow}((t+\Delta t) - \tfrac{L}{w}) + k_{\mathrm{j}}L\} \tag{6.8}$$

$$R(t) = \min\{q_{max}\Delta t, (N^{\downarrow}((t+\Delta t) - \tfrac{L}{w}) + k_{\mathrm{j}}L) - N^{\uparrow}(t)\} \tag{6.9}$$

Now that we have determined how to carry out the network loading step, the next step in the model is for drivers to use the travel times of links to determine the shortest path for them to take. This is also where we modify the dynamic traffic assignment model so that connected vehicles will re-route to use SPaT nodes. Pathfinding is

completed using Dijkstra's Algorithm and the node network at the current time step [9]. The travel time used in standard dynamic traffic assignment is the saved observed average travel time.

For this project, we diverge from the standard Dijkstra's algorithm for a road network to construct a generalized cost function, where the cost of traveling each link is the travel time minus a discount for the money saved from traveling through a SPaT node (which is only applied on links which terminate with a SPaT node). We do this to model drivers traveling slightly out of their way to save money on gas. We calculate the SPaT discount by determining the gallons used on the link from its length L, the average mile per gallon of vehicles from the EPA of $22mpg$ [4], and the average cost per gallon in Minnesota as of 10/18/2021 \$3.1 [5]. From this cost of fuel used on the link, we use the federal value of time saved $\$13.60/hour$ [19]. This study occurs during the peak commuting hour, and the federal guidance for value of time states that this value is sufficient for commuter travel. We also use the calculated energy benefit e for CAVs in a ten-vehicle platoon at each market penetration rate from Task 5.

$$\text{Travel Time Cost} = \text{Travel Time} - \text{SPaT Discount} \tag{6.10}$$

$$\text{SPaT Discount} = \left(\frac{L}{22mpg}\right) e * \frac{\$3.01/gal}{\$13.60/hr} \tag{6.11}$$

Note that the magnitude of the discount is sensitive to all of these parameters. An increase in average fuel mileage would cause less gas to be used on the SPaT link, making it less likely to be worthwhile to re-route for the increased efficiency. An increased value of time would make it more important that a driver reaches their destination as fast as possible and thus reduce SPaT discount and the likelihood of a driver rerouting for the SPaT node. An upwards shock in gas prices could make it significantly more worthwhile to re-route to the SPaT node to save on fuel, and an avenue for future consideration would be to examine the impact of the increased fuel efficiency from SPaT if a hefty carbon tax were to be imposed.

The final step is to update the path flows and solve for dynamic user equilibrium.

Dynamic user equilibrium is achieved when the gap between the travel cost on the paths used by drivers and the minimum possible travel costs is zero. We approach dynamic user equilibrium as the gap gets smaller, once it is sufficiently small we say that the solution is sufficiently close to dynamic user equilibrium. More precisely, we define the shortest path travel time (SPTT) as the sum of the shortest path travel time costs across all origin destination pairs. Let each origin-destination pair be denoted (r, s) for departure time t, the least possible travel time between (r, s) at t be $\tau^*_{rs,t}$, the demand at the same time d^{rs}_t, and the set of starting or ending nodes $\mathcal{Z}$. Then:

$$SPTT = \sum_{(r,s)\in\mathcal{Z}^2} \sum_t d^{rs}_t \tau^*_{rs,t} \tag{6.12}$$

Total system travel time (TSTT) is the sum of the actual total travel time cost experienced by all drivers on the network. We use travel time cost in this report to clarify that the TSTT is the sum of all travel time costs, including travel times that have been discounted thanks to the SPaT node. Let Π be the set of all paths π, h_t^π be the number of vehicles traveling on path π during time t, and τ_π^t be the travel time cost of π at t. Then:

$$TSTT = \sum_{\pi \in \Pi} \sum_{t} h_t^\pi \tau_\pi^t \tag{6.13}$$

Finally, the gap that approaches 0 as dynamic user equilibrium is approached is $\frac{TSTT - SPTT}{SPTT}$.[7]

To find dynamic user equilibrium, use the method of successive averages. To do this, we follow the algorithm:

1. Initialize the path flows to a feasible value
2. Preform network loading to obtain path travel times
3. Identify time-dependent shortest paths
4. Check if gap is small enough. Terminate if it is and if it is not, update route choices towards equilibrium and go back to step 2

For each iteration, we do not want to change all the paths as some portion of travelers have already chosen their best path. At the start, all travelers make their optimum choice. Then, the network loading and time-dependent shortest path steps occur. For some amount of travelers, their new time-dependent shortest path will be different because of new congestion from other travelers re-routed. This re-routing will again mean that the shortest path for some travelers will be different, but this will only be true for a decreasing amount of travelers at each iteration as more travelers have found an optimal route. Thus, a step size λ is chosen at each iteration for the proportion of travelers to move onto new paths. In the method of successive averages, $\lambda = \frac{1}{iteration}$. So in the first iteration $\lambda = 1$ as all travelers are adjusted, but it decreases for each iteration as dynamic user equilibrium is approached. [7]

In order to demonstrate that the new formulation for travel time cost models traveler route choice changes due to the SPaT eco-driving discount, a simulation is ran on a 5-node test network with 175 vehicles at different levels of market penetration. In Figure 7.4, node 3 is a SPaT enabled node. The free-flow time of taking the path from (1,2,4,5) is 62 seconds. The free-flow time without a SPaT travel time discount of taking the path from (1,2,3,4,5) is 80 seconds. Figure 6.2 shows the route choices for the CVs in the network. At 20% and 25% fuel economy discount, the total travel time cost for both routes is about equal, so most but not all vehicles use the

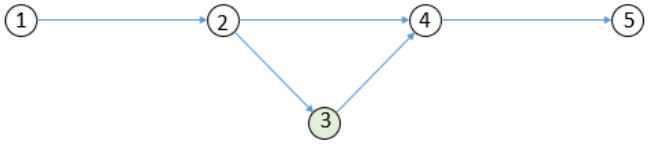

Figure 6.1: Test Network

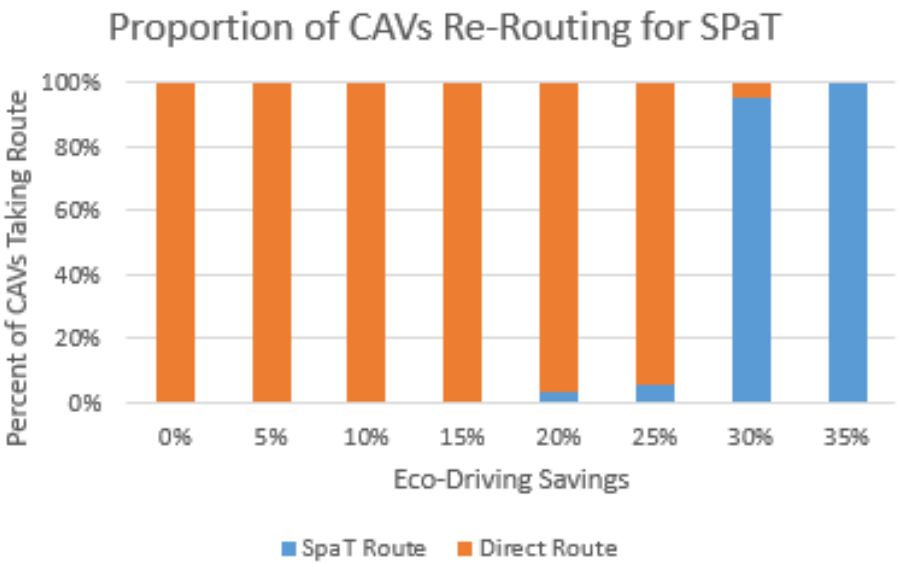

Figure 6.2: Proportion of CAVs Who Take Longer Spat Route

more direct path. At 30% or beyond, the eco-driving discount is sufficient that the SPaT-enabled route has a lower travel time cost than the direct route, so the majority of vehicles take the more circuitous SPaT-enabled route.

6.3 Twin Cities Network

For this study, we use the DynusT network and demand model provided by MnDOT and converted for use with Dynamic Traffic Assignment. In this model, there are 29,013 links and 10,943 nodes (see Figure 6.3). We designate the 22 SPaT nodes on TH-55 as a special case of a SPaT intersection. The list of origin-destination pairs across all time periods comes out to more than 60 origin-destination pairs, so we limit the scope of the study to just one hour at 8am (during peak commuting time) to ensure the simulation can complete in a reasonable amount of time. Task 7 will include more simulations for the entire day and consider other connected-corridor installation locations for a thorough cost-benefit analysis. At this hour, there are 710,052 vehicles who travel on the network across 1,593,813 possible origin-destination pairs. We set the duration of an assignment interval to be 15 minutes (900s), and the duration of the demand interval for the hour of 8am to 2 hours (7200s).

As a result of the large magnitude of the 710,052 vehicles, the data was discretized in units of 10. The

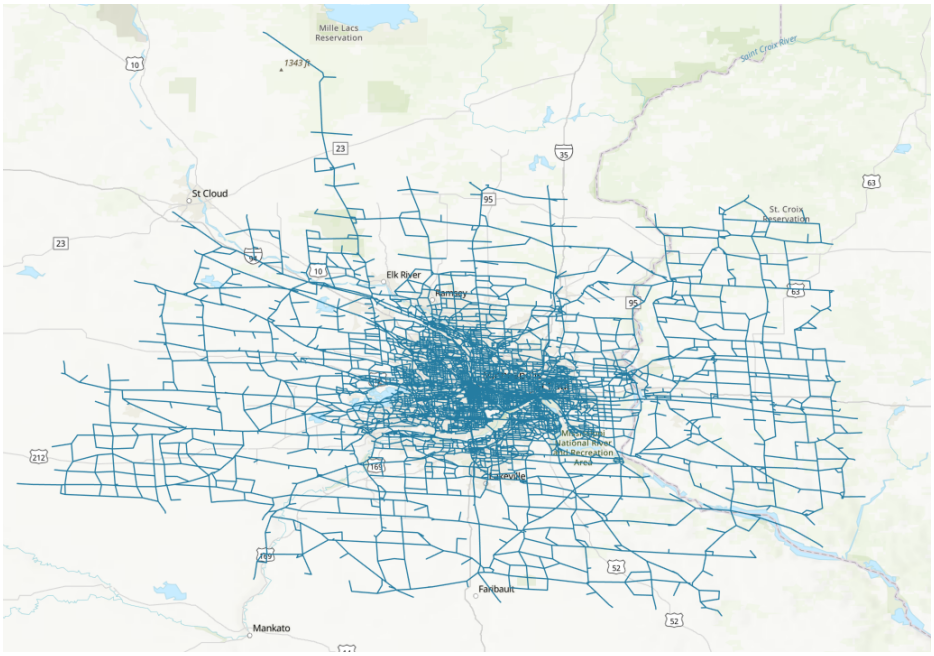

Figure 6.3: Twin Cities Network Model

simulation is ran for units representing ten vehicles for a total of 71,148 units. This does not impact the congestion modeling of the simulation as the capacity was also scaled down by ten, but not the congested wave speed or free flow speed. Thus vehicles travel just as quickly though the network and links become just as congested with one unit of ten vehicles as they would with ten individual vehicles. When observing the data for fuel savings, the value from the simulation is multiplied by ten so as to show the total fuel saved for all the vehicles, and not on a per-unit basis.

6.4 Numerical Results

Five different simulations were run at different market penetration rates of CAVs. The observed market penetration rate of the TH-55 was observed, as well as the travel time of CAVs taking TH-55, and the total distance traveled by CVs on the highway. This distance was used to determine total fuel savings from the eco-driving discount during this hour of the morning commute. Simulations ran for 25 hours on average. They were run on three machines, one with an Intel Xeon CPU E3-1230 v6 @ 3.50GHz, 3501 Mhz with 4 Cores and 8 Logical Processors, an Intel Core i5-7500 CPU @ 3.40GHz, 3408 Mhz with 4 Cores and 4 Logical Processor(s), and an Intel Core i7-6700K processor Quad-core 4 GHz. Figure 6.4 shows that we were able to find dynamic user equilibrium.

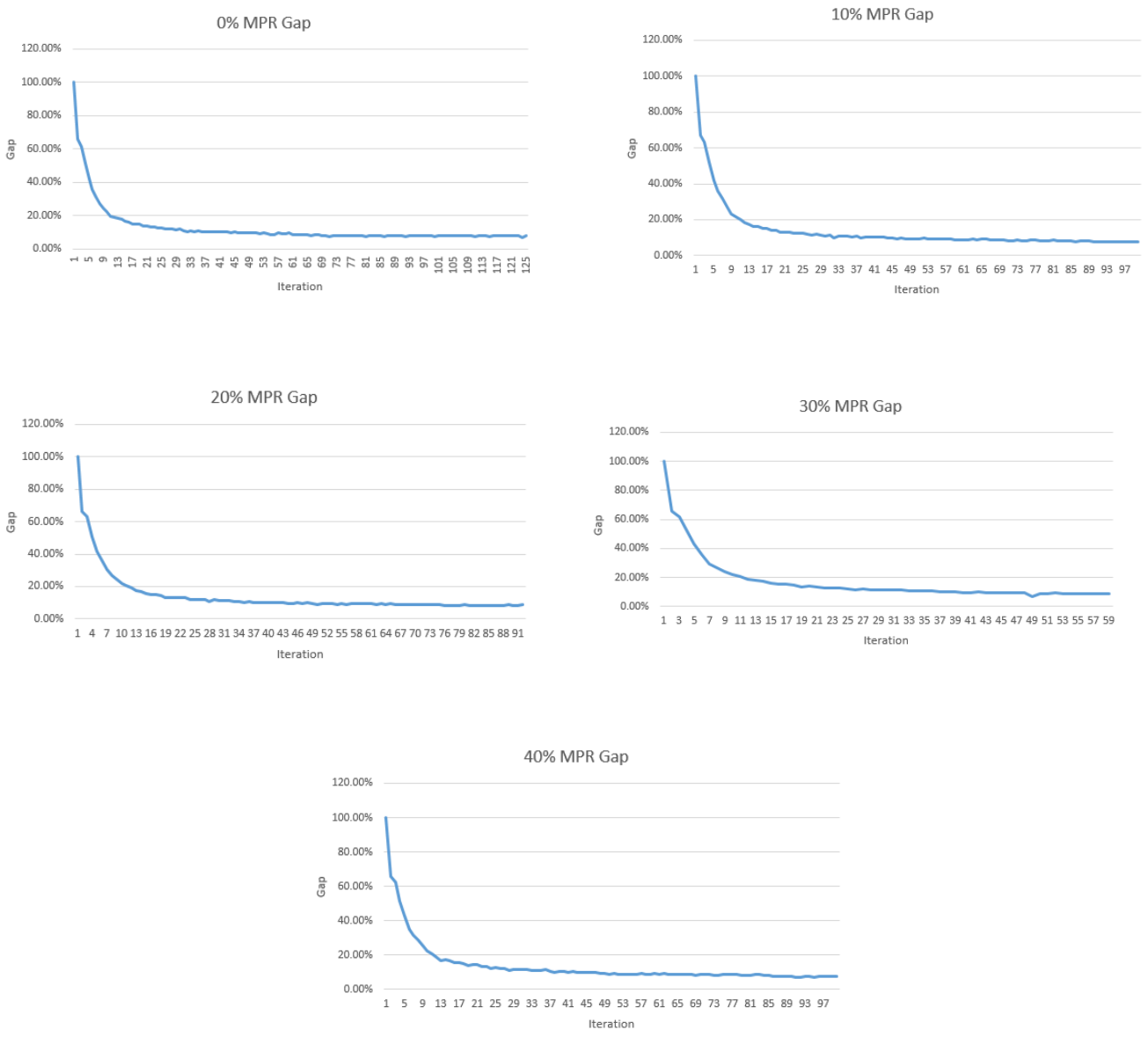

Figure 6.4: Gap Proportions

Figure 6.5 shows the observed market penetration rate of TH-55 compared to the market penetration rate of CAVs for all vehicles in the network. They are similar, showing that there was not a significant amount of extra CAVs re-routing specifically for TH-55. This tracks with Figure 6.6, which shows the average travel time of all vehicles who used TH-55. If there were to be significant re-routing, then we would expect to see market penetration rates above the base market penetration rate of all demand. This re-routing would potentially increase the congestion of TH-55, which would show in Figure 6 as lower average travel times as demand increases. These results are reasonable as most commuters are already taking their fastest route, so it would require a significant incentive to switch to a completely different thoroughfare. The total length of the SPaT corridor traveled by all CAVs is 47.64 miles, so the actual travel time discount listed in Table 1 ranges from 3.8 - 4.2 minutes. This compared

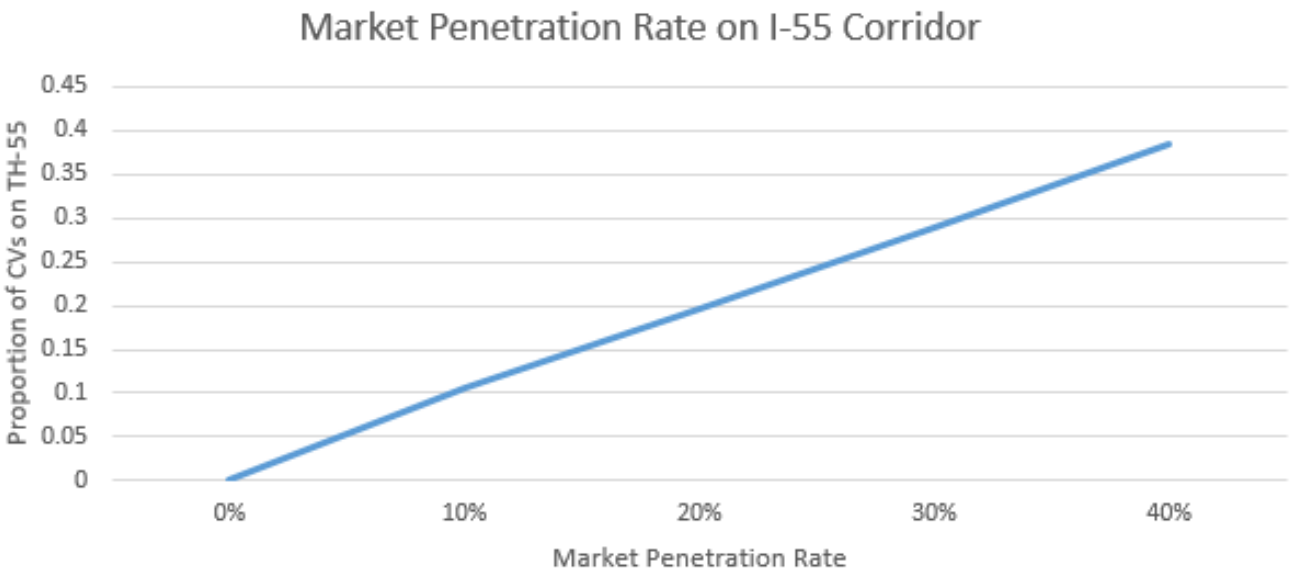

Figure 6.5: Observed TH-55 Market Penetration Rate

MPR	Fuel Savings (from Task 5)	Travel Time Discount (min)	Gallons Saved for 1 Hour on TH-55	Number of CAVs using TH-55	Gallons Saved per Vehicle
0%	0%	0	0	0	0
10%	13.33%	3.83	9.54	2,050	0.047
20%	14.24%	4.10	21.78	3,780	0.058
30%	14.64%	4.21	30.69	5,848	0.053
40%	14.31%	4.11	38.27	7,470	0.051

Table 6.1: Eco-driving Fuel Savings

to the average travel times in Figure 6 of around an hour, the magnitude of the discount is small compared to the total travel time that it takes for vehicles on TH-55 to get to their destination. To demonstrate this, we observe average travel times on the free-way that is roughly parallel to TH-55, I-394, at the 40% MPR level. We find travel times ranging between 20 and 50 minutes, more than 4 minutes less than the around 60 minute travel times on TH-55. The four minutes in reduced travel time cost are not enough to make taking TH-55 cheaper for those vehicles, especially the vehicles only taking 20 minutes to reach their destination, so they stay on the larger and faster I394.

Figure 7 and Table 1 show the amount of fuel saved through the use of eco-driving on TH-55 for only the CAVs who use it. Table 1 also shows the values for e, the eco-driving fuel savings for a 10 vehicle CAV platoon from Task 5. At a market penetration rate of 40%, that is 38 gallons of fuel saved in total during this one hour of the day for only those $7,470$ vehicles. Task 7 will extend this analysis to include all hours of the day with more

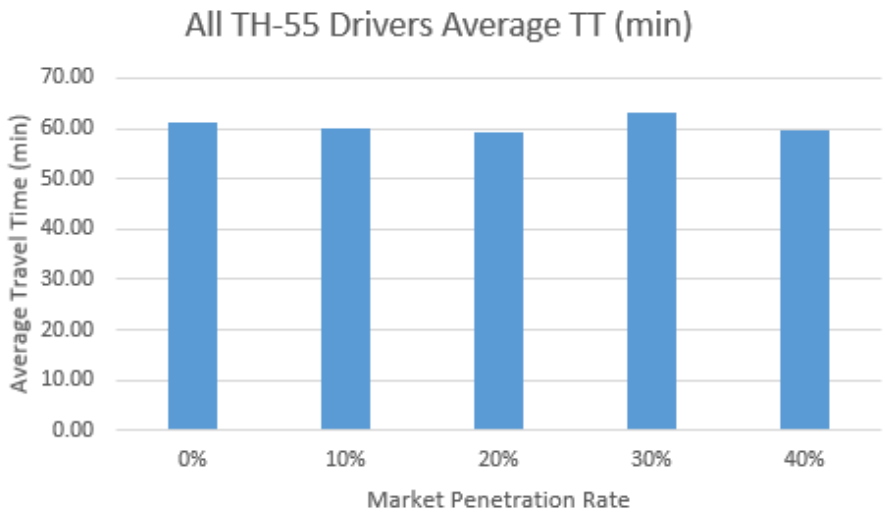

Figure 6.6: Average TT of drivers who used TH-55

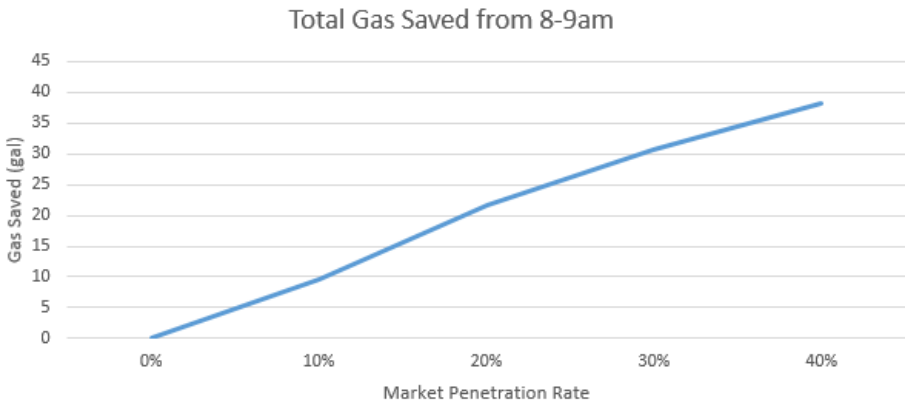

Figure 6.7: Fuel Savings from the CAVs on TH-55 from 8 - 9am

simulations from the MnDOT data. Assuming that this 1 hour is representative of all weekday trips at this hour, across the 261 working days of the year that is 9,918 gallons of fuel saved per year at 40% MPR and 2,490 gallons per year at 10% MPR.

6.5 Summary

In the previous tasks, it was shown that signal phase and timing (SPaT) can increase fuel efficiency when deployed with connected autonomous vehicles that drive at eco-speed on the approach to a stoplight. The purpose of this task was to model what the magnitude of those fuel savings were at the network-level. Dynamic traffic assignment was chosen to model the entire Twin Cities. The dynamic traffic assignment model was modified so that instead of seeking just to minimize travel time, drivers in the system seek to minimize travel time cost, which is travel time discounted for CAVs that travel using Trunk Highway 55 where SPaT signals are installed. It was decided to run

the simulation at peak hour in the morning when the most vehicles were on the road. Due to the enormous size of the Twin Cities network model, as well as the large number of vehicles on the road at peak hour, the simulation was run for one hour from 8 to 9 am in discretized units of 10. While there were not significant route changes observed because of the eco-speed fuel discount, it was observed that even for just one hour, many gallons of fuel were saved.

Task 7 will observe the magnitude of fuel savings across a larger time-horizon, as well as consider other highways that could be chosen to have SPaT equipment installed. We will then compare the benefits of increased SPaT connectivity to the costs. As more routes are chosen, more vehicles will use the SPaT route and so more fuel will be saved. It is also worth noting that vehicle route preferences, especially around fuel economy, are elastic. If there is a significant increase in the price of carbon, then the eco-benefits observed in this study will only become more important and desirable, and a follow-up could also consider a sensitivity analysis for the cost of fuel.

Chapter 7

Task 7: Cost/benefit analyses of connected corridor installation

December 31, 2021

Dynamic Traffic Assignment Model to Show Impact of Signal Phasing and Timing (SPaT) on Route Choice

Description: Using the fuel savings predictions from Tasks 4, 5, and 6, the project team will conduct a cost/benefit analysis of future SPaT deployments, comparing the benefits in fuel savings to drivers against the costs of installation, operations, and maintenance. This task will also consider the cost impacts of higher travel times caused by route choice changes. Different CV market penetration rates will be included in the analyses. The outcome will be a case study of scenarios indicating the cost/benefit of various connected corridor deployment options for MnDOT. The objective is to identify the optimal timing to deploy SPaT on other corridors for driver benefits.

7.1 Introduction

In the previous tasks, it has been shown that the use of signal phase and timing (SPaT) can increase fuel efficiency when deployed with connected autonomous vehicles (CAVs). In Task 5, the traffic prediction and vehicle speed optimization data from Task 3 were used to develop a holistic simulation methodology to predict the benefits in fuel consumption for vehicle platoons at various market penetration rates of CAVs. In Task 6, this method was applied to study the impact of CAV market penetrations on fuel consumption of vehicle platoons using vehicle speed data collected along Trunk Highway 55. While no significant re-routing behavior was discovered, it was observed that the fuel benefits from vehicles traveling along the connected corridor have the potential to be significant. In this task, the same dynamic traffic assignment methodology from Task 6 was used to discover the benefits of several prospective locations to install a new connected corridor in the Twin Cities region.

For the purposes of this analysis, three signalized highways were selected along with the already installed SPaT equipment along Trunk highway TH-55. The highways selected were Hiawatha Avenue, Highway 51, and Highway 3. 7.1 shows the location for the signalized highways included in the study.

7.2 Costs

The main costs involved with eco-driving control for SPaT deployments are for installation and maintenance of the SPaT units at signalized intersections. At each intersection, it is minimally necessary to deploy a signal controller, a roadside unit (RSU), and cables connecting the signal controller and the RSU. An optional connected vehicle roadside processor might be required if the functionality is not performed at the signal controller or at the RSU. The costs for deployment are highly dependent on the signal hardware that currently exists at an intersection. For example, signal controllers are already deployed at signalized intersections.

SPaT deployment depends on the signal controller's capability to send SPaT data and on software to translate the data from the controller into standard messages sent to connected vehicles by the RSU. The amount of equipment required for the signal controller to complete the task will depend on the model and age of the controller. The cost of software will depend on whether existing software meets the project needs or if MnDOT needs to develop proprietary software. In general, it is assumed that power is already available at the intersection. Cost estimates based on limited early deployments indicate that installation of a working system at an intersection is approximately $4,150 [Georgia DOT], which includes $1,300 per RSU, $850 per RSU deployment, and $2,000 per RSU configuration. According to [National Operations Center of Excellence (NOCoE)], it is expected that the equipment will commit to operating the SPaT broadcasts for a minimum of 10 years. For analysis, it is assumed that, on average, the cost of deploying SPaT at each intersection is $4,150 as reported in [Georgia DOT]. The 10-year costs for each corridor are thus estimated based off the number of traffic signals in for each intersection in

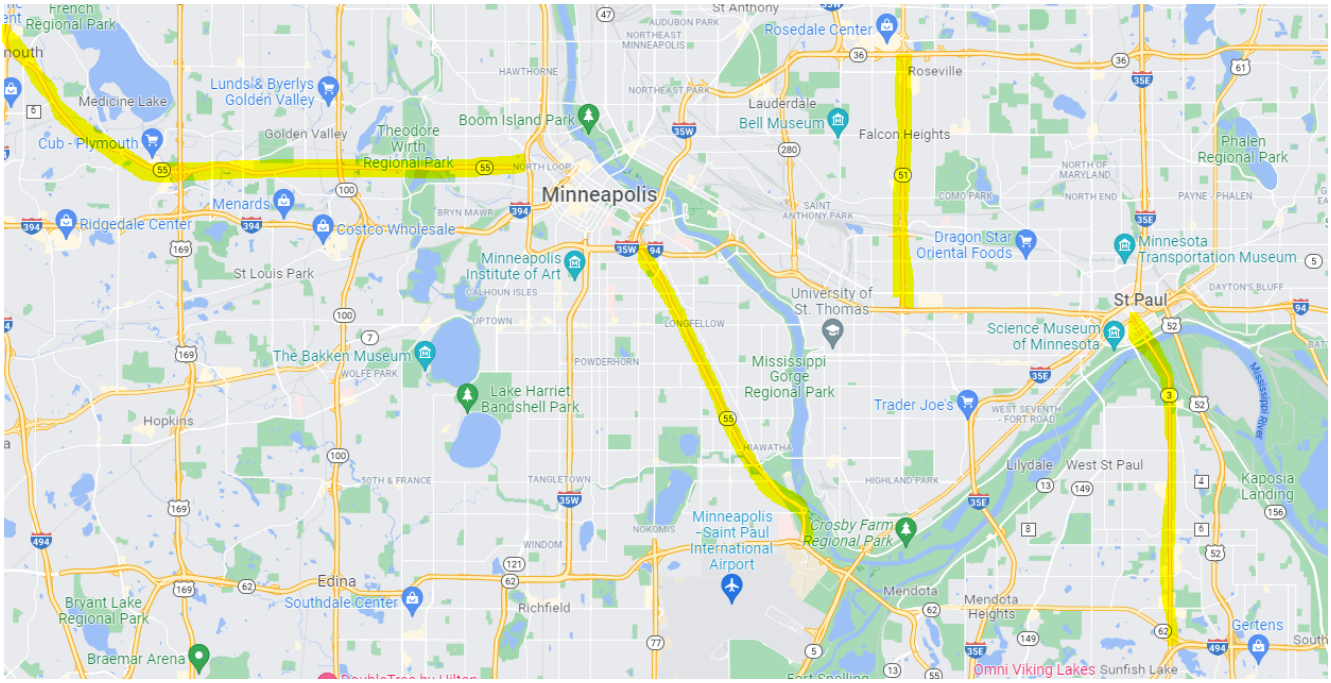

Figure 7.1: Study Corridors

Highway	Number of Intersections	10-Year Cost
Trunk Highway TH-55	23	$95,450
Hiawatha Avenue	15	$65,250
Highway 51	17	$70,550
Highway 3	16	$66,400

Table 7.1: SPaT Installation Costs

table 1.

In order to calculate the benefits accrued for each corridor over the 10-year study time, the same modified dynamic traffic assignment model as in Task 6 was used and is explained below. The model was run for the three hour rush hour at different market penetration rates. There were 1,654,830 trips, so due to the large magnitude of the simulation, the data was discretized in units of 10. The simulation is ran for units representing ten vehicles for a total of 165,483 units. This does not impact the congestion modeling of the simulation as the capacity was also scaled down by ten, but not the congested wave speed or free flow speed. Thus vehicles travel just as quickly though the network and links become just as congested with one unit of ten vehicles as they would with ten individual vehicles. When observing the data for fuel savings, the value from the simulation is multiplied by ten so as to show the total fuel saved for all the vehicles, and not on a per-unit basis. The model was run across the entire Twin Cities node network (see Figure 7.2), using data from the MnDOT's Dynus-T model. The process took 135 hours with 1,654,830 vehicle trips. It was run on an Intel Xeon CPU E3-1230 v6 @ 3.50GHz, 3501 Mhz with 4

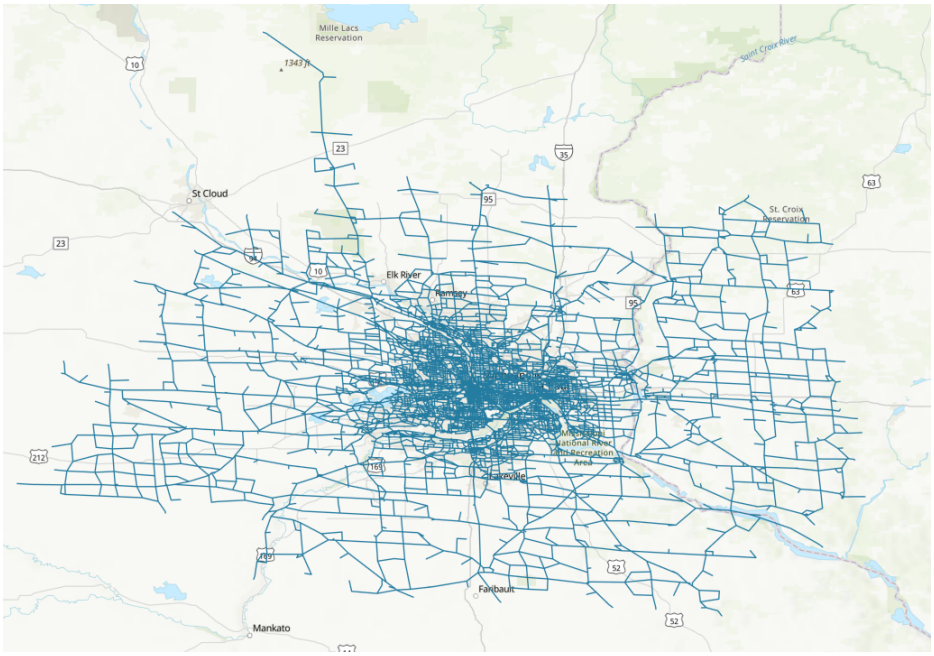

Figure 7.2: Twin Cities Network Model

Cores and 8 Logical Processors. As a result of how long the simulation was run for, it was necessary to create sub-networks to consider each corridor under different market penetration rates. Sub-networks were created by selected each corridor to be selected and the surrounding roads, and then isolating this new network from the large-scale Twin-Cities network. These sub-networks are shown in Figure 7.3. The demand was created for each of these sub-networks from the vehicle paths generated by the overall Dynamic Traffic Assignment model. The convergence rates of the gap for the model are shown in Figures 7.6–7.9 for all the sub-networks.

7.3 Benefits

7.4 Modified Dynamic Traffic Assignment Methodology

Traffic assignment modeling is the process of using networks to model real-life roadway conditions and congestion. The roadway system is modeled with links and nodes, where links represent roads and nodes represent intersections. A traffic assignment model is used to predict the flow of drivers on each roadway segment, called a link flow. There are two main types of traffic assignment models, static and dynamic.

Static models were the first to be developed, and do not consider the element of time. They assign trips from the demand data and predict travel times using a link performance function, typically dependent on the free flow time and capacity of each link. Dynamic traffic assignment models track changes to congestion over time, which requires storing the location of vehicles on the network at the same level of detail as the link flows to be

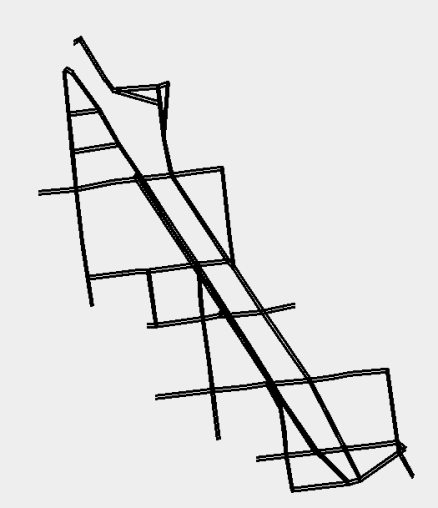

(a) Hiawatha Avenue Sub-network

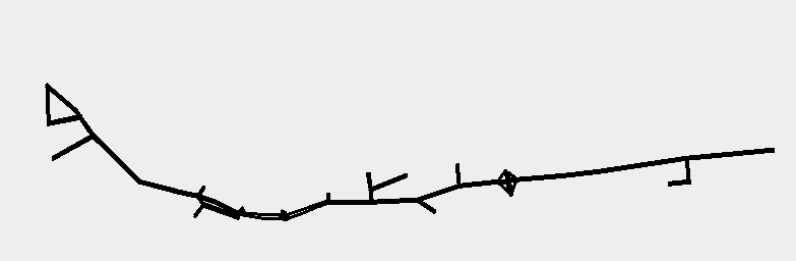

(b) TH-55 Sub-Network

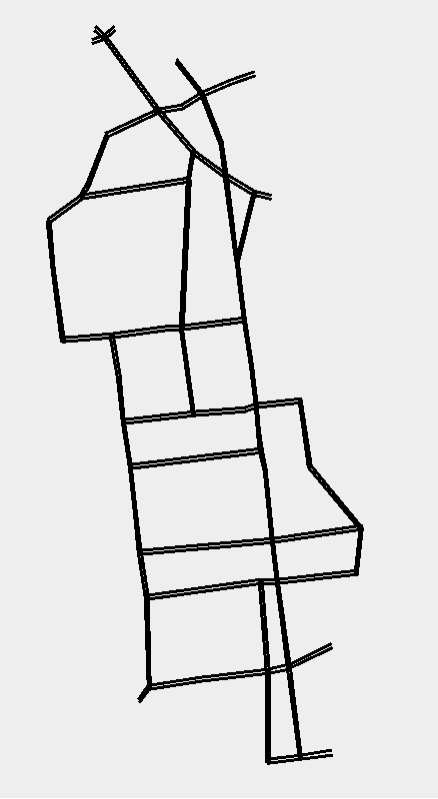

(c) Highway 3 Sub-Network

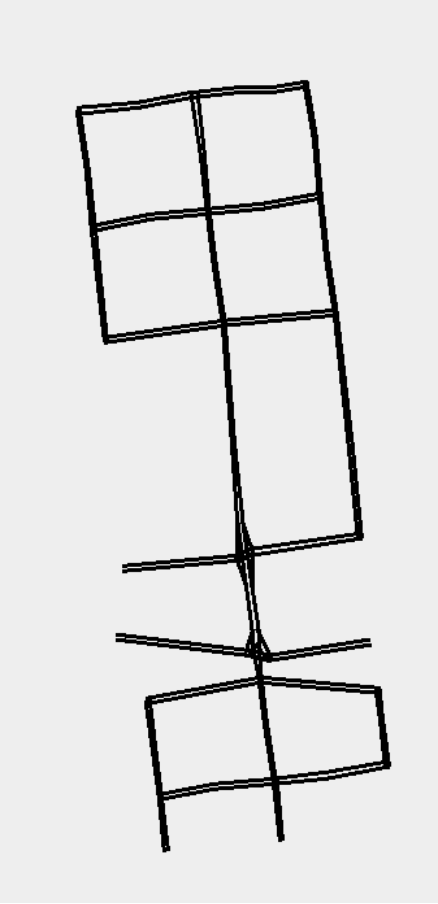

(d) Highway 51 Sub-Network

Figure 7.3: Sub-Networks

tracked. As congestion changes over time, the model is solved when *dynamic user equilibrium* is reached. This is achieved when all the paths used by drivers departing the same origin, for the same destination, at the same time, have equal and minimal travel times. Due to the dynamic nature of dynamic traffic assignment, it is possible for there to be multiple equilibrium states or no equilibrium. In dynamic user equilibrium, drivers choose routes based off of their experienced travel times, with the underlying assumption being that drivers are familiar enough with the network to anticipate likely changes in congestion (and thus travel time) in order to make an informed decision on their route choice. As we model the morning commute in this study, this is a reasonable assumption. This means that it is only possible to solve the problem through an iterative process, such as the method of successive averages used in this study. [7].

As this task uses dynamic traffic assignment, we will focus solely on it. There is a three step process for dynamic traffic assignment.

1. Network Loading: The traffic flow model is used to predict the time dependent travel times on each link, with the routes and departure times of drivers as input.

2. Path Finding: With the travel time of each link obtained from network loading, all the drivers at a certain time find the shortest route to their destination

3. Route Updating: Vehicles are shifted from their current paths onto the new, shorter paths. The traffic flow model is updated with the new vehicle paths.

To perform the network loading step, it is necessary to model the state of each link and node. As the model is time dynamic, time is discretized into time steps Δt. Each link outputs a sending and receiving flow $S(t), R(t)$ for a particular timestep, which denotes the number of vehicles leaving and entering the link respectively. Nodes, which are between links, take the sending flow of all the links going to the node and the receiving flow of the links going from the node and calculate the turning movement flow for each possible movement (ie, which link a vehicle turns onto when as it crosses an intersection). The Newell-Daganzo method is used to calculate the sending and receiving flow for links ([18], [8]).

In order to have a realistic model of vehicle flows, it is necessary to use traffic flow theory. The most basic assumption in traffic flow theory is from the Lighthill-Whitham-Richards model relating flow q (rate at which vehicles pass a certain point), density k (spatial concentration of vehicles), and speed u (the average rate of travel) [15].

$$q = uk \tag{7.1}$$

Although equation (7.1) was originally developed for freeway flow, it has been used extensively in the literature

for signalized roads. To use traffic flow theory to find the counts of vehicles at certain points on the network, we introduce another variable $N(t,x)$ which is defined as the cumulative count of vehicles that have passed point x at time t. This allows us to create the relationship between q, u, and k:

$$\frac{\partial N}{\partial t} = q \tag{7.2}$$

$$\frac{\partial N}{\partial x} = -k \tag{7.3}$$

$$\frac{\partial q}{\partial x} + \frac{\partial k}{\partial t} = 0 \tag{7.4}$$

$\frac{\partial N}{\partial x} = -k$ because the cumulative count decreases as the x position increases. This allows us to find the flow $q(t,x)$, density $k(t,x)$, and speed $u(t,x)$ if we are given $N(t,x)$ [18].

With this traffic theory in mind, we now seek to find the cumulative counts at both ends of each link. Let L be the length of a given link, u_{f} the free flow speed of the link, w the congested wave speed, k_{j} the jam density, and $q_{\max}$ the link capacity. We use the Newell-Daganzo [18] method to find the fundamental diagram (in this case, trapezoidal):

$$Q(k) = \min\{u_{\mathrm{f}}k, q_{\max}, w(k_{\mathrm{j}} - k)\} \tag{7.5}$$

In this study, we use the link transmission model to calculate the sending and receiving flows for links [38]. It only involves calculations at each end of the link, but requires storing the previous values of information about the link. We use the Newell-Daganzo method to calculate the upstream and downstream cumulative vehicle counts for a given node at a point Δt in the future:

$$N^{\downarrow}(t+\Delta t) = \min\{N^{\uparrow}((t+\Delta t) - \tfrac{L}{u_{\mathrm{f}}}), q_{max}\Delta t\} \tag{7.6}$$

We can then get the sending flow as the difference between $N^{\downarrow}(t+1)$ and $N^{\downarrow}(t)$.

$$S(t) = \min\{N^{\uparrow}((t+\Delta t) - \frac{L}{u_{\mathrm{f}}}) - N^{\downarrow}(t), q_{max}\Delta t\} \tag{7.7}$$

In order to get the receiving flow, we have to consider the congested wave speed $-w$ to include the case where the upstream end of the link is congested. We consider the difference between a stationary point at the start of the link $N(0,t)$ and the point at the end of the link $N(L, t - \frac{L}{w})$ along with the possible flows from equation (7.5) to get:

$$N^{\uparrow}(t+\Delta t) = \min\{N^{\uparrow}(t) + q_{max}\Delta t, N^{\downarrow}((t+\Delta t) - \tfrac{L}{w}) + k_{\mathrm{j}}L\} \tag{7.8}$$

$$R(t) = \min\{q_{max}\Delta t, (N^{\downarrow}((t+\Delta t) - \tfrac{L}{w}) + k_{\mathrm{j}}L) - N^{\uparrow}(t)\} \tag{7.9}$$

Now that we have determined how to carry out the network loading step, the next step in the model is for drivers to use the travel times of links to determine the shortest path for them to take. This is also where we modify the dynamic traffic assignment model so that connected vehicles will re-route to use SPaT nodes. Pathfinding is completed using Dijkstra's Algorithm and the node network at the current time step [9]. The travel time used in standard dynamic traffic assignment is the saved observed average travel time.

For this project, we diverge from the standard Dijkstra's algorithm for a road network to construct a generalized cost function, where the cost of traveling each link is the travel time minus a discount for the money saved from traveling through a SPaT node (which is only applied on links which terminate with a SPaT node). We do this to model drivers traveling slightly out of their way to save money on gas. We calculate the SPaT discount by determining the gallons used on the link from its length L, the average mile per gallon of vehicles from the EPA of $22mpg$ [4], and the average cost per gallon in Minnesota as of 10/18/2021 of \$3.01 [5]. From this cost of fuel used on the link, we use the federal value of time saved $\$13.60/hour$ [19]. This study occurs during the peak commuting hour, and the federal guidance for value of time states that this value is sufficient for commuter travel. We also use the calculated energy benefit e for CAVs in a ten-vehicle platoon at each market penetration rate from Task 5. The energy benefit is the value of fuel savings converted to units of time via the cost of fuel and the value of time.

$$\text{Travel Time Cost} = \text{Travel Time} - \text{SPaT Discount} \tag{7.10}$$

$$\text{SPaT Discount} = \left(\frac{L}{22mpg}\right) e * \frac{\$3.01/gal}{\$13.60/hr} \tag{7.11}$$

Note that the magnitude of the discount is sensitive to all of these parameters. An increase in average fuel mileage would cause less gas to be used on the SPaT link, making it less likely to be worthwhile to re-route for the increased efficiency. An increased value of time would make it more important that a driver reaches their destination as fast as possible and thus reduce SPaT discount and the likelihood of a driver rerouting for the SPaT node. An upwards shock in gas prices could make it significantly more worthwhile to re-route to the SPaT node to save on fuel, and an avenue for future consideration would be to examine the impact of the increased fuel efficiency from SPaT if a hefty carbon tax were to be imposed.

The final step is to update the path flows and solve for dynamic user equilibrium.

Dynamic user equilibrium is achieved when the gap between the travel cost on the paths used by drivers and the minimum possible travel costs is zero. We approach dynamic user equilibrium as the gap gets smaller, once it is sufficiently small we say that the solution is sufficiently close to dynamic user equilibrium. More precisely, we define the shortest path travel time (SPTT) as the sum of the shortest path travel time costs across all origin destination pairs. Let each origin-destination pair be denoted (r, s) for departure time t, the least possible travel

time between (r, s) at t be $\tau^*_{rs,t}$, the demand at the same time d^{rs}_t, and the set of starting or ending nodes $\mathcal{Z}$. Then:

$$SPTT = \sum_{(r,s)\in\mathcal{Z}^2} \sum_t d^{rs}_t \tau^*_{rs,t} \tag{7.12}$$

Total system travel time (TSTT) is the sum of the actual total travel time cost experienced by all drivers on the network. We use travel time cost in this report to clarify that the TSTT is the sum of all travel time costs, including travel times that have been discounted thanks to the SPaT node. Let Π be the set of all paths π, h^π_t be the number of vehicles traveling on path π during time t, and τ^t_π be the travel time cost of π at t. Then:

$$TSTT = \sum_{\pi\in\Pi} \sum_t h^\pi_t \tau^t_\pi \tag{7.13}$$

Finally, the gap that approaches 0 as dynamic user equilibrium is approached is $\frac{TSTT-SPTT}{SPTT}$.[7]

To find dynamic user equilibrium, use the method of successive averages. To do this, we follow the algorithm:

1. Initialize the path flows to a feasible value
2. Perform network loading to obtain path travel times
3. Identify time-dependent shortest paths
4. Check if gap is small enough. Terminate if it is and if it is not, update route choices towards equilibrium and go back to step 2

For each iteration, we do not want to change all the paths as some portion of travelers have already chosen their best path. At the start, all travelers make their optimum choice. Then, the network loading and time-dependent shortest path steps occur. For some amount of travelers, their new time-dependent shortest path will be different because of new congestion from other travelers re-routed. This re-routing will again mean that the shortest path for some travelers will be different, but this will only be true for a decreasing amount of travelers at each iteration as more travelers have found an optimal route. Thus, a step size λ is chosen at each iteration for the proportion of travelers to move onto new paths. In the method of successive averages, $\lambda = \frac{1}{iteration}$. So in the first iteration $\lambda = 1$ as all travelers are adjusted, but it decreases for each iteration as dynamic user equilibrium is approached. [7]

In order to demonstrate that the new formulation for travel time cost models traveler route choice changes

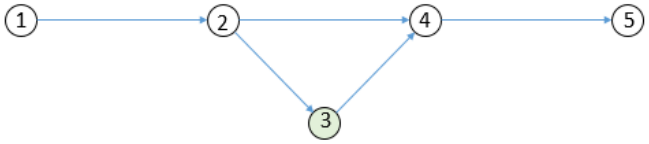

Figure 7.4: Test Network

due to the SPaT eco-driving discount, a simulation is ran on a 5-node test network with 175 vehicles at different levels of market penetration. In Figure **??**, node 3 is a SPaT enabled node. The free-flow time of taking the path from (1,2,4,5) is 62 seconds. The free-flow time without a SPaT travel time discount discount of taking the path from (1,2,3,4,5) is 80 seconds. Figure 7.5 shows the route choices for the CVs in the network. At 20% and 25% fuel economy discount, the total travel time cost for both routes is about equal, so most but not all vehicles use the more direct path. At 30% or beyond, the eco-driving discount is sufficient that the SPaT-enabled route has a lower travel time cost than the direct route, so the majority of vehicles take the more circuitous SPaT-enabled route.

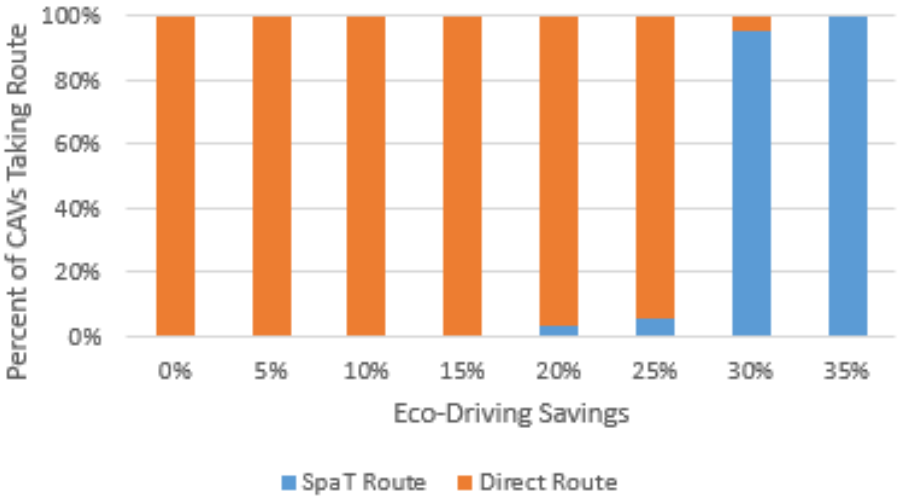

Figure 7.5: Proportion of CAVs Who Take Longer Spat Route in Test Network

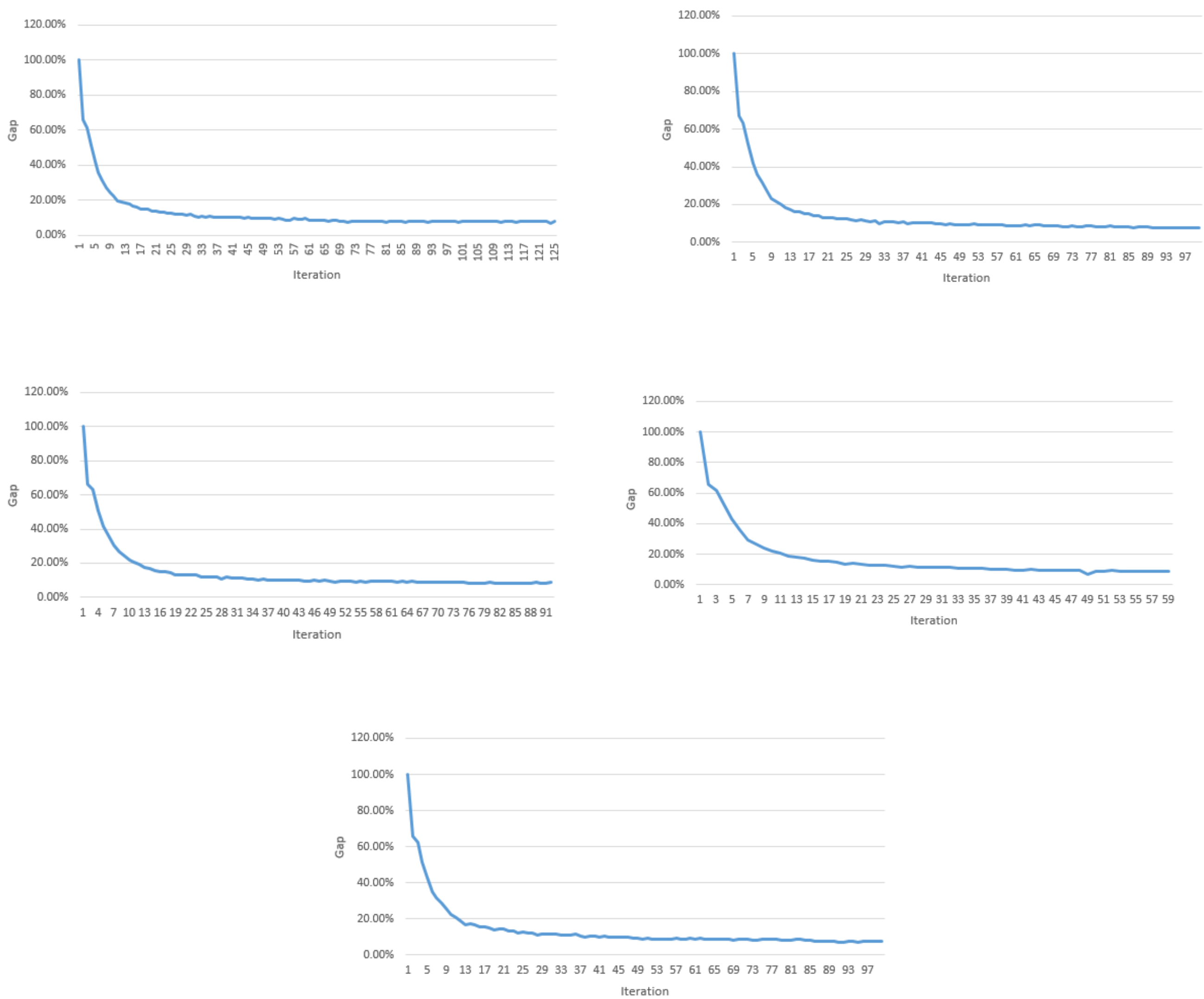

Figure 7.6: Gap Proportions — Trunk Highway TH55

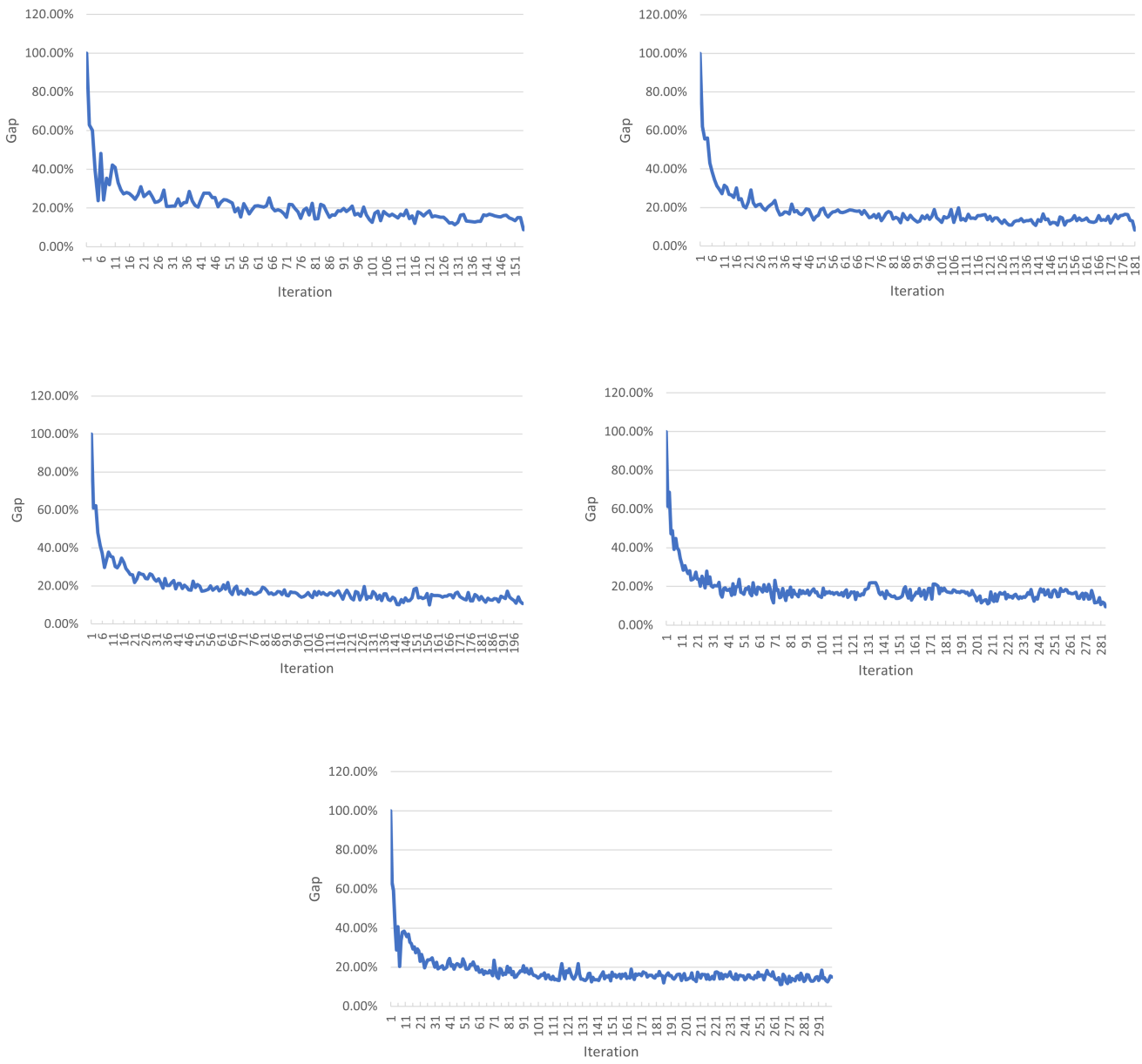

Figure 7.7: Gap Proportions — Hiawatha Avenue

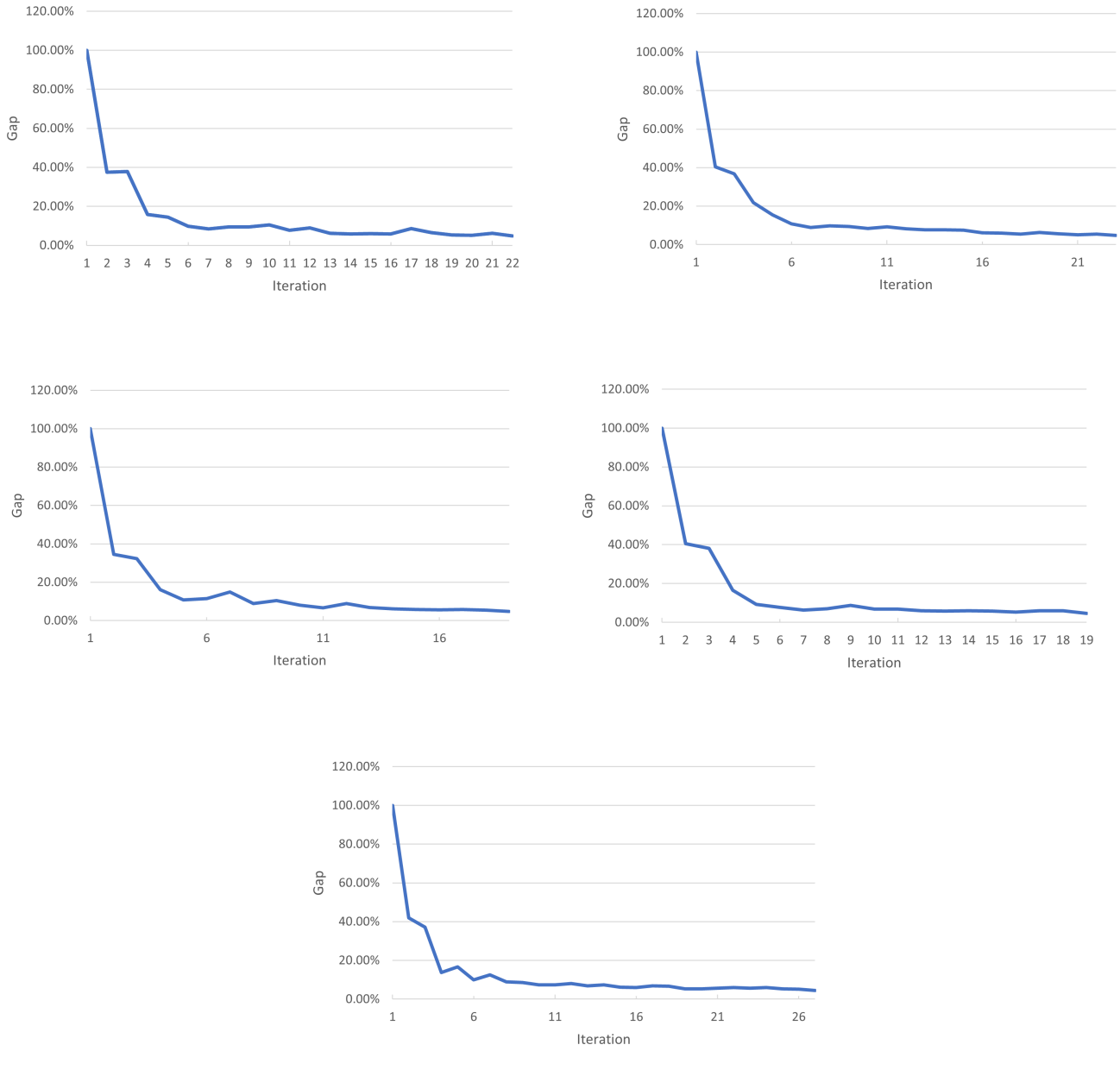

Figure 7.8: Gap Proportions — Highway 3

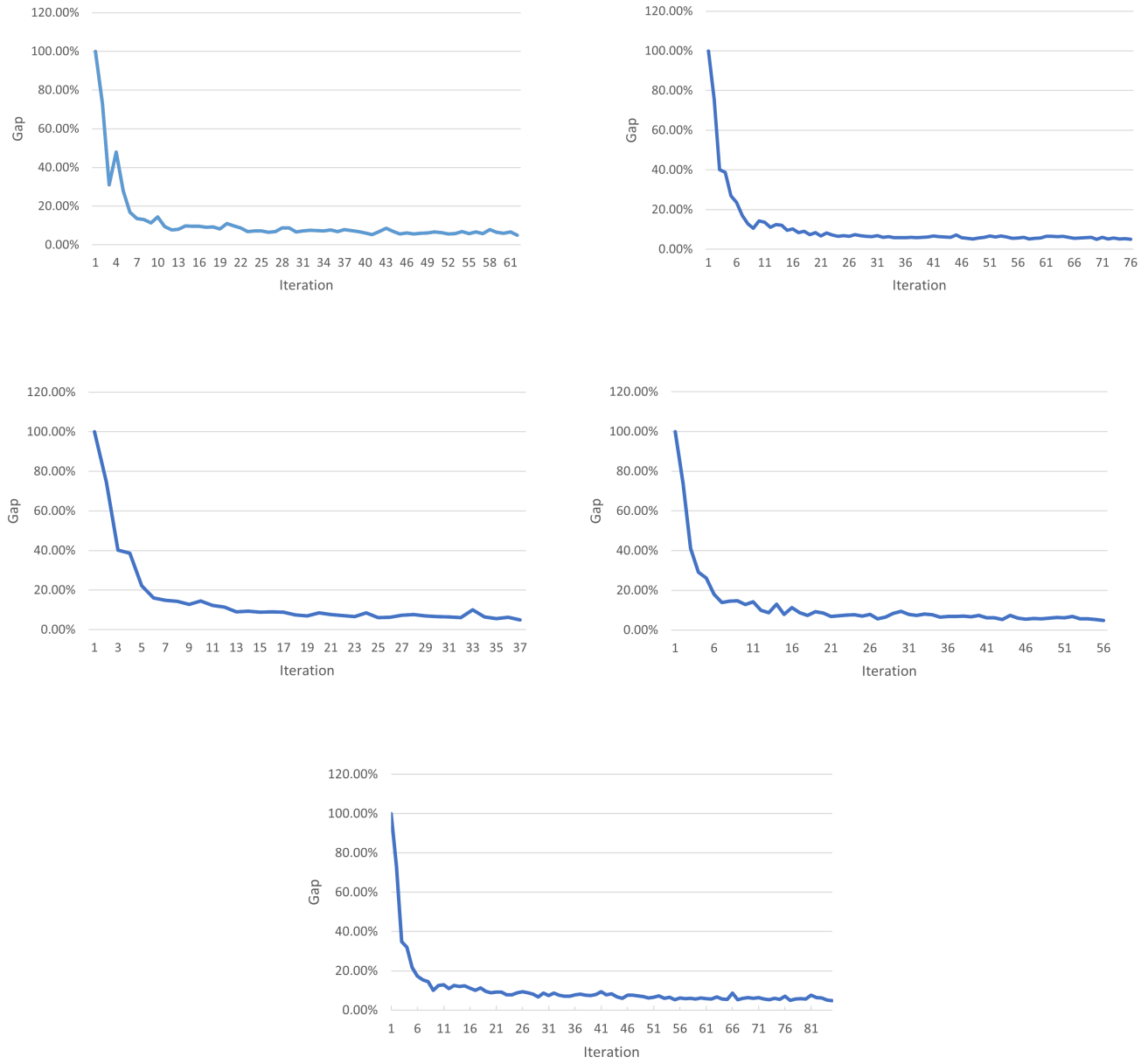

Figure 7.9: Gap Proportions — Highway 51

7.5 Results

The miles traveled by CAVs along eco-speed control routes (roads controlled by SPaT-enabled signals) are divided by the Minnesota average fuel mileage of 22mpg [4] to get the total amount of fuel consumed. This fuel mileage is then multiplied by the percent fuel savings calculated in the previous task. These three hours at maximum rush are assumed to be similar both in the morning and evening peak. Thus the total six hour fuel savings are considered for the benefits for a single day, which was then multiplied by 261 to to consider all the weekdays in a year, which was then multiplied by 10 to consider the entire 10-year period. As a result of this step in the analysis, the benefits

were underestimated as the vehicles who traverse the SPaT-enabled nodes at an off-peak time are not considered, so the fuel benefits calculated here are likely to be an underestimation. At the end of the traffic assignment period, the miles of road that Connected Autonomous Vehicles traveled along each SPaT corridor was determined. This was then used with the fuel savings observed in the previous tasks to determine how many gallons of fuel were saved, from which the dollar value of the fuel saved was determined for the purpose of the analysis. The detailed results can be seen in table 7.2. The results from that table were then extracted to determine the cost-benefit ratio for install the entire SPaT corridor in table 7.3, and also calculated on a per-unit basis in table 7.4.

Highway:		0% MPR	10%MPR	20%MPR	30%MPR	40%MPR
Fuel Savings (From Task 5)		0%	13.44%	14.24%	14.67$	14.31%
Th-55	1 Day CAV SPaT Miles	0	5000.6	9446.44	14652.64	19395.64
	1 Day Fuel Savings (gal)	0.00	30.30	61.16	97.71	126.16
	1 Year Fuel Savings (gal)	0.00	7908.06	15963.13	25501.39	32927.71
23 SPaT Intersections	10 Year Fuel Savings (gal)	0.00	79080.62	159631.27	255013.88	329277.14
	10 Year Dollar Savings	$ -	$ 245,149.94	$ 494,856.93	$ 790,543.03	$ 1,020,759.12
	10 Years Benefits Per Node	$ -	$ 10,658.69	$ 21,515.52	$ 34,371.44	$ 44,380.83
Hiawatha Ave.	1 Day CAV SPaT Miles	0.00	6040.20	12001.20	18064.00	23969.64
	1 Day Fuel Savings (gal)	0.00	36.60	77.70	120.45	155.91
	1 Year Fuel Savings (gal)	0.00	9552.11	20280.30	31438.50	40692.93
15 SPaT Intersections	10 Year Fuel Savings (gal)	0.00	95521.10	202803.04	314385.03	406929.31
	10 Year Dollar Savings	0	$ 296,115.40	$ 628,689.43	$ 974,593.61	$ 1,261,480.86
	10 Years Benefits Per Node	$ -	$ 19,741.03	$ 41,912.63	$ 64,972.91	$ 84,098.72
Highway 51	1 Day CAV SPaT Miles	0.00	4040.80	9402.00	12963.40	16473.00
	1 Day Fuel Savings (gal)	0.00	24.48	60.87	86.44	107.15
	1 Year Fuel Savings (gal)	0.00	6390.21	15888.03	22561.44	27965.99
17 SPaT Intersections	10 Year Fuel Savings (gal)	0.00	63902.13	158880.30	225614.42	279659.87
	10 Year Dollar Savings	$ -	$ 198,096.60	$ 492,528.92	$ 699,404.72	$ 866,945.61
	10 Years Benefits Per Node	$ -	$ 11,652.74	$ 28,972.29	$ 41,141.45	$ 50,996.80
Highway 3	1 Day CAV SPaT Miles	0.00	2291.00	4593.80	6216.80	9305.56
	1 Day Fuel Savings (gal)	0.00	13.88	29.74	41.45	60.53
	1 Year Fuel Savings (gal)	0.00	3623.04	7762.86	10819.69	15797.92
16 SPaT Intersections	10 Year Fuel Savings (gal)	0.00	36230.39	77628.62	108196.90	157979.22
	10 Year Dollar Savings	$ -	$ 112,314.22	$ 240,648.73	$ 335,410.40	$ 489,735.59
	10 Years Benefits Per Node	$ -	$ 7,019.64	$ 15,040.55	$ 20,963.15	$ 30,608.47

Table 7.2: Detailed Benefits Information

		0% MPR	10%MPR	20%MPR	30%MPR	40%MPR
Trunk Highway TH-55	10 Year Cost	$ 95,450.00	$ 95,450.00	$ 95,450.00	$ 95,450.00	$ 95,450.00
	10 Year Benefits	$ -	$ 245,149.94	$ 494,856.93	$ 790,543.03	$ 1,020,759.12
	B/C Ratio	0.00	2.57	5.18	8.28	10.69
Hiawatha Avenue	10 Year Cost	$ 65,250.00	$ 65,250.00	$ 65,250.00	$ 65,250.00	$ 65,250.00
	10 Year Benefits	0	$ 296,115.40	$ 628,689.43	$ 974,593.61	$ 1,261,480.86
	B/C Ratio	0.00	4.54	9.64	14.94	19.33
Highway 51	10 Year Cost	$ 70,550.00	$ 70,550.00	$ 70,550.00	$ 70,550.00	$ 70,550.00
	10 Year Benefits	$ -	$ 198,096.60	$ 492,528.92	$ 699,404.72	$ 866,945.61
	B/C Ratio	0.00	2.81	6.98	9.91	12.29
Highway 3	10 Year Cost	$ 66,400.00	$ 66,400.00	$ 66,400.00	$ 66,400.00	$ 66,400.00
	10 Year Benefits	$ -	$ 112,314.22	$ 240,648.73	$ 335,410.40	$ 489,735.59
	B/C Ratio	0.00	1.69	3.62	5.05	7.38

Table 7.3: Cost-Benefit Ratio Calculation of the Entire Corridor

The results show that at any level for the 10 year time-span of the survey, the fuel benefits saved by drivers clearly outweigh the costs of installing the connected SPaT corridors. The corridor with the greatest cost-benefit ratio at any market penetration rate is Hiawatha Avenue. It is evident that the economic efficiency of installing the SPaT nodes increases as the market penetration rate of Eco-speed control enabled connected vehicles increases. This make sense as the installation of SPaT nodes is a fixed cost, while benefits are variable with the magnitude of vehicles enjoying who enjoy the benefits of Eco-speed control.

There are several limitations to this study. As previously stated, due to the fact that we measured for the 6 peak hours of the day, the number of vehicles who take advantage of the SPaT nodes, and thus the total benefits, are under-counted. There is also the fact that the costs come from the estimated already published, but do not take into account variable costs. Only after the SPaT nodes have been installed over a long period will the true cost of both installation and maintenance be discovered. There is also a limitation in how the model processes Eco-speed behavior. An analog is developed with the travel time cost calculation to model re-routing behavior, but the actual driver behavior of slowing down to save on fuel on approach to a SPaT node is not modeled. It is possible that this anomalous driving behavior may cause more congestion, thus reducing capacity, reducing the drivers who use the node and its benefits. This analysis also takes fuel mileage and costs as fixed parameters. As fuel mileage increases, the benefits from Eco-speed control driving may decrease as less fuel is burned overall. On the other hand, it is likely that fuel costs will increase, meaning that the 10% of fuel saved account for a greater magnitude of dollar benefits, increasing the cost-benefit ratio. This entire study has been conducted on internal combustion motors, so electric vehicles will not be able to take advantage of Eco-speed control and so benefits will decrease with increasing

		0% MPR	10%MPR	20%MPR	30%MPR	40%MPR
Trunk Highway TH-55	10 Year Cost	$ 4,150.00	$ 4,150.00	$ 4,150.00	$ 4,150.00	$ 4,150.00
	10 Year Benefits	$ -	$ 10,658.69	$ 21,515.52	$ 34,371.44	$ 44,380.83
	B/C Ratio	0.00	2.57	5.18	8.28	10.69
Hiawatha Avenue	10 Year Cost	$ 4,150.00	$ 4,150.00	$ 4,150.00	$ 4,150.00	$ 4,150.00
	10 Year Benefits	$ -	$ 19,741.03	$ 41,912.63	$ 64,972.91	$ 84,098.72
	B/C Ratio	0.00	4.76	10.10	15.66	20.26
Highway 51	10 Year Cost	$ 4,150.00	$ 4,150.00	$ 4,150.00	$ 4,150.00	$ 4,150.00
	10 Year Benefits	$ -	$ 11,652.74	$ 28,972.29	$ 41,141.45	$ 50,996.80
	B/C Ratio	0.00	2.81	6.98	9.91	12.29
Highway 3	10 Year Cost	$ 4,150.00	$ 4,150.00	$ 4,150.00	$ 4,150.00	$ 4,150.00
	10 Year Benefits	$ -	$ 7,019.64	$ 15,040.55	$ 20,963.15	$ 30,608.47
	B/C Ratio	0.00	1.69	3.62	5.05	7.38

Table 7.4: Cost-Benefit Ratio Calculation for a Single SPaT Signal

market penetration rate of electric vehicles. This study also did not capture the environmental benefits from the fuel saved, as saving on fuel leads to less carbon emissions.

7.6 Summary

In the previous tasks, Eco-speed control with Signal Phasing and Timing (SPaT) enabled intersections was precisely measured to determine how much fuel can be saved with this new optimal driving behavior that is made possible with autonomous driving. This data was then used in Task 6 with a dynamic traffic assignment model built from MnDOT data to determine what kind of fuel benefits can be observed on the already installed SPaT corridor on Trunk Highway TH-55.

In this task, the model was extended to calculate the 10-year cost-benefit ratio of installing a SPaT corridor both on TH-55, and also on Hiawatha Avenue, Highway 51, and Highway 3. The model was run for the highest traffic concentration period of the day, and then that data was extended out to cover all the working days for the entire length of the study. It was determined that at any market penetration rate of connected vehicles above zero, the benefits from fuel saved outweigh the costs of installation. In particular, it was determined that Hiawatha Avenue in Minneapolis is the best candidate for SPaT - enabled signals of the corridors studied. Eco-speed driving is a powerful tool that saves fuel for motorists, with costs borne by the government during SPaT installation and maintenance. In a time when awareness of the costs associated with fuel consumption is rising, the combination of connected infrastructure and Eco-speed driving is a powerful new tool with the potential to prevent millions of gallons of fuel from being burned if properly used.

Chapter 8

Task 8: Final Memorandum on Research Benefits and Implementation Steps

December ,2022

Description: Using the traffic predictions in Task 5, and network-wide cost-benefit analysis from Tasks 6 and 7, the project team had provided a final overview for 4 candidate corridors for SPaT method deploying.

8.1 Introduction

Anticipating future signal phases creates significant opportunities for individual vehicles to optimize their speed profiles on arterial corridors. A major source of fuel consumption is acceleration/deceleration cycles caused by stopping at red lights; acceleration from a full stop requires significant power. Since a significant number of miles are traveled by Minnesotans everyday, optimized vehicle speeds will reduce daily fuel consumption for many of these travelers. In addition, the associated greenhouse gas emissions will be considerably reduced for the state of Minnesota.

The signal phase and timing (SPaT) information has promising potential to achieve fuel efficiency when appropriately utilized. Currently, most vehicle manufacturers are integrating adaptive cruise control which can be used with SPaT data and traffic estimation to adjust the speed of target vehicles equipped with vehicle-to-infrastructure communications. Prior research has shown the benefits of vehicle speed control with SPaT in terms of fuel savings and GHG reductions. It is shown that fuel benefits increase with the increase in the market penetration rate of connected vehicles. This is also validated through real-world experiments which indicate that worthwhile fuel benefits can be achieved for a connected vehicle utilizing SPaT information in the presence of two connected preceding vehicles. With reduced fuel consumption, CO_2 emissions of the target connected vehicle are significantly reduced [26], due to the fact that CO_2 emissions considerably depend on the fuel consumption of a gasoline engine. It is therefore expected that fuel efficiency and emission reductions will be achieved for Minnesotans if vehicle speed control is employed using signal phasing and timing data in the state of Minnesota.

In the previous tasks, it has been shown that the use of signal phase and timing (SPaT) can increase fuel efficiency when deployed with connected autonomous vehicles (CAVs). In Task 5, the traffic prediction and vehicle speed optimization data from Task 3 were used to develop a holistic simulation methodology to predict the benefits in fuel consumption for vehicle platoons at various market penetration rates of CAVs. In Task 6, this method was applied to study the impact of CAV market penetrations on fuel consumption of vehicle platoons using vehicle speed data collected along Trunk Highway 55. While no significant re-routing behavior was discovered, it was observed that the fuel benefits from vehicles traveling along the connected corridor have the potential to be significant. In Task 7, the same dynamic traffic assignment methodology from Task 6 was utilized to discover the benefits of several prospective locations to install a new connected corridor in the Twin Cities region. For this task, the final cost and benefit analysis is presented based on data from Task 6 and 7 which implements the method on the Minneapolis/St. Paul network.

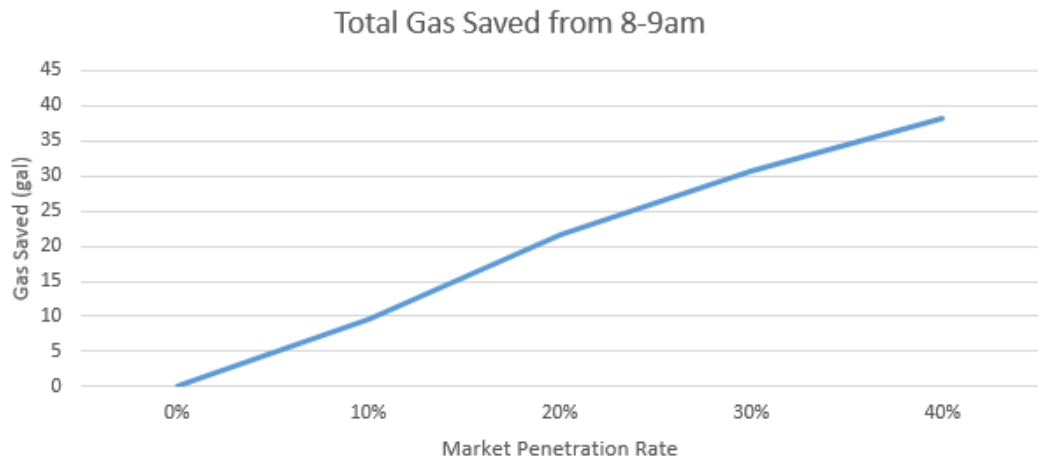

Figure 8.1: Fuel Savings from the CAVs on TH-55 from 8–9am

8.2 Benefits

Benefits of fuel savings will be more realistic by modeling what the magnitude of those fuel savings are at the network-level. For modeling, dynamic traffic assignment was chosen for the entire Twin Cities. Three steps of traffic assignment construction are: network loading, path finding, and route updating.

The dynamic traffic assignment model was modified so that instead of seeking just to minimize travel time, drivers in the system seek to minimize travel time cost, which is travel time discounted for CAVs that travel using TH-55 where SPaT signals were installed. In other words, dynamic traffic assignment was applied to see re-routing phenomena to TH-55 to enjoy fuel saving. It was decided to run the simulation at peak hour in the morning when there were the most vehicles on the road.

For this study, we used the DynusT network and demand model provided by MnDOT and converted for use with dynamic traffic assignment. In this model, there are 29,013 links and 10,943 nodes. We designate the 22 SPaT nodes on TH-55 as a special case of a SPaT intersection. Then, we limit the scope of the study to just one hour at 8 am (during peak commuting time) to ensure the simulation can complete in a reasonable amount of time. At this hour, there are 710,052 vehicles that travel on the network across 1,593,813 possible origin-destination pairs. We set the duration of an assignment interval to be 15 minutes (900s) and the duration of the demand interval for two hours beginning at 8am (7200s).

Simulating peak hour shows that there is no increase in market penetration of target route (TH-55) compared to alternative paths. So, there is no significant re-routing from alternative paths to the SPaT path. In this case, route changes observed were due of the eco-speed fuel discount. Also, total travel time savings for TH-55 is 4 minutes. The total travel time in this route is around 60 minutes; however travel times for I-394 range between 20–50 minutes in 40 percent MPR level. Therefore, the difference of travel time between I-394 and TH-55 is more

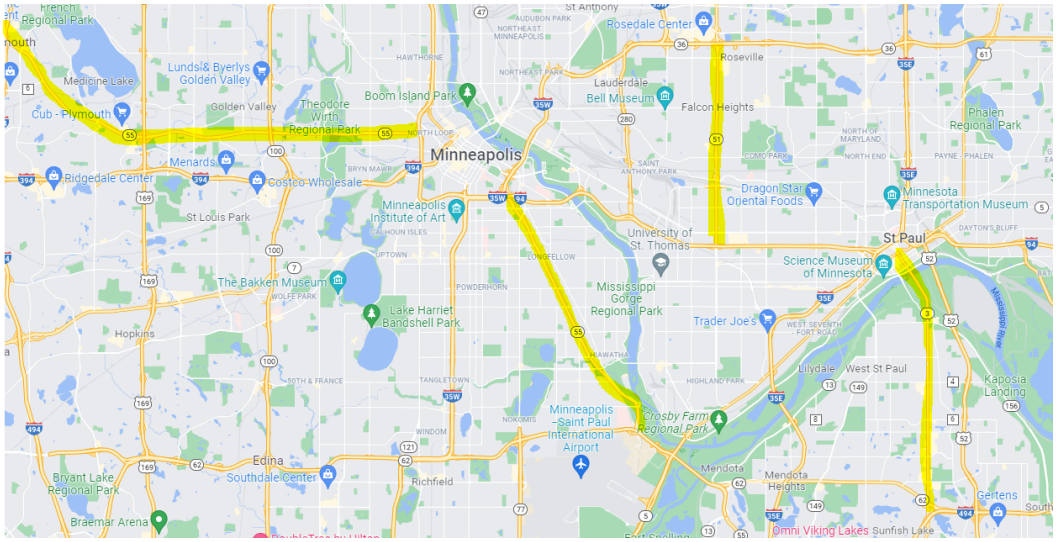

Figure 8.2: Study Corridors

than 4 minutes, and this discounted time is not enough. As a result, drivers still stay on the larger and faster road, I-394.

Although no re routing, there is an impressive fuel saving for vehicles that already are in the road. As mentioned, discounted travel times are between 3.8 to 4.2 minutes, and Figure 8.1 presents fuel savings during the peak hour. At a market penetration rate of 40 percent, 38 gallons of fuel were saved during this one hour of the day for only those 7470 CAV vehicles. Assuming that this 1 hour is representative of all weekday trips at this hour, across the 261 working days of the year that is 9,918 gallons of fuel saved per year at 40 percent MPR and 2,490 gallons per year at 10 percent MPR.

8.3 Benefits predicted by peak hour model on TH-55 and candidate highways

In Task 7, traffic assignment is implemented for three hours peak hour. There are two peak periods during a day; morning and afternoon. In addition, goal is to discover the benefits of several prospective locations to install a new connected corridor in the Twin Cities region. For the purposes of this analysis, three signalized highways were selected along with the already installed SPaT equipment along Trunk highway TH-55. The highways selected were Hiawatha Avenue, Highway 51, and Highway 3 provided in Figure 8.2. The costs for deploying SPaT include installation and maintenance of the SPaT units at signalized intersections. At each intersection, it is minimally necessary to deploy a signal controller, a roadside unit (RSU), and cables connecting the signal controller and the RSU. Signalized intersections already have signal controllers, so a part of expenses are reduced. Finally, the model is extended to calculate the 10-year cost-benefit ratio of installing a SPaT corridor.

		0% MPR	10%MPR	20%MPR	30%MPR	40%MPR
TH-55	10 Year Cost	$ 95,450.00	$ 95,450.00	$ 95,450.00	$ 95,450.00	$ 95,450.00
	10 Year Benefits	$ -	$ 245,149.94	$ 494,856.93	$ 790,543.03	$ 1,020,759.12
	B/C Ratio	0.00	2.57	5.18	8.28	10.69
Hiawatha	10 Year Cost	$ 65,250.00	$ 65,250.00	$ 65,250.00	$ 65,250.00	$ 65,250.00
	10 Year Benefits	0	$ 296,115.40	$ 628,689.43	$ 974,593.61	$ 1,261,480.86
	B/C Ratio	0.00	4.54	9.64	14.94	19.33
Highway 51	10 Year Cost	$ 70,550.00	$ 70,550.00	$ 70,550.00	$ 70,550.00	$ 70,550.00
	10 Year Benefits	$ -	$ 198,096.60	$ 492,528.92	$ 699,404.72	$ 866,945.61
	B/C Ratio	0.00	2.81	6.98	9.91	12.29
Highway 3	10 Year Cost	$ 66,400.00	$ 66,400.00	$ 66,400.00	$ 66,400.00	$ 66,400.00
	10 Year Benefits	$ -	$ 112,314.22	$ 240,648.73	$ 335,410.40	$ 489,735.59
	B/C Ratio	0.00	1.69	3.62	5.05	7.38

Table 8.1: Cost-Benefit Ratio Calculation of the Entire Corridor

The model was run for the three hour peak hour at different market penetration rates. There were 1,654,830 trips, so due to the large magnitude of the simulation, the data was discretized in units of 10. The simulation is ran for units representing ten vehicles for a total of 165,483 units. This does not impact the congestion modeling of the simulation. Moreover, sub-networks were created in modeling process to consider each corridor under different market penetration rates. This study also did not capture the environmental benefits from the fuel saved, as saving on fuel leads to fewer carbon emissions.

The miles traveled by CAVs along eco-speed control routes (roads controlled by SPaT enabled signals) are divided by the Minnesota average fuel mileage of 22mpg [4] to get the total amount of fuel consumed. This fuel mileage is then multiplied by the percent fuel savings calculated in the last section (1 hour simulation). These three hours at peak are assumed to be similar both in the morning and evening peak. Thus the total six hour fuel savings are considered for the benefits for a single day, which was then multiplied by 261 to consider all the weekdays in a year, which was then multiplied by 10 to consider the entire 10-year period. Dollar savings are calculated assuming $3.01 as average fuel cost per gallon in Minnesota. As a result of this step in the analysis, the benefits were underestimated as the vehicles who traverse the SPaT-enabled nodes at an off-peak time are not considered, so the fuel benefits calculated here are likely to be an underestimation. At the end of the traffic assignment period, the miles of road that connected autonomous vehicles traveled along each SPaT corridor was determined. This was then used with the fuel savings observed in the previous tasks to determine how many gallons of fuel were saved, from which the dollar value of the fuel saved was determined for the purpose of the analysis. The detailed results of the cost-benefit analysis for the candidate highways can be seen in Table 8.1 and 8.2. Table 8.1 presents analysis

		0% MPR	10%MPR	20%MPR	30%MPR	40%MPR
TH-55	10 Year Cost	$ 4,150.00	$ 4,150.00	$ 4,150.00	$ 4,150.00	$ 4,150.00
	10 Year Benefits	$ -	$ 10,658.69	$ 21,515.52	$ 34,371.44	$ 44,380.83
	B/C Ratio	0.00	2.57	5.18	8.28	10.69
Hiawatha	10 Year Cost	$ 4,150.00	$ 4,150.00	$ 4,150.00	$ 4,150.00	$ 4,150.00
	10 Year Benefits	$ -	$ 19,741.03	$ 41,912.63	$ 64,972.91	$ 84,098.72
	B/C Ratio	0.00	4.76	10.10	15.66	20.26
Highway 51	10 Year Cost	$ 4,150.00	$ 4,150.00	$ 4,150.00	$ 4,150.00	$ 4,150.00
	10 Year Benefits	$ -	$ 11,652.74	$ 28,972.29	$ 41,141.45	$ 50,996.80
	B/C Ratio	0.00	2.81	6.98	9.91	12.29
Highway 3	10 Year Cost	$ 4,150.00	$ 4,150.00	$ 4,150.00	$ 4,150.00	$ 4,150.00
	10 Year Benefits	$ -	$ 7,019.64	$ 15,040.55	$ 20,963.15	$ 30,608.47
	B/C Ratio	0.00	1.69	3.62	5.05	7.38

Table 8.2: Cost-Benefit Ratio Calculation for a Single SPaT Signal

for entire corridor, and Table 8.2 presents potential benefit ratio for one single signal. As example, the cost-benefit ratio for 40 percent of market penetration rate varies between 7.38 to 19.33 for this ten years period. In general, Hiawatha Avenue showed highest benefits with respect to the market penetration tested.

MPR	TH-55	Hiawatha	Highway 51	Highway 3
0%	0	0	0	0
10%	3.9	2.2	3.6	5.9
20%	1.9	1	1.9	2.8
30%	1.3	0.7	1	2
40%	0.9	0.5	0.8	1.4

Table 8.3: Eco-strategy return on investment in years

8.4 Cost-Benefit Overview

For selected corridors, fuel savings during peak hours will be around 14% (13.44% to 14.67%). Starting from 10% MPR, they can bring $100M to 300$ profit in a 10 year period. At maximum considered rate for MPR which is 40%, we can see up to $1,260M with the proposed control system. Since the platform may require an instant investment at the start point of study, one may ask for horizon to return the original fund. In other words, it will be valuable if we take a look at the return of investment (or capital turnover) for each corridor or a single signal. Table 8.3 shows that how many years takes for each corridor to its earning equals to the costs. As visible, typically if market penetration exceeds 20%, just in two years all of costs are returned. Also, for Hiawatha Avenue its even better and it needs one year. This statement is also valid for single signals.

8.5 Summary

Overall, eco-speed control with Signal Phasing and Timing (SPaT) enabled will provide fuel saving benefits in network view. Although SPaT controlled corridor was not chosen by drivers of other paths, drivers who already were driving in the target road will enjoy fuel savings. Hourly ranges for fuel savings is 9–38 gallon based on the MPR for the total number of CAVs using the corridor. As expected, value of benefits varies by connected vehicles market penetration. Also, three options were presented beside TH-55 as candidates to deploy the controlling system. Model was extended to calculate the 10-year cost-benefit ratio of installing a SPaT corridor on TH-55, Hiawatha Avenue, Highway 51, and Highway 3. Average B-C ratio in 10% MPR for these four corridors is around 2.9 for ten years. Therefore, current project reveals that by choosing the best corridor for eco-control, people can sense the fuel consumption by this method even in low market penetration rates (10 % MPR).

It was determined that at any market penetration rate of connected vehicles above zero, the benefits from fuel saved outweigh the costs of installation. In particular, it was determined that Hiawatha Avenue in Minneapolis was the best candidate for SPaT-enabled signals of the corridors studied. Modeling daily peak hours over ten years was revealed that deploying such a system can provide worthwhile profits for the entire society of road users due

to thousands gallons of fuel saved.

Chapter 9

Conclusions

The scope of this research provided benefits including: 1) reduce road user costs via reduced fuel consumption, and 2) reduce environmental impact via reduced greenhouse gas emissions. Signal phasing and timing data was used to help avoid complete stops at signalized intersections, which provided vehicle fuel consumption savings since acceleration from a full stop requires significant power. Also, since the emissions considerably depend on the fuel consumption of a gasoline engine, reductions in fuel consumption were also expected to reduce CO2 emissions of the target connected vehicle.

The overall cost of deploying the control system was based on the RSU equipment, installations, and support. However, the overall benefit was the total amount of fuel that saved in plan's horizon. The benefit value was the product of fuel savings, the total number of target vehicles (and price of the fuel). Our estimation for a certain corridor was that the cost of infrastructure deployment would be $3,612,000 and the benefits would be be around $1,354,000,000 for a period of 10 years and market penetration of 40%. Also, assuming 7.95% reduction in CO2 by eco driving using SPaT data, greenhouse gas emissions will be reduced by 2,553,540 tons of CO2 in 10 years.

9.1 Data Collection and Map Analysis

The project team researched vendors (for OBUs) of connected vehicle equipment, then discussed the requirements for software, hardware, and warranty support. Fig 9.1 presents how OBUs equipment were installed as package of driving test. This process collected data and generated the vehicle trajectory of each CV. The OBU received the MAP messages (The MAP message is used to convey many types of geometric information of the intersection) broadcast to CVs at the intersection via the RSU once per second. In order to interpret the MAP messages, an

Figure 9.1: OBU installation inside a vehicle

online message decoder was used to figure out the location of intersections and signal groups.

Analysis of the results showed that the SPaT messages broadcast at Theodore Wirth Pkwy, Meadow Ln and Schaper Rd include a few issues: 1) time offsets, 2) inaccurate signal timing, and 3) unsteady signal timing. It was also noticed that the MAP messages broadcast at Douglass Dr have the wrong signal group allocation. Therefore, the research team corrected the issues in the data processing process. Through this project, the performance of traffic prediction and optimal control for energy saving was demonstrated with the collected and preprocessed data. The proposed approach can be applied on a corridor with multiple intersections and is verified by real traffic data.

9.2 Speed Control Based on Traffic Flow Prediction

To provide a fuel efficient control for CVs, future traffic conditions (next 10–15s) was predicted using traffic flow model. A second order traffic flow model used speed and location of other vehicles to estimate the speed and the density of the traffic flow. The SPaT information provided the current and future signal states at the intersection. This platform was shown to work for different CV market penetration rates. The prediction of future traffic conditions determined the car following constraints for the target CV. Under all constraints, the speed control of the target CV could be obtained by solving an optimal control problem which aims for minimum fuel consumption.

The preliminary result focused on a segment of TH-55 consisting of four intersections, as shown in Fig. 3.6. The four 'CAVs' were driven from west to east (left to right in the figure). The preliminary results showed that, for a segment of road with 4 intersections, the fuel benefits could be 12.19%.

9.3 Control Benefits Evaluation by HIL Testbed

After optimal controlling of the target CV, a hardware-in-the-loop (HIL) testbed was used to experimentally evaluate the performance of target vehicle. HIL testbed allowed a virtual target vehicle to interact with traffic while maintaining the fidelity of the fuel measurement with laboratory instruments. A laboratory powertrain research platform was employed to represent the virtual target vehicle, including an actual engine, an engine loading device (hydrostatic dynamometer), and vehicle dynamic models. The main advantage was that by using an actual engine the target vehicle simulated by the powertrain research platform could accurately represent the dynamics of the target vehicle without safety concerns.

Comparing the performances of connected and autonomous vehicles driven by the proposed co-optimization technique with traditional vehicles, the optimal control could achieve 11.35% energy benefits. The energy benefits came from less deceleration when approaching the intersections when the signal is red and smoother acceleration when leaving intersections. Connected vehicles did not come to a complete stop, which reduced the amount of braking and avoids idling waste. Thus, CVs could achieve significant benefits on fuel consumption.

9.4 Various Market Penetration Analysis

A series of simulation experiments was conducted for a platoon consisting of 10 vehicles following a lead LV (11 vehicles in total). In this setting, 10 different penetration rates of CAVs were simulated, ranging from 10% to 100%. A similar study was also conducted on a platoon with 20 vehicles to verify results. The baseline scenario was considered with a 0% penetration rate of CAVs, i.e., all the vehicles were LVs. It was observed from the results that the fuel benefits of the vehicle platoon appear to increase with the increase of CAV penetrations due to smoother traffic. The fuel savings could be seen in different ways ranging from only CAV to impacts on whole platoon. In addition to fuel savings for those target CAVs, they could also provide fuel savings for other following human driven vehicles due to smoother reactions. Therefore, CAVs could show fuel savings for the whole platoon. Based on simulation data, the fuel savings on the CAVs started from 5% for the lowest MPR, and rose up to 15% improvement for the highest possible MPR (all vehicles are CAV). Also, fuel savings for the whole platoon caused by CAV started from around 3% and increased up to 12%.

In addition to the fuel benefits obtained by LVs behind CAVs, LVs also experienced a smaller travel time compared scenarios without CAVs. With a penetration rate varying from 10% to 90%, the corresponding reduction in average travel time for LVs ranged from around 1% to nearly 5%. As a result, LVs experienced a larger average speed at a higher penetration rate of CAVs, as opposed to the scenario with a lower penetration rate. The results were encouraging in the sense that more vehicles driving on Minnesota roads would benefit from the deployment of future connected corridors with an increasing number of CAVs present.

MPR	Time Discount (min)	Gallons Saved	Number of CAVs
0%	0	0	0
10%	3.83	9.54	2,050
20%	4.10	21.78	3,780
30%	4.21	30.69	5,848
40%	4.11	38.27	7,470

Table 9.1: Eco-driving Fuel Savings for 1 hour driving in TH-55 corridor

9.5 Network Model and Route Choice

Studying the corridor, simulations revealed that the discounted travel time based on MPR varied from 3.8 to 4.2 minutes for the deployed SPaT corridor. The total travel time for this section was around an hour while the alternate path had travel times ranging between 20 and 50 minutes. Since the discounted travel time and fuel savings were not sufficient to overcome the time savings and drivers would still choose the alternate route (I-394). Thus, there was no significant route-change from other routes to this eco route. Although re-routing did not occur, many gallons of fuel were saved by the vehicles already using TH-55. Assuming that this 1 hour was representative of all weekday trips at this hour, across the 261 working days of the year that was 9,918 gallons of fuel saved per year at 40% MPR and 2,490 gallons per year at 10% MPR. Table 9.1 shows how many CAVs would use the target corridor and how many gallons would be saved daily.

9.6 Cost/Benefit Analysis of Connected Corridors

Following the last step, three signalized corridors were selected along with the already installed SPaT equipment along trunk highway TH-55. The selected routes were Hiawatha Avenue, Highway 51, and Highway 3. The costs for deploying SPat included installation and maintenance of the SPaT units at signalized intersections. The signalized intersections had signal controllers, so controller hardware was not included in the cost. For candidates in this study, SPaT installations' cost based on the number of intersections varied from \$65K to \$95K.

For selected corridors, the fuel savings during rush hours would be around 14% (13.44% to 14.67%). Starting from 10% MPR, they could bring \$100M to 300\$ in net benefits in a 10 year period. At maximum considered rate for MPR which was 40%, we could see up to \$1,260M with the proposed control system. In a 10 year period, the benefit-cost ratio increased up to 20.26 for the most cost efficient route of Hiawatha Avenue (in 40% MPR). The average benefit-cost ratio in 10% MPR for these four corridors was around 2.9 for the ten year period. Therefore, by choosing the best corridor as the priority for eco-control, people experienced reductions in fuel consumption even in low market penetration rates (10% MPR). Since the platform might require an initial

investment at the start point. It was possible to evaluate the expected horizon to see the value of benefits exceeded the original investment. Table 9.1 shows that how many years takes for each corridor to its earning equals to the costs. As demonstrated, typically if the market penetration exceeds 20%, in two years all of costs are returned. Hiawatha Avenue only requires 1 year for this demonstration. This statement is also valid for single signals.

Overall, eco-speed driving is a powerful mechanism that saves fuel for motorists with costs borne by the government during SPaT installation and maintenance. In a time when awareness of the costs associated with fuel consumption is rising, the combination of connected infrastructure and eco-speed driving is a new tool with the potential to prevent millions of gallons of fuel (and tons of emissions) from being burned if properly utilized.

Bibliography

[SAE] Dedicated short range communications (dsrc) message set dictionary. SAE Standard J2735, Jan. 2016.

[MAR] Marben products: Asn.1 messages decoder.

[wir] Neal probert: Wireshark-dsrc, github repository. Nov. 2022.

[4] (2020). The 2020 EPA Automotive Trends Report. techreport, U.S. Environmental Protection Agency.

[5] AAA Gas Prices (2021). https://gasprices.aaa.com/?state=MN.

[Bemporad and Morari] Bemporad, A. and Morari, M. Control of systems integrating logic, dynamics, and constraints. In *Hybrid Systems" publisher "Lecture Notes in Computer Science, Springer*, Berlin, Heidelberg.

[7] Boyles, S. D., Lownes, N. E., and Unnikrishnan, A. (2021). *Transportation Network Analysis*, volume 1. 0.89 edition.

[8] Daganzo, C. F. (1995). The cell transmission model, part ii: Network traffic. *Transportation Research Part B: Methodological*, 29(2):79–93.

[9] Dijkstra, E. W. (1959). A note on two problems in connexion with graphs. *Numerische Mathematik*, 1:269–271.

[Georgia DOT] Georgia DOT. Georgia dot statewide connected vehicles deployment experience and future plans. Accessed: 2020-08-30.

[J.Ma and J.Hu] J.Ma and J.Hu. Eco-drive experiment on rolling terrain for fuel consumption optimization summary report (no. fhwa-hrt-18-037). Federal Highway Administration, U.S. Department of Transportation. McLean, VA.

[12] Laval, J. A. and Daganzo, C. F. (2006). Lane-changing in traffic streams. *Transportation Research Part B: Methodological*, 40(3):251–264.

[13] Liberti, L., P. C. (2006). An exact reformulation algorithm for large nonconvex nlps involving bilinear terms. *J Glob Optim*, 36(2):161–189.

[14] Lighthill, M. J. and Whitham, G. B. (1955a). On kinematic waves ii. a theory of traffic flow on long crowded roads. *Proceedings of the Royal Society of London. Series A. Mathematical and Physical Sciences*, 229(1178):317–345.

[15] Lighthill, M. J. and Whitham, G. B. (1955b). On kinematic waves ii. a theory of traffic flow on long crowded roads. *Proceedings of the Royal Society of London. Series A. Mathematical and Physical Sciences*, 229(1178):317–345.

[16] Ma, J., Hu, J., Leslie, E., Zhou, F., Huang, P., and Bared, J. (2019). An eco-drive experiment on rolling terrains for fuel consumption optimization with connected automated vehicles.

[National Operations Center of Excellence (NOCoE)] National Operations Center of Excellence (NOCoE). The spat challenge. Accessed: 2020-08-30.

[18] Newell, G. F. (1993). A simplified theory of kinematic waves in highway traffic, part II: Queueing at freeway bottlenecks. *Transportation Research Part B: Methodological*, 27(4):289–303.

[19] Office of the Assistant Secretary for Transportation Policy (2016). Revised Departmental Guidance on Valuation of Travel Time in Economic Analysis. Technical report, U.S. Department of Transportation. Washington, DC.

[20] Payne, H. (1971). Shock waves on the highway. In *Mathematical Models of Public Systems*, volume 1, pages 51–61. La Jolla, Calif., Simulation Councils.

[21] Richards, P. I. (1956). Shock waves on the highway. *Operations Research*, 4(1):42–51.

[22] Ross, I. M. and Karpenko (2012). A review of pseudospectral optimal control: From theory to flight. 36(2):182–197.

[Savari Inc.] Savari Inc. Savari mobiwave1000 user guide v6.1.0.

[Shao and Sun] Shao, Y. and Sun, Z. Optimal speed control for a connected and autonomous electric vehicle considering battery aging and regenerative braking limits. In *Proceedings of the ASME 2019 Dynamic Systems and Control Conference*, volume 1. ASME.

[25] Shao, Y. and Sun, Z. (2019). Optimal vehicle speed and gear position control for connected and autonomous vehicles. In *2019 American Control Conference (ACC)*, pages 545–550. IEEE.

[26] Shao, Y. and Sun, Z. (2021). Eco-approach with traffic prediction and experimental validation for connected and autonomous vehicles. *IEEE Transactions on Intelligent Transportation Systems*, 22(3):1562–1572.

[27] Simon, D. (2006). *Optimal State Estimation: Kalman, H, and Nonlinear Approaches*. Wiley-Interscience. Hoboken, New Jersey.

[28] Suh, B., Shao, Y., and Sun, Z. (2020). Vehicle speed prediction for connected and autonomous vehicles using communication and perception. In *2020 American Control Conference (ACC)*, pages 448–453. IEEE.

[29] Sun, W., Wang, S., Shao, Y., Sun, Z., and Levin, M. W. (under review). Traffic prediction for connected vehicles on a signalized arterial. In *2021 IEEE Intelligent Transportation Systems Conference (ITSC)*. IEEE.

[30] Treiber, M., Hennecke, A., and Helbing, D. (2000). Congested traffic states in empirical observations and microscopic simulations. *Physical Review E*, 62(2):1805.

[31] Treiber, M. and Kesting, A. (2013). *Traffic flow dynamics*. Springer. Verlag Berlin Heidelberg.

[32] Wang, Y. and Papageorgiou, M. (2005). Real-time freeway traffic state estimation based on extended kalman filter: a general approach. *Transportation Research Part B: Methodological*, 39(2):141–167.

[Wang and Sun] Wang, Y. and Sun, Z. Dynamic analysis and multivariable transient control of the power-split hybrid powertrain. *IEEE/ASME Trans. Mechatron*, 20(6):3085–3097.

[34] Whitham, G. B. (2011). *Linear and nonlinear waves*, volume 42. John Wiley & Sons. New York.

[35] Wilson, R. E. and Ward, J. A. (2011). Car-following models: fifty years of linear stability analysis–a mathematical perspective. *Transportation Planning and Technology*, 34(1):3–18.

[Xianan Huang, Ding Zhao, and Huei Peng] Xianan Huang, Ding Zhao, and Huei Peng. Empirical study of dsrc performance based on safety pilot model deployment data. IEEE Transactions on Intelligent Transportation Systems, vol. 18, Oct. 2017.

[Y. Wang, Z. Sun and K.A. Stelson] Y. Wang, Z. Sun and K.A. Stelson. Modeling, control, and experiment validation of a transient hydrostatic dynamometer. IEEE Trans. Control Syst. Technol. 19(6),1578-1586.

[38] Yperman, I., Logghe, S., and Immers, B. (2005). The link transmission model: An efficient implementation of the kinematic wave theory in traffic networks. *Proceedings of the 10th EWGT Meeting and 16th Mini-Euro Conference*.

[Z.Sun and G.G.Zhu] Z.Sun and G.G.Zhu. Design and control of automotive propulsion system. CRC Press, 2014.